



SAND REPORT

SAND2002-1084
Unlimited Release
Printed April 2002

Assembly of LIGA using Electric Fields

John T. Feddema, Larry K. Warne, William A. Johnson, Allison J. Ogden, David L. Armour

Prepared by
Sandia National Laboratories
Albuquerque, New Mexico 87185 and Livermore, California 94550

Sandia is a multiprogram laboratory operated by Sandia Corporation, a Lockheed Martin Company, for the United States Department of Energy under Contract DE-AC04-94AL85000.

Approved for public release; further dissemination unlimited.



Sandia National Laboratories

Issued by Sandia National Laboratories, operated for the United States
Department of Energy by Sandia Corporation.

NOTICE: This report was prepared as an account of work sponsored by an agency of the United States Government. Neither the United States Government, nor any agency thereof, nor any of their employees, nor any of their contractors, subcontractors, or their employees, make any warranty, express or implied, or assume any legal liability or responsibility for the accuracy, completeness, or usefulness of any information, apparatus, product, or process disclosed, or represent that its use would not infringe privately owned rights. Reference herein to any specific commercial product, process, or service by trade name, trademark, manufacturer, or otherwise, does not necessarily constitute or imply its endorsement, recommendation, or favoring by the United States Government, any agency thereof, or any of their contractors or subcontractors. The views and opinions expressed herein do not necessarily state or reflect those of the United States Government, any agency thereof, or any of their contractors.

Printed in the United States of America. This report has been reproduced directly from the best available copy.

Available to DOE and DOE contractors from
U.S. Department of Energy
Office of Scientific and Technical Information
P.O. Box 62
Oak Ridge, TN 37831

Telephone: (865)576-8401
Facsimile: (865)576-5728
E-Mail: reports@adonis.osti.gov
Online ordering: <http://www.doe.gov/bridge>

Available to the public from
U.S. Department of Commerce
National Technical Information Service
5285 Port Royal Rd
Springfield, VA 22161

Telephone: (800)553-6847
Facsimile: (703)605-6900
E-Mail: orders@ntis.fedworld.gov
Online order: <http://www.ntis.gov/ordering.htm>



SAND2002-1084
Unlimited Release
Printed April 2002

Assembly of LIGA using Electric Fields

John T. Feddema
Intelligent Systems, Sensors & Controls Department

Larry K. Warne
EM & Plasma Physics Analysis Department

William A. Johnson
EM & Plasma Physics Analysis Department

Allison J. Ogden
Mechanical Systems Design Department

David L. Armour
Electromechanical Engineering Department

Sandia National Laboratories
P.O. Box 5800
Albuquerque, NM 87185-1003

Abstract

The goal of this project was to develop a device that uses electric fields to grasp and possibly levitate LIGA parts. This non-contact form of grasping would solve many of the problems associated with grasping parts that are only a few microns in dimensions. Scaling laws show that for parts this size, electrostatic and electromagnetic forces are dominant over gravitational forces. This is why micro-parts often stick to mechanical tweezers. If these forces can be controlled under feedback control, the parts could be levitated, possibly even rotated in air. In this project, we designed, fabricated, and tested several grippers that use electrostatic and electromagnetic fields to grasp and release metal LIGA parts. The eventual use of this tool will be to assemble metal and non-metal LIGA parts into small electromechanical systems.

Acknowledgements

The authors would like to thank William Derr (of Derr Enterprises) for expertise in providing the high frequency current required to drive the magnetic repulsion coils.

Contents

1.0 Introduction	1
2.0 Electromagnetic Analysis and Simulation	4
3.0 Experimental Tests.....	20
3.1 Electrostatic Gripper	20
3.2 Combined Electrostatic/Electromagnetic Gripper	23
4.0 Conclusions and Future Directions.....	28
References	29
Appendix A – Derivation of van der Waals Force	31
Appendix B – Stability Analysis Report for Magnetically Levitated Disc, Larry Warne.....	35

Figures

Figure 1. Forces of attraction.	1
Figure 2. Van der Waals force of attraction	2
Figure 3. Geometry of circular part and stator (or gripper).....	4
Figure 4 Electrostatic attractive force, electromagnetic repulsive force, and gravity.	7
Figure 5. Side view of stator picking up part off a surface	7
Figure 6. Response in the z direction without the derivative control term. $a = 0 \text{ mm}$, $b = 1.5 \text{ mm}$, $c = d = 2 \text{ mm}$, $\Delta = 150 \text{ }\mu\text{m}$, $t = 100 \text{ }\mu\text{m}$, $t_w = 10 \text{ }\mu\text{m}$, $h^* = 30 \text{ }\mu\text{m}$, $K_p = 10000$, and $K_v = 0$. The initial condition is $z_o = 1 \text{ }\mu\text{m}$	10
Figure 7. Response in the z direction with the derivative control term. $a = 0 \text{ mm}$, $b = 1.5 \text{ mm}$, $c = d = 2 \text{ mm}$, $\Delta = 150 \text{ }\mu\text{m}$, $t = 100 \text{ }\mu\text{m}$, $t_w = 10 \text{ }\mu\text{m}$, $h^* = 30 \text{ }\mu\text{m}$, $K_p = 10000$, and $K_v = 500$. The initial condition is $z_o = 1 \text{ }\mu\text{m}$	11
Figure 8. Response in the z direction with the electromagnetic force and the derivative control term. The parameters are $a = 0 \text{ mm}$, $b = 1.5 \text{ mm}$, $c = d = 2 \text{ mm}$, $\Delta = 150 \text{ }\mu\text{m}$, $t = 100 \text{ }\mu\text{m}$, $t_w = 10 \text{ }\mu\text{m}$, $h^* = 30 \text{ }\mu\text{m}$, $K_p = 15000$, $K_v = 500$, $I = 0.1 \text{ A}$, and $\omega = 2\pi(10^7) \text{ rad/s}$. The initial condition is $z_o = 1 \text{ }\mu\text{m}$	12
Figure 9. Simulation of electrostatic force between gripper array and cylinder shaped part.....	15
Figure 10. Simulation of electrostatic force between gripper array and a plate	16
Figure 11. Simulation of electrostatic force between gripper array and a C-shaped part.....	17
Figure 12. Simulation of electrostatic force between gripper array and an L-shaped part.	18
Figure 13. Simulation of electrostatic force between gripper array and a T-shaped part.....	19
Figure 14. Picking up 4mm diameter copper plate using electrostatics	20

Figure 15. Capacitance sensor readings in experiment. Capacitance reading of 1 indicates plate is picked up.....	21
Figure 16. Theoretical electrostatic force of attraction.....	22
Figure 17. Combined electrostatic/electromagnetic stator. The electrostatic force of attraction is created by applying up to 150 volts to the four inner pads. The electromagnetic force of repulsion is created by applying up to 1 Amp of current to the coils surrounding the inner pads. The center circle is used to sense the stand-off distance between the part and the stator	23
Figure 18. Two array designs for nonsymmetric parts. The cross-shaped pads in the middle of each coil are individually addressable electrostatic pads. The coils are individually addressable electromagnetic coils. The diamond-shaped pads are capacitive sensors	24
Figure 19. The measured probability that the copper plate would stick to the gripper after the voltage is returned to zero	25
Figure 20. Probability of sticking when a 10MHz, 1A current is applied to the electromagnetic coil.	26
Figure 21. Probability of sticking when a 1A DC current is applied to the coil	27

1.0 Introduction

Since 1996, Sandia National Laboratories' Intelligent Systems and Robotics Center has been investigating techniques for the assembly of miniaturized electromechanical systems. Great strides have been made in developing a semi-automated CAD-driven workcell for assembling LIGA (Lithographie Galvanoformung Abformung) parts with 100 micron outer dimensions and submicron tolerances [1-3]. In the course of this past work, one area that has continued to cause difficulty is accurate grasping and releasing of such small parts. As the size of parts drop below 1 mm in outside dimensions, the parts tend to stick to the gripper surfaces. The attractive forces that cause this effect are electrostatic, magnetic, surface tension, and van der Waals. Figure 1 shows that these forces are dominant over gravity as the radius of a particle drops below 1 mm [4-5].

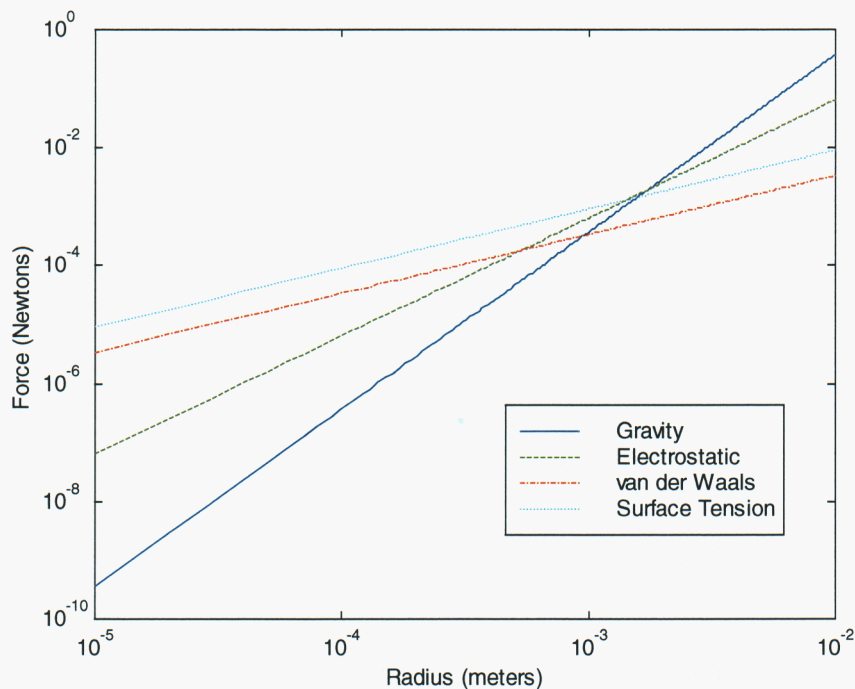


Figure 1. Forces of attraction.

All of these forces can be reduced with careful preparation and design of materials. For instance, surface tension can be reduced by performing the assembly in a low humidity clean room environment. Van der Waals forces can be reduced by roughing the tweezer surface [4]. Magnetic forces can be reduced by using dissimilar non-magnetic materials. For example, in our experiments, we used Permalloy (a magnetic material) for the gears being assembled and copper (a non-magnetic material) for the tweezers. And lastly, electrostatics may be reduced by grounding conductive surfaces; although, oxides quickly build up on most conductive surfaces, thus trapping electrostatic charge.

Unfortunately, it is impossible to completely eliminate these forces, and as parts become smaller, these forces do affect the handling of parts. Therefore, in this project, we investigated the use of electromagnetic fields to pick up and hopefully levitate a part so that it can be manipulated without actually touching the part. If the part can be levitated only a few microns from a tweezer tip, van der Waals forces are nearly eliminated as shown in Figure 2. The two curves in this figure represent the upper and lower bounds of the van der Waals force of attraction between a 2 micron diameter copper sphere and a tweezer tip which varies in size from 1 micron³ to an infinite plane [3]. This figure shows that van der Waals forces drop between 4 to 6 orders of magnitude if the sphere is only 5 microns away from the tip. Similarly, surface tension forces will be negligible if the tweezer tip never touches the part. This has an important economic benefit in that a clean room may not be needed to assemble parts if they can be levitated and never touched.

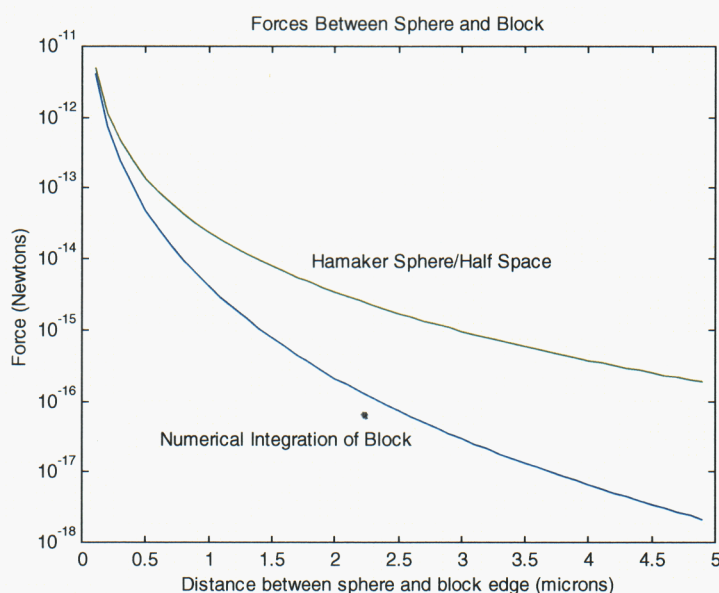


Figure 2. Van der Waals force of attraction.

There are several previous works that lead us to believe that it is feasible to develop an electromagnetic levitation probe for assembly. The first is a 1997 paper by Williams, et.al., at the University of Sheffield in the United Kingdom [6]. They have demonstrated the ability to levitate a 500 micron diameter, 10 micron thick aluminum plate using high-frequency (1-10 MHz) magnetic fields generated by a multi-pole stator coil. Induced eddy currents in the aluminum plate (rotor) cause the plate to be repelled from stator coil and levitate at a height of 5 to 35 microns above the substrate. By using three coils and phasing the applied current, they have demonstrated that they can even rotate the aluminum rotor at 1000 rpm.

Another relevant work is a paper by Rulison, et. al., at Loral Space Systems [7]. They have developed an Electrostatic Containerless Processing System (ESCAPES) which levitates 1 to 3 mm diameter specimens of metals, ceramics, and semiconductors using electrostatic fields. The system was designed to

investigate thermophysical properties of materials. The specimens are heated with a deuterium lamp to maintain their electrostatic charge. An optical feedback system using HeNe lasers and position sensitive detectors (PSD) is used to control the x, y, and z position of the specimens.

Other work by Allison and Kenall at the Pennsylvania State University [8] have developed an electrodynamic suspension system which stably levitates solid and liquid particles ranging from 1 to 100 microns diameter without the need for feedback control. Also unique to their suspension system is that six transparent electrodes are arranged as faces of a hollow cube, allowing easy access for an optical measurement. Four of the electrodes are drive by a variable-frequency two-phase AC source operating in the low audio frequency range.

There is one last levitation approach worth mentioning, but not worth pursuing. The optical laser trap as developed by Cell Robotics has been successful at moving semi-transparent materials such as blood cells in a liquid medium [9]. We have previously taken a LIGA gear to Cell Robotics and tried to move it. There were two problems. First, the gear had to be placed in liquid, and second, the trapping phenomenon did not occur because the gear was not semi-transparent.

To realize an electromagnetic levitation scheme that could be used to assemble LIGA and micro-optoelectronic components, the following issues must be resolved:

1. An analysis must be performed to understand how electrostatics, magnetics, and electromagnetics can be combined to levitate both metallic and non-metal parts.
2. Micro-coils and electrostatically charged structures need to be designed, fabricated, and tested to produce the desired electromagnetic fields.
3. An optical, inductive, or capacitance feedback sensor needs to be designed, fabricated, and tested to control the stand-off of the part.

This report describes the work performed in these areas over the course of this project.

2.0 Electromagnetic Analysis and Simulation

During this project, the Electromagnetic and Plasma Physics Analysis Department has performed extensive electromagnetic analysis and simulation to determine the attractive and repulsive forces that can be expected between the gripper and the part to be picked up. The initial analysis was based on a flat circular metal part being picked up by a circular shaped gripper (or stator) as shown in Figure 3. The part on the left has a radius d , thickness t , and density ρ_m . The stator on the right consists of a circle of radius b with a DC voltage $\pm(V/2)$ applied to each quadrant. The sign of the applied voltage is alternated between adjacent quadrants so that the part can remain neutrally charged.

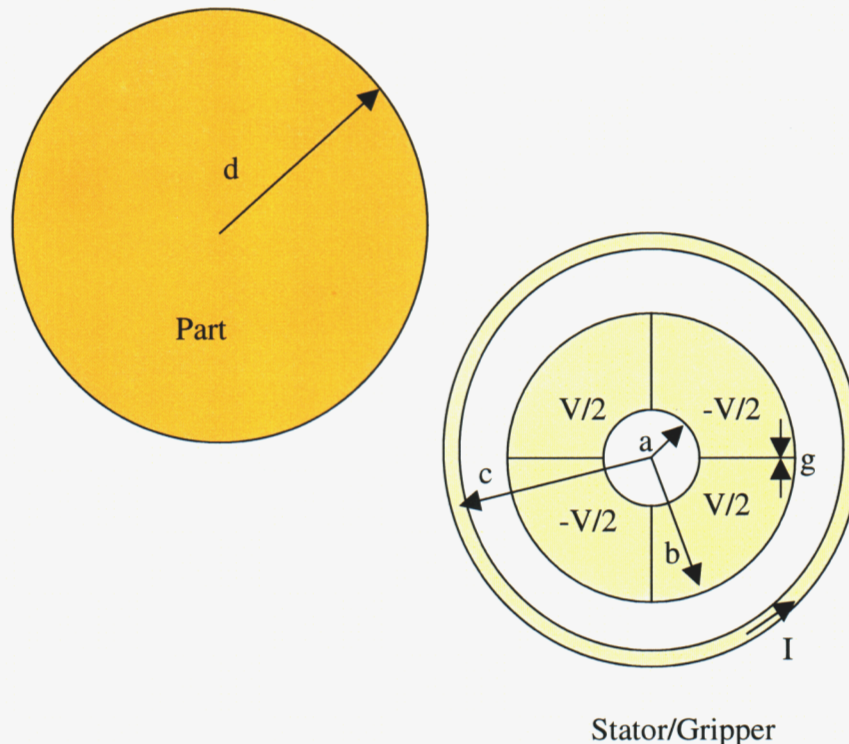


Figure 3. Geometry of circular part and stator (or gripper).

When the stator is directly over the part and the distance between the two is small compared to the diameter (i.e. neglecting fringe fields), they act as a parallel plate capacitor with capacitance

$$C = \frac{\epsilon_o \pi (b^2 - a^2)}{h} \quad (1)$$

where ϵ_o is the permittivity of free space ($\epsilon_o = \frac{1}{36\pi} \times 10^{-9} \text{ F/m}$), a is the inner radius of the stator pad, b is the outer radius of the stator pad, and h is the height of the stator above the part. The energy stored in the capacitor is given by

$$E = \frac{1}{2} C \left(\frac{V}{2} \right)^2 \quad (2)$$

where $(V/2)$ is the applied voltage to the stator. The electrostatic force of attraction between the part and the stator in the z direction perpendicular to the plates is given by

$$F_z^e = \frac{\partial E}{\partial h} = -\frac{1}{2} \epsilon_o \left(\frac{V}{2} \right)^2 \frac{\pi (b^2 - a^2)}{h^2} \quad (3)$$

In order to pick up the part, the magnitude of the electrostatic force must be larger than the magnitude of the weight of the part. The weight of the part is given by

$$F_z^w = \rho_m \pi d^2 t G \quad (4)$$

where ρ_m is the density of the part, d is the radius of the part, t is the thickness of the part, and G is gravitational acceleration ($G = 9.8 \text{ m/s}^2$). Assuming the outer radius of the stator is equal to the radius of the part ($b = d$), the inner radius is zero ($a = 0$), and using Equations (3) and (4), the part is picked up if

$$V > \sqrt{\frac{8 \rho_m t G h^2}{\epsilon_o}} \quad (5)$$

For values of $h = 10 \mu\text{m}$, $t = 100 \mu\text{m}$, and $\rho_m = 19281 \text{ kg/m}^3$ (for gold), we find that $V > 41.3$ volts. This is well within the Pachen voltage breakdown curves at standard pressure and temperature. The Pachen curves show the maximum arcing voltage for two planes to be 300 volts at $10 \mu\text{m}$, and 900 volts at $100 \mu\text{m}$. The actual geometry may give somewhat smaller breakdown voltages as a result of field enhancements near the device or stator edges. As another example, suppose we design for twice gravitational acceleration, a maximum thickness of $100 \mu\text{m}$ and a

maximum gap of $100\mu m$. The applied voltage must be greater than 585 volts in order to pick up the part. From a voltage breakdown point of view, this is tolerable if the voltage is scaled back at closer distances. However, this is on the edge of the current state of the art in drive electronics. Therefore, in our studies we have only considered parts that are $100\mu m$ in thickness and less than $50\mu m$ between the part and the gripper. In this range, the applied voltage ($V/2$) is less than 150 volts.

If the stator is above the part and the electrostatic force is counteracting gravity, it should be possible to levitate the part when the electrostatic force is equal to the gravitational force. Unfortunately, the attractive forces between the part and the surface it is on tends to hold the part down, requiring us to increase the electrostatic force to break it away from the surface. When the electrostatic force is finally increased to the point where the part is broken away from the surface, the part accelerates towards the stator with such force that it jumps to the stator and stays stuck to it. To overcome this effect, we have added a repulsive force to counteract the attractive force. This repulsive force was created with an electromagnetic field.

If an alternating current is applied to a coil surrounding the stator as shown in Figure 3, then it is possible to induce a circular Eddy current in the metal part that will cause the part to be repelled from the stator. This electromagnetic force is approximated by

$$F_z^m \approx \frac{\mu_o I^2}{2\pi D} 2\pi c \quad (6)$$

where μ_o is the permeability of free space ($\mu_o = 4\pi \times 10^{-7} H/m$), I is the rms magnitude of the current applied to the coil, and c is the radius of the coil. The distance

$$D = \frac{2\bar{h}^2 + 2\bar{h}\delta + 3\delta^2/4}{\bar{h} + \delta/2} \quad (7)$$

is a modified Sunde approximation where $\bar{h} = h + \frac{t_w}{2}$ and t_w is the thickness of the coil. The skin depth of the induced electromagnetic field is

$$\delta = \sqrt{\frac{2}{\omega \mu_o \sigma}} \quad (8)$$

where ω is the frequency of the current through the coil, and σ is the conductance of the part. Figure 4 shows the relative magnitude of the electrostatic attractive force, the electromagnetic repulsive force, and gravity as a function of distance between the part and the stator.

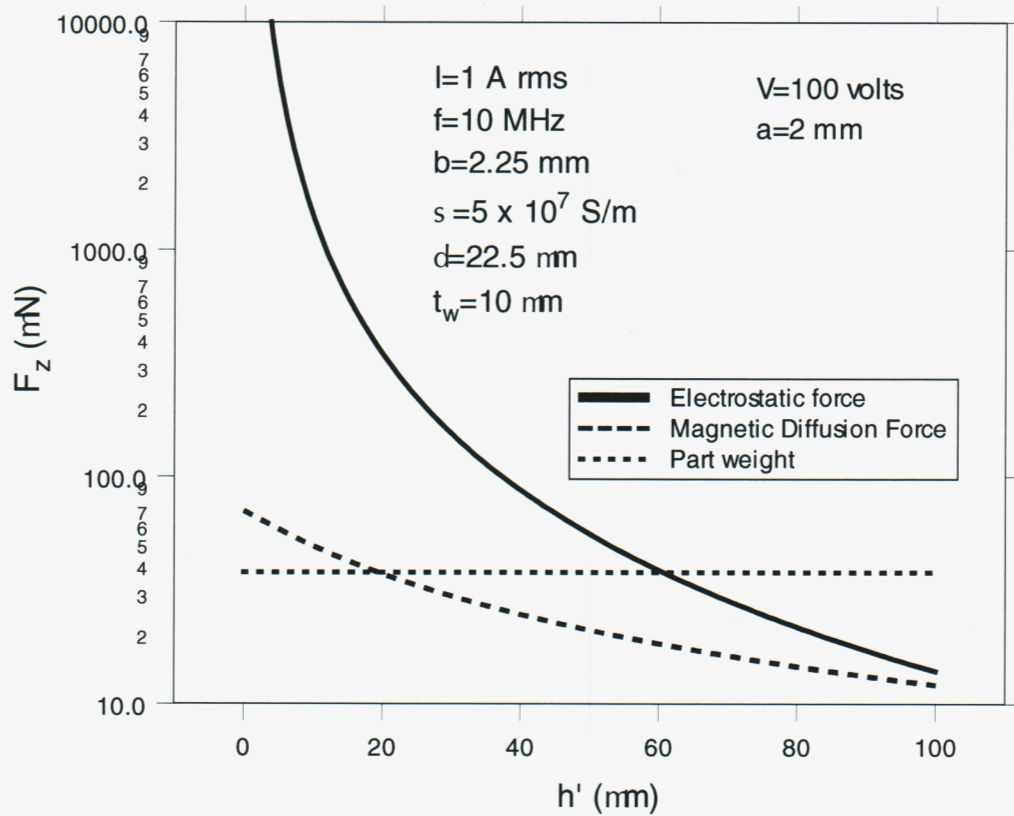


Figure 4. Electrostatic attractive force, electromagnetic repulsive force, and gravity.

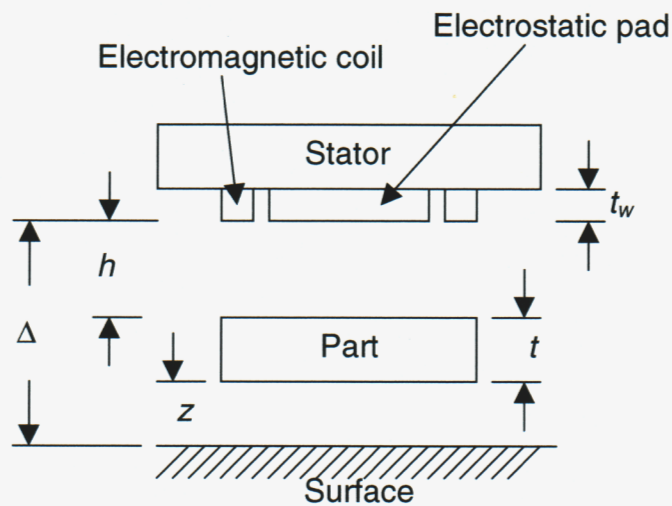


Figure 5. Side view of stator picking up part off a surface.

Next we consider the dynamics of the problem and a feedback control scheme for levitating the part. Assume the stator is above the part and the part is above a flat surface as shown in Figure 5, and that surface tension can be neglected. The equation of motion along the z axis for the disk is given by

$$m\ddot{z} = -mG + \frac{1}{2}\epsilon_o\left(\frac{V}{2}\right)^2 \frac{\pi(b^2 - a^2)}{(\Delta - t - z)^2} - \frac{\mu_o I^2 c}{D} + \frac{H d^2}{6} \left[\frac{1}{(z+t)^3} - \frac{1}{z^3} \right] \quad (9)$$

where $m = \rho_m \pi d^2 t$, $D = \frac{2(\Delta - z - t + t_w/2)^2 + 2(\Delta - z - t + t_w/2)\delta + 3\delta^2/4}{(\Delta - z - t + t_w/2) + \delta/2}$, and

H is Hamaker's constant (assumed to be $40 \times 10^{-20} J$ for gold). The first term on the right is gravity, the second term is the electrostatic force acting upwards, the third term is the electromagnetic force acting downward, and the last term is the nonretarded van der Waals force holding the part against the surface it is on (see Appendix A for the derivation).

For the moment, assume that the current running through the coil is zero, and, therefore, the electromagnetic force is zero. To levitate the part, one possible control law would be to vary the applied voltage to the electrostatic pad as a function of measured gap between the electrostatic pad and the part. This control could be written as

$$V = 2h \sqrt{\frac{2mG}{\pi\epsilon_o(b^2 - a^2)}} + K_p(h - h^*) + K_v \dot{h} \quad (10)$$

where $h = \Delta - t - z$ is the measured gap and h^* is the desired gap. The first term is a feedforward gravity compensation term, and the second and third terms are proportional and derivative control terms with user-defined gains K_p and K_v .

Figures 6 and 7 show the response of this control without and with the derivative control term. Without the derivative term, there is no damping, and the part oscillates at a frequency of 5 Hz. With the derivative term, a near critically damped response can be achieved. The difficulty in producing this more desirable response is that the measurement of the gap must be noise free since the derivative of this measurement is multiplied by a gain of $K_v = 500$.

Figure 8 shows the response of this control when a constant electromagnetic field is added. The electromagnetic field pushes the part away from the stator, causing it to never reach the desired gap $h^* = 30 \mu m$.

For dielectric parts, an electrostatic field may still be used to lift the dielectric part although it will have substantially less force than a metal part. And unfortunately, in the dielectric case it is impossible to repel the part with an electromagnetic field. Assuming the part acts as a dielectric half space, the equivalent capacitance between a stator and a dielectric part can be approximated from a series circuit as

$$C \approx \frac{(2C_o)(C_p/2)}{2C_o + C_p/2} \quad (11)$$

where each gap has capacitance

$$C_p = \frac{\epsilon_o(b^2 - a^2)\pi}{2h} \quad (12)$$

and the approximate capacitance through the dielectric when $h = 0$ is

$$C_o = \frac{\epsilon}{\pi} 2(b-a) \ln\left(\frac{8t}{g}\right) \quad (13)$$

where ϵ is the permittivity of the dielectric part and g is the gap between the electrostatic pads on the stator. The associated electrostatic force is

$$F_z = \frac{1}{2} V^2 \frac{\partial C}{\partial h} = -\frac{1}{2} V^2 \frac{2C_o^2}{(2C_o + C_p/2)^2} \epsilon_o \frac{(b^2 - a^2)\pi/2}{h^2}. \quad (14)$$

The ratio of the force for a dielectric part to the force for the conducting part is

$$\frac{F_z}{F_z^e} = \left(\frac{2C_o}{2C_o + C_p/2} \right)^2 = \frac{1}{\left[1 + \frac{\epsilon_o \pi^2 (b+a)}{\epsilon 16h \ln(8t/g)} \right]^2} \quad (15)$$

If the relative permittivity of the part is $\epsilon/\epsilon_o = 8$, $a = 0\text{ mm}$, $b = 2\text{ mm}$, $h = 10\mu\text{m}$, and

$t = g = 100\mu\text{m}$, then $\frac{F_z}{F_z^e} = 0.014$. Therefore, the attractive electrostatic force for a

dielectric part is substantially less than for a conductive part, which implies that in order to pick up the part, the gripper will have to be much closer to the dielectric part than the conductive part. Surface conduction on the part may eventually give rise to larger forces at later times.

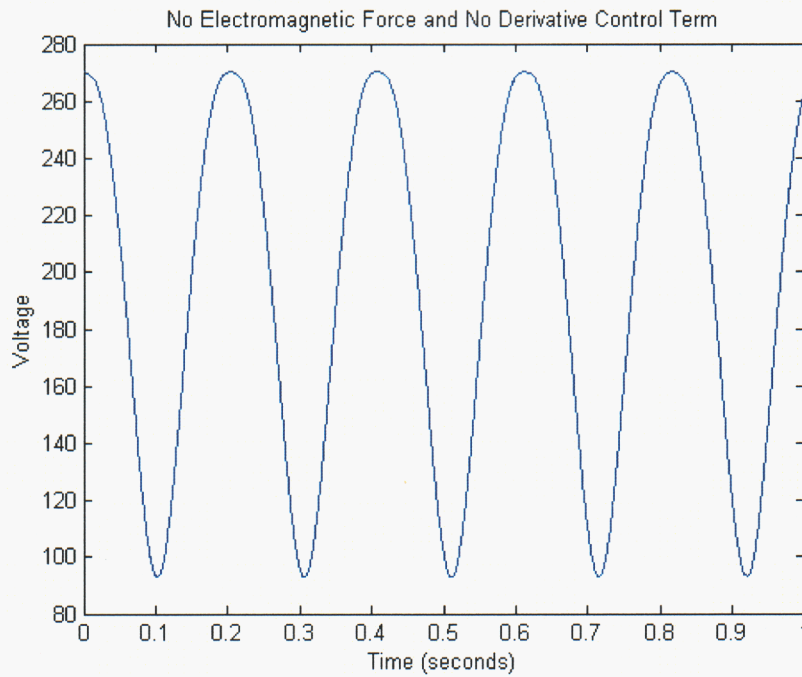
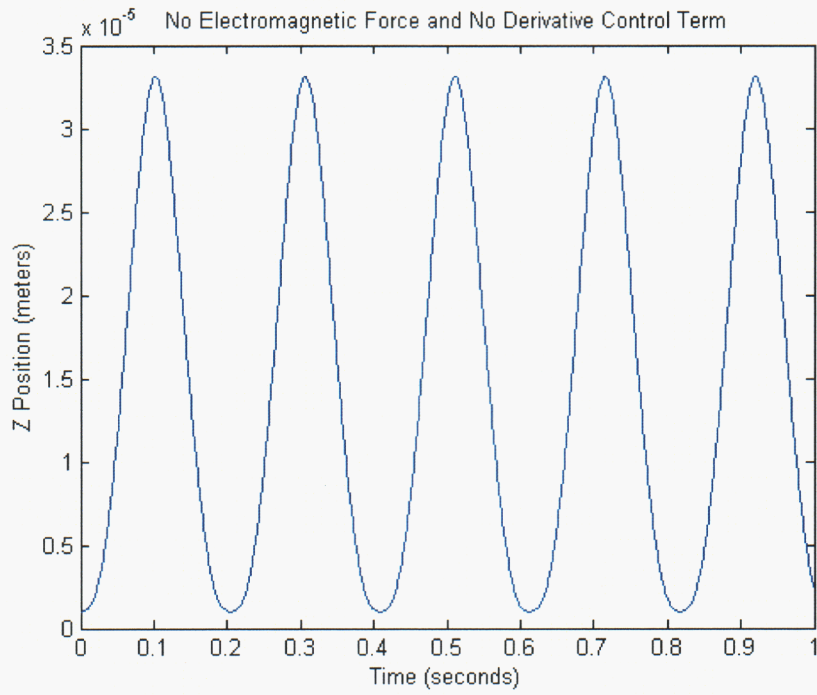


Figure 6. Response in the z direction without the derivative control term. $a = 0 \text{ mm}$, $b = 1.5 \text{ mm}$, $c = d = 2 \text{ mm}$, $\Delta = 150 \text{ }\mu\text{m}$, $t = 100 \text{ }\mu\text{m}$, $t_w = 10 \text{ }\mu\text{m}$, $h^* = 30 \text{ }\mu\text{m}$, $K_p = 10000$, and $K_v = 0$. The initial condition is $z_o = 1 \text{ }\mu\text{m}$.

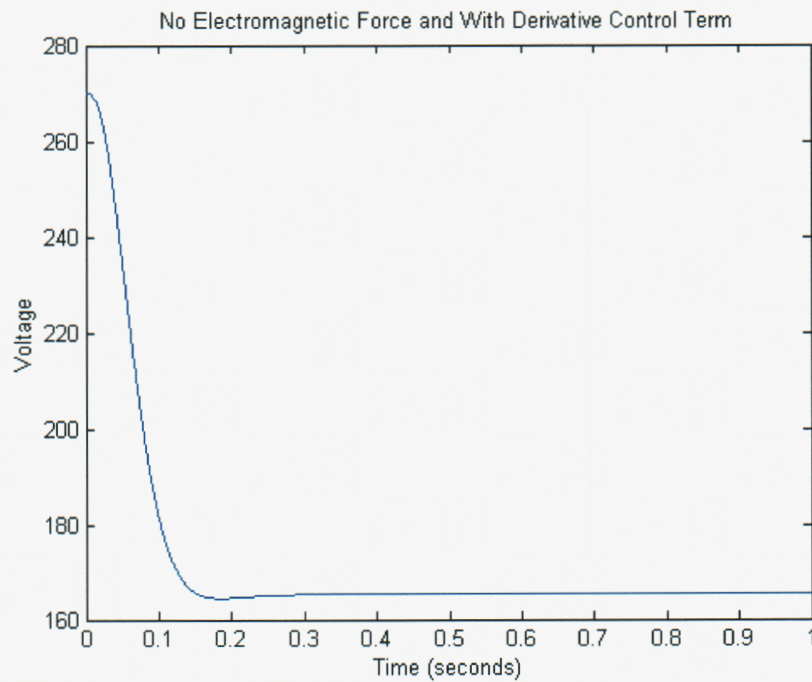
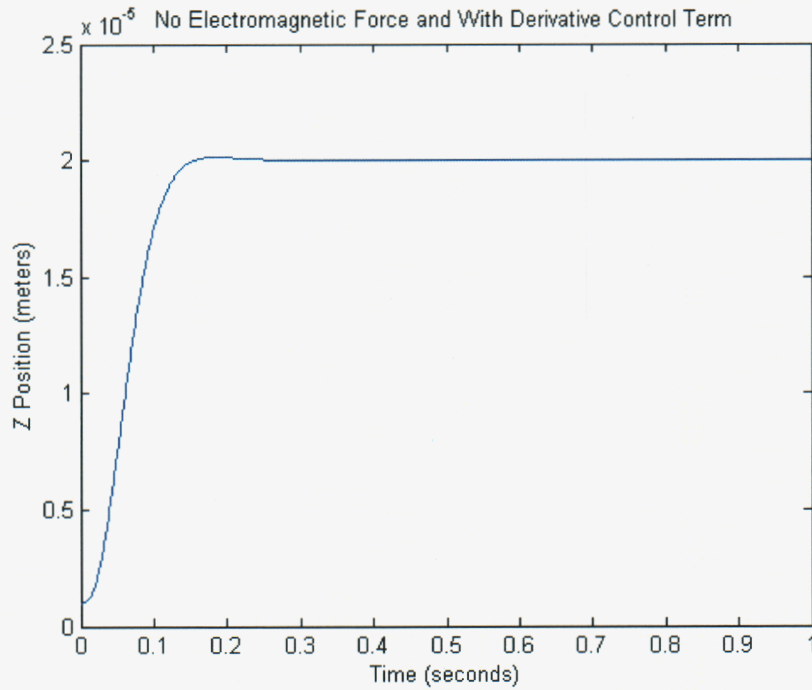


Figure 7. Response in the z direction with the derivative control term. $a = 0 \text{ mm}$, $b = 1.5 \text{ mm}$, $c = d = 2 \text{ mm}$, $\Delta = 150 \text{ }\mu\text{m}$, $t = 100 \text{ }\mu\text{m}$, $t_w = 10 \text{ }\mu\text{m}$, $h^* = 30 \text{ }\mu\text{m}$, $K_p = 10000$, and $K_v = 500$. The initial condition is $z_0 = 1 \text{ }\mu\text{m}$.

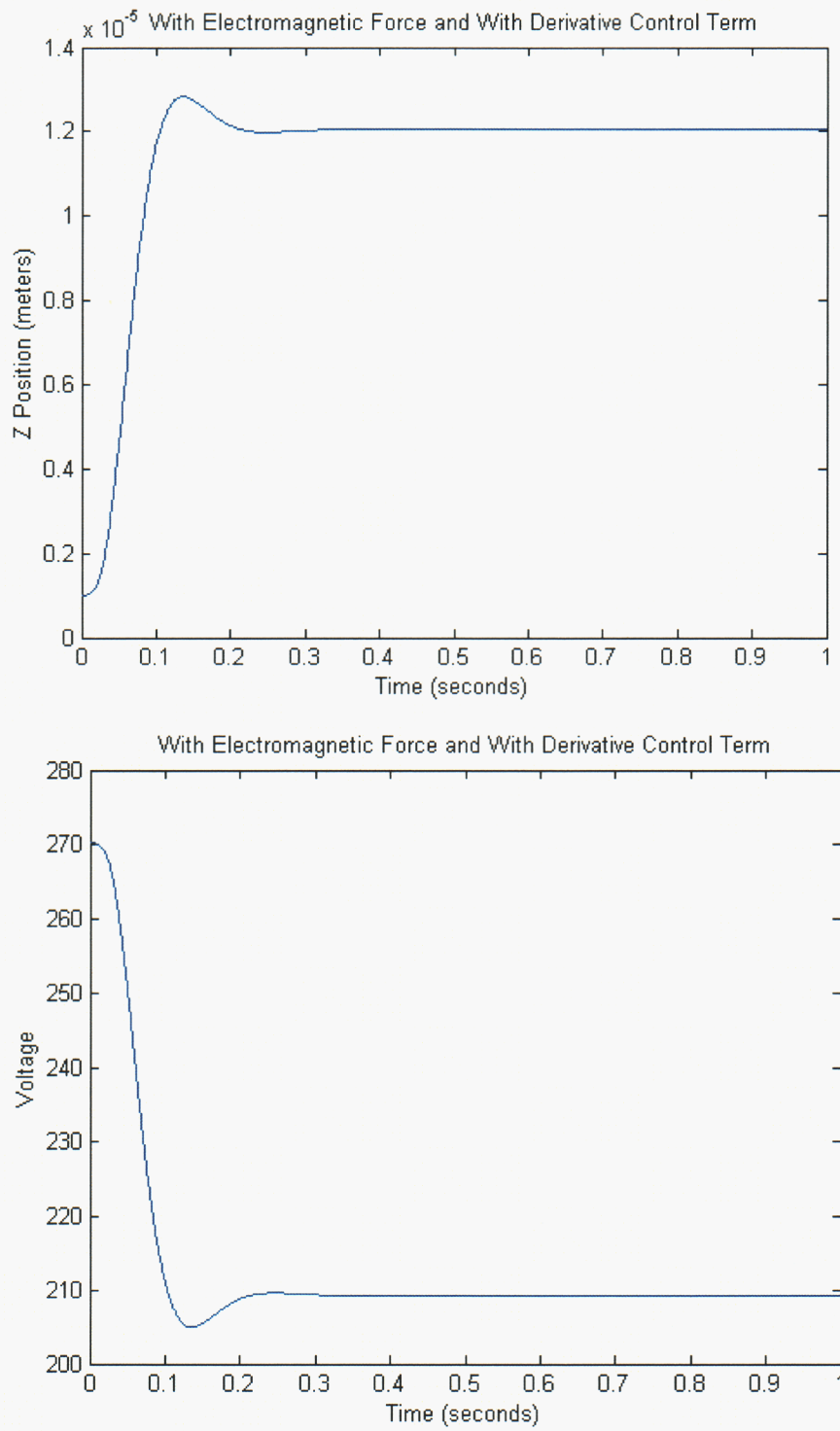


Figure 8. Response in the z direction with the electromagnetic force and the derivative control term. The parameters are $a = 0 \text{ mm}$, $b = 1.5 \text{ mm}$, $c = d = 2 \text{ mm}$, $\Delta = 150 \text{ }\mu\text{m}$, $t = 100 \text{ }\mu\text{m}$, $t_w = 10 \text{ }\mu\text{m}$, $h^* = 30 \text{ }\mu\text{m}$, $K_p = 15000$, $K_v = 500$, $I = 0.1 \text{ A}$, and $\omega = 2\pi(10^7) \text{ rad/s}$. The initial condition is $z_o = 1 \text{ }\mu\text{m}$

Several other simulations were performed to investigate the required voltages and maximum distance required to pick up a variety of non-symmetric parts. In these cases, simple formulas do not exist as they do for the parallel plate example. Instead, the Sandia-developed boundary element electrostatic code called EIGER_S was used to solve for the micro-scale forces and moments between two bodies (a gripper and the part to be grasped). This software was originally developed by Sandia National Laboratories to evaluate the electrostatic fields on various weapons components. In this project, we have expanded it's capabilities to compute the electrostatic forces and torques between multiple bodies, and to perform these calculations on a parallel computer.

A standard method of solution [10], based on the electrostatic potential, is employed to obtain the charge density on the metal surfaces. The unknown surface charge density is expanded in piecewise constant pulses over each panel, and then the electrostatic potential at the center of each panel is set to $V_i + C$ where $V_i + C$ is the potential of the i^{th} body. The constant C in the potential is determined by the constraint that the total charge in the problem is zero.

The inputs to the code are the potential voltage of each body and a mesh (panels are either triangles or squares) of each body. To compute the charge distribution, the code uses LU decomposition to solve the equation

$$\mathbf{P}\mathbf{q} = \mathbf{p} \quad (16)$$

for \mathbf{q} , a vector containing the charge density of each panel on each body. The vector \mathbf{p} is the potential of each panel on all bodies, and the matrix \mathbf{P} is a function of the integral of the inverse of the distance between each panel. The dimensions of matrix \mathbf{P} are quite large. For example, if there are 2 bodies and each body contains 1000 panels, then the dimensions of matrix \mathbf{P} are 2000×2000 . EIGER_S uses closed form solutions to evaluate the matrix \mathbf{P} for triangular and square panels. Most of the other electrostatic codes use numerical techniques to compute the matrix \mathbf{P} for both triangular and square panels as well as curved parametric surfaces. The advantage of using a closed form solution is that it does not become numerically unstable as the panels come very close together. At present, the closed form solutions do not allow us to solve for the electric fields of a curved parametric surface.

Once the charge distribution on the body panels has been calculated, the electrostatic force and moment between bodies is calculated using Coulomb's law. The force on each panel j of body i is given by

$$\vec{F}_{ij} = -\frac{q_{ij}}{4\pi\epsilon_o} \sum_{\substack{b=0 \\ b \neq i}}^n \sum_{p=0}^{m_b} q_{bp} \nabla \iint_{bq} \frac{1}{\|\vec{r}_{ij} - \vec{r}'\|} ds' \quad (17)$$

where q_{ij} is the accumulated charge on panel j of body i , \vec{r}_{ij} is the position of the center of panel j of body i , ϵ_o is the permittivity of free space, n is the number of

bodies, m_b is the number of panels in body b and the intergral is over pannel q of body b. In this expression, self-forces ($b = i, p \neq j$) are ignored since the bodies are assumed to be rigid. The total force acting on body i is the sum of the forces of the individual panels.

$$\vec{F}_i = \sum_{j=0}^{m_i} \vec{F}_{ij} \quad (18)$$

The torque acting on a body with respect to it's center of mass is the sum of the cross products of the vector distance from the center of mass of the body (\vec{r}_{cgi}) to the center of each panel and the individual forces acting on each panel.

$$\vec{M}_i = \sum_{j=0}^{m_i} (\vec{r}_{ij} - \vec{r}_{cgi}) \times \vec{F}_{ij} \quad (19)$$

Examples of simulations that were performed are illustrated in Figures 9-13.

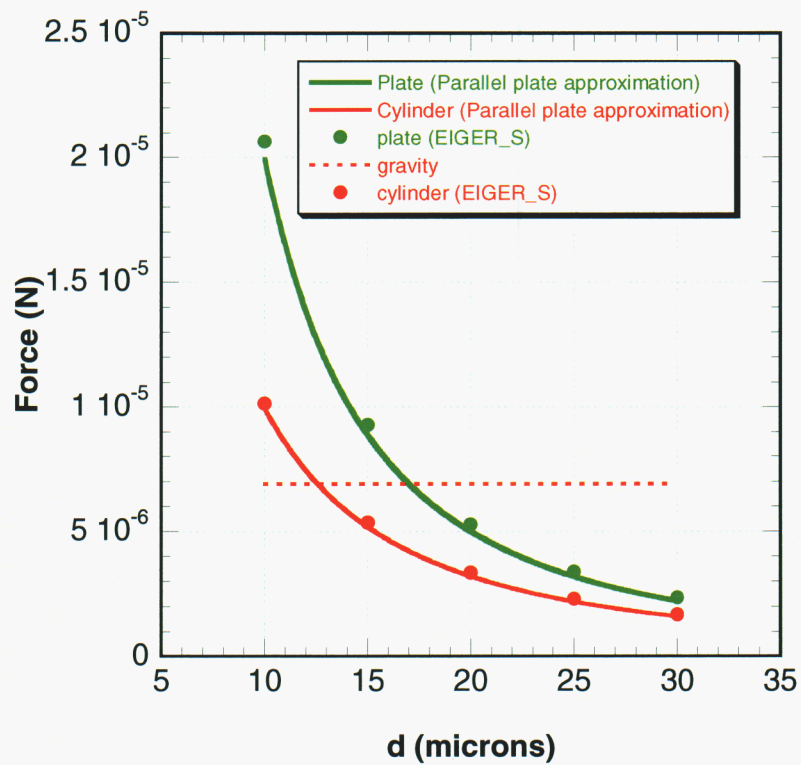
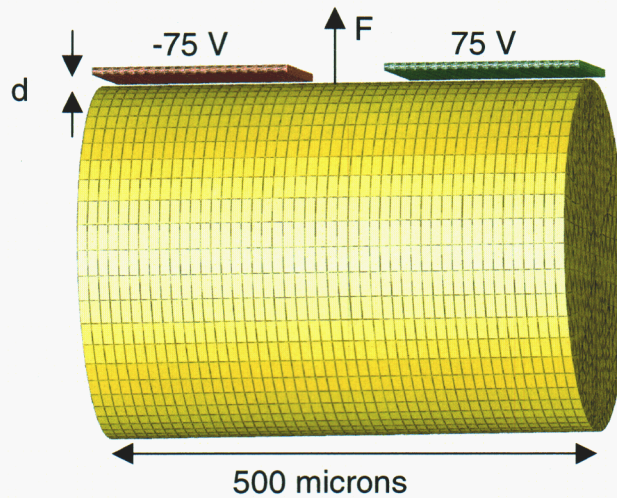


Figure 9. Simulation of electrostatic force between gripper array and cylinder shaped part.

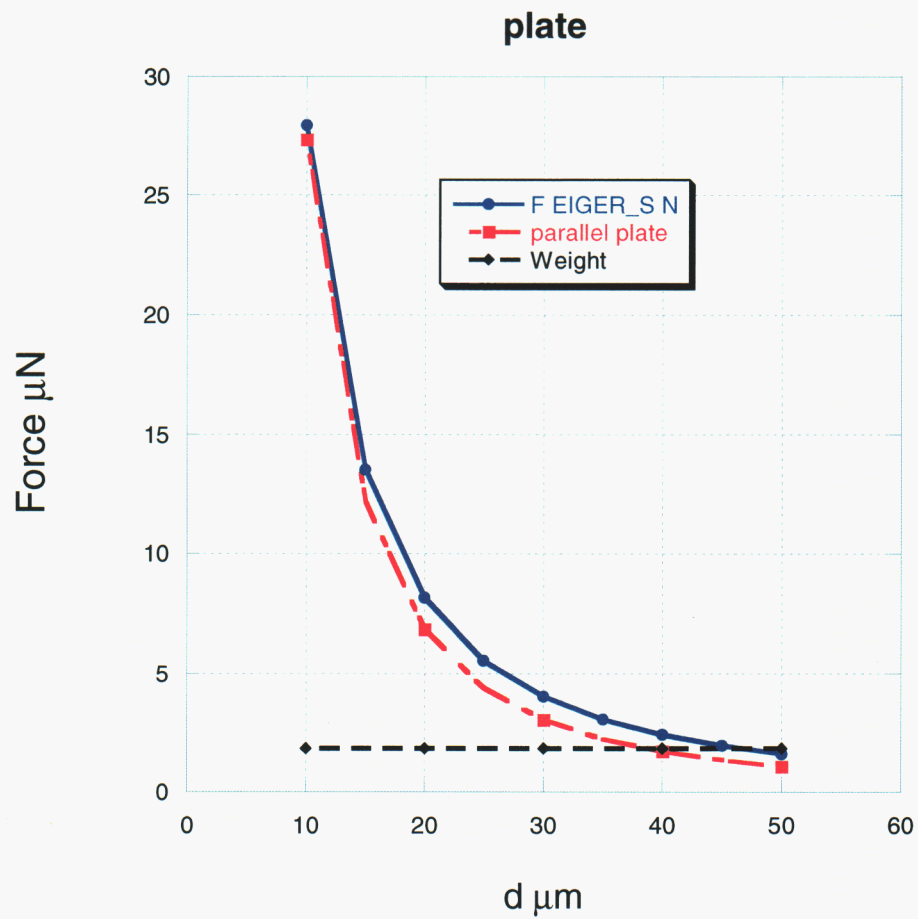
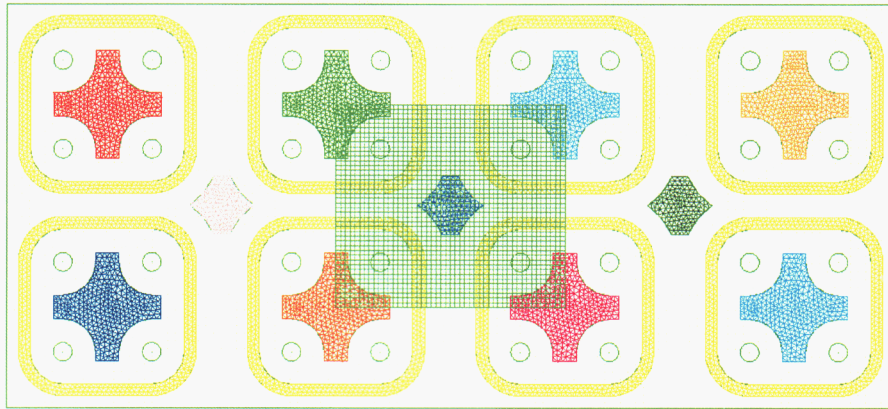


Figure 10. Simulation of electrostatic force between gripper array and a plate.

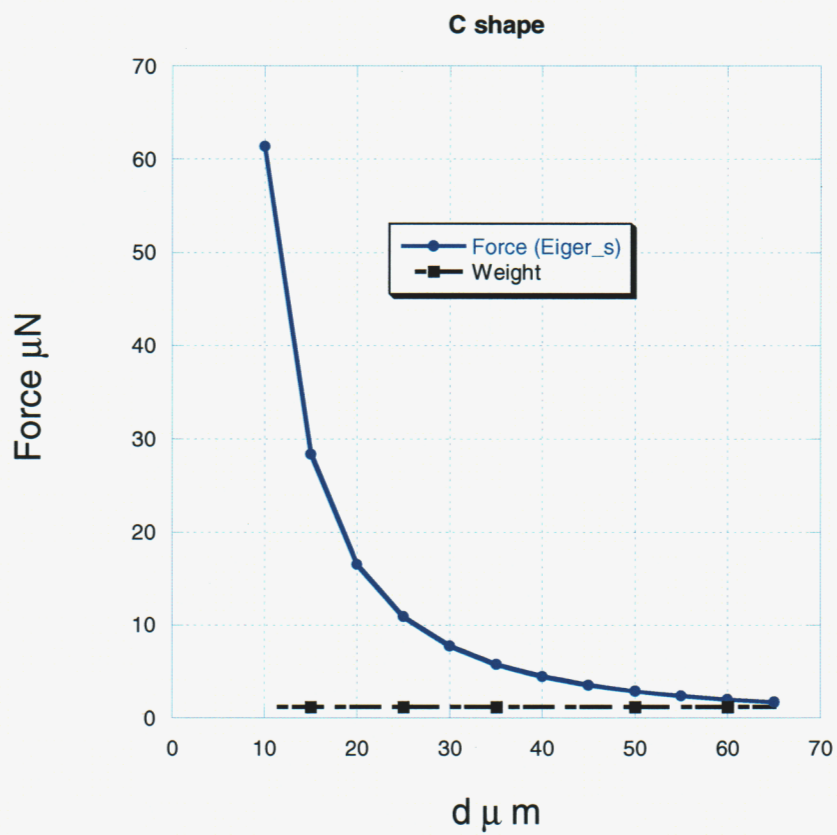
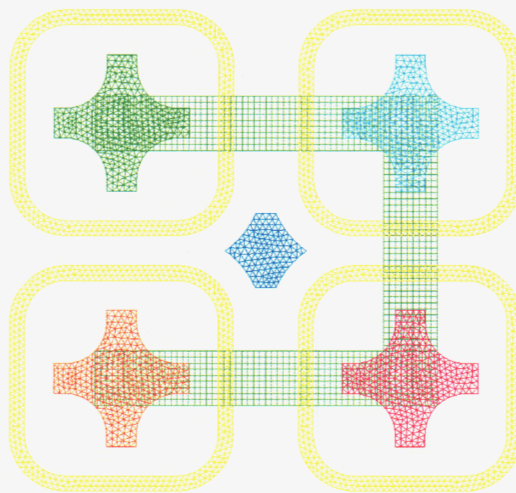


Figure 11. Simulation of electrostatic force between gripper array and a C-shaped part.

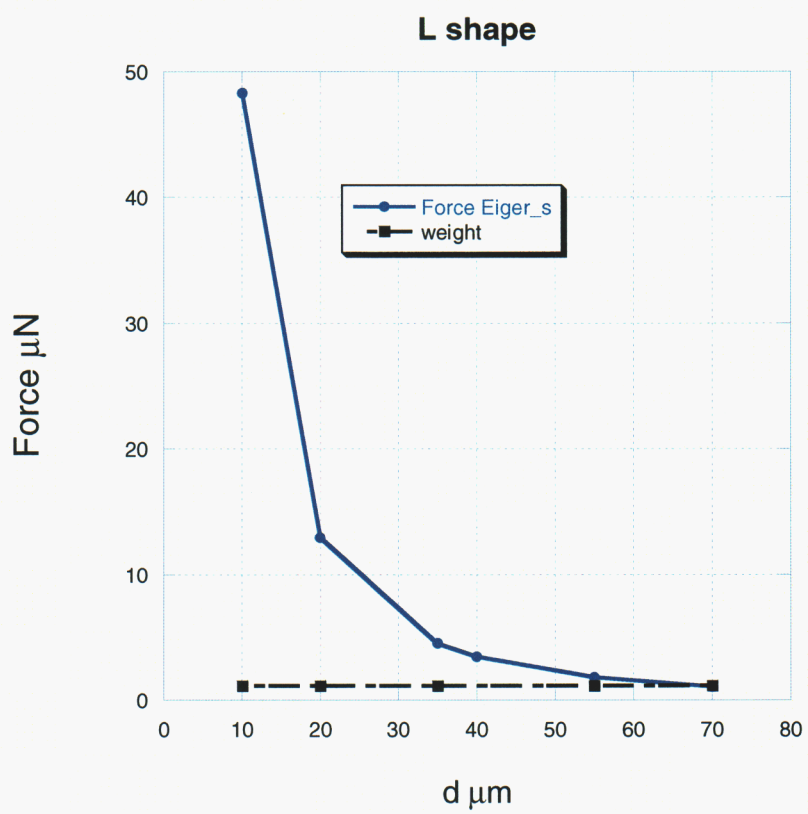
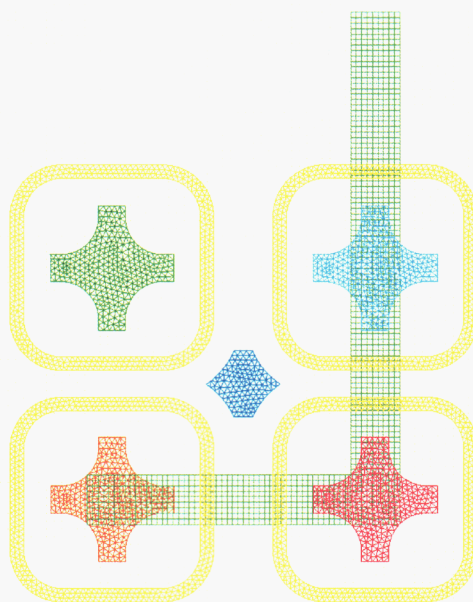


Figure 12. Simulation of electrostatic force between gripper array and an L-shaped part.

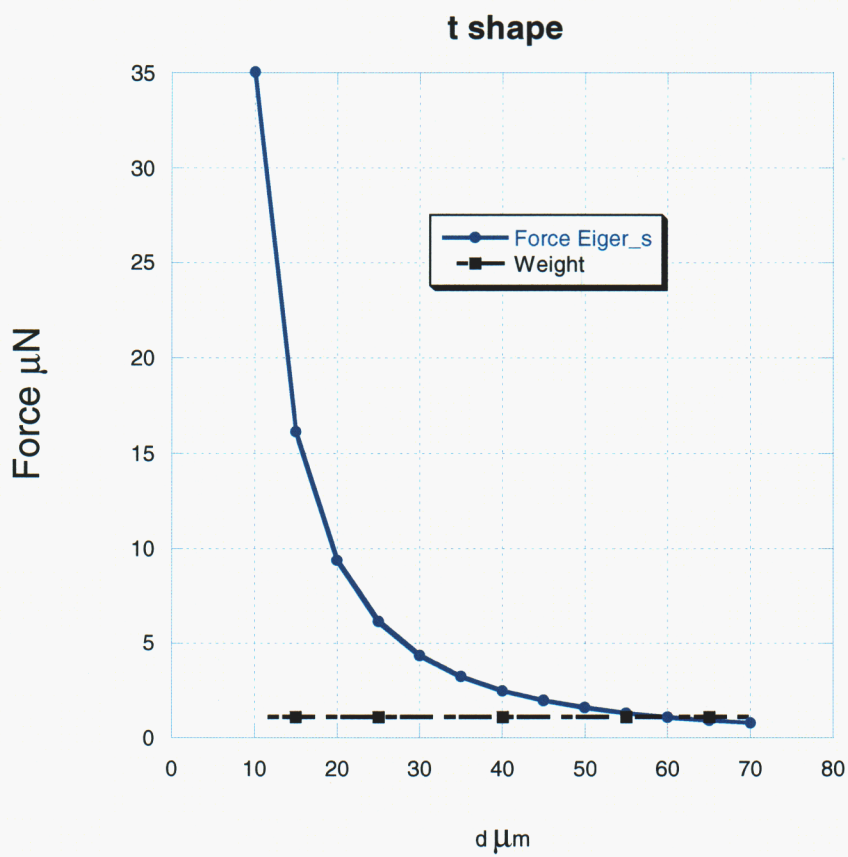
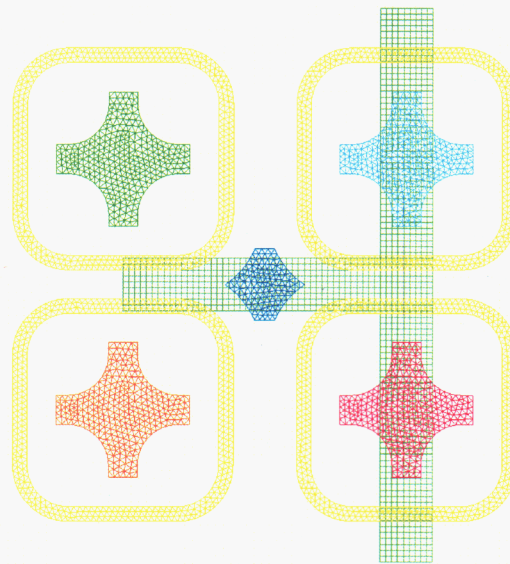


Figure 13. Simulation of electrostatic force between gripper array and a T-shaped part.

3.0 Experimental Tests

Along with the analysis and simulation discussed in the previous section, we experimentally tested several gripper designs. The next two sections discuss the test results of the electrostatic and combined electrostatic/electromagnetic grippers.

3.1 Electrostatic Gripper

Within the first six months of this project, we demonstrated that we could pick up and release a 4 mm diameter copper plate using electric fields. A 4mm diameter, 4-electrode stator from the Micro-Gyro project was mounted in our microassembly workcell in an inverted position (see Figure 14). We designed and fabricated a robot tool interface plate and a custom printed circuit board to hold the stator package and provide interface electronics to the power amplifiers and synchronous detection circuitry. We also designed and fabricated a pedestal on which to place the copper plate. Software was written to position the stator at varying heights above the copper plate while varying the voltage to the stator. A capacitance sensor on the stator was used to measure the distance between the stator and plate.

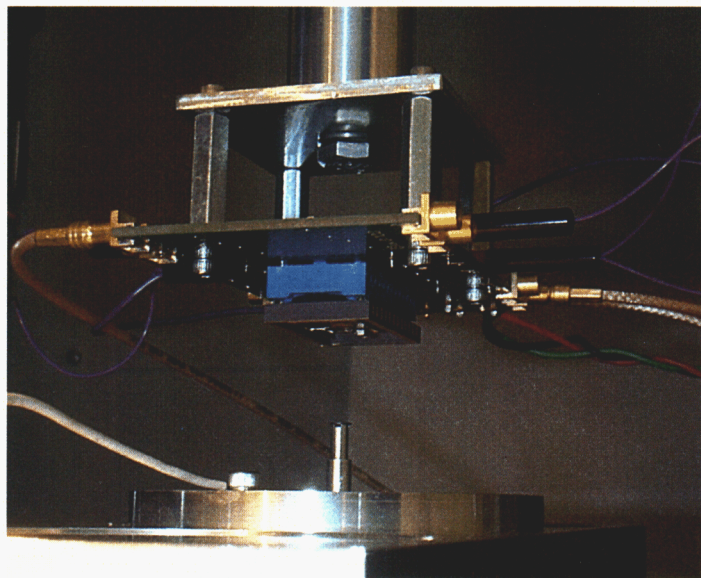


Figure 14. Picking up 4mm diameter copper plate using electrostatics.

Tests showed good correlation between theoretical analysis and experiments. Figure 15 shows how the gap between the plate and the stator depends on the voltage applied to the stator and the initial gap (at zero potential). The x-axis in the figure is the initial gap, while the y-axis is the capacitance sensor reading. The color of the curve is the voltage applied to the stator. The capacitance sensor reading represents the change in the gap when the voltage is applied. When the plate has been picked up, the capacitance sensor reading is 1. Any value less than this means that the plate has been released. From this figure, we see that the plate is picked up when stator voltage is 120V and the distance is 80 microns. However, the stator must be closer to the plate if the stator voltage is 96 V. For the stator configuration used in the experiments, the theoretical electrostatic force is given by

$$F = \frac{1}{2} \frac{\left(\frac{V}{2}\right)^2 \pi r^2}{h^2} \quad (20)$$

where V is the stator voltage, r is the radius of the stator and h is the gap. When the electrostatic force is greater than gravity, the copper plate is drawn into the stator. Comparing Figure 16 to Figure 15, we see that the experimental results closely match the theoretical expected values.

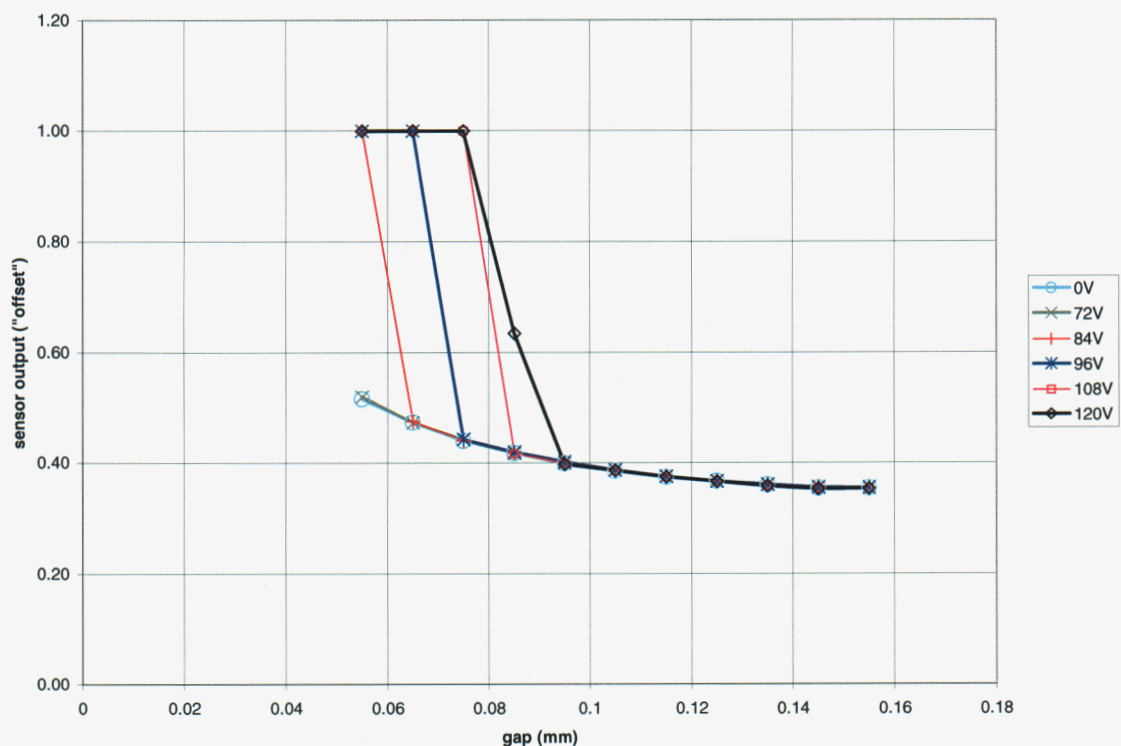


Figure 15. Capacitance sensor readings in experiment. Capacitance reading of 1 indicates plate is picked up.

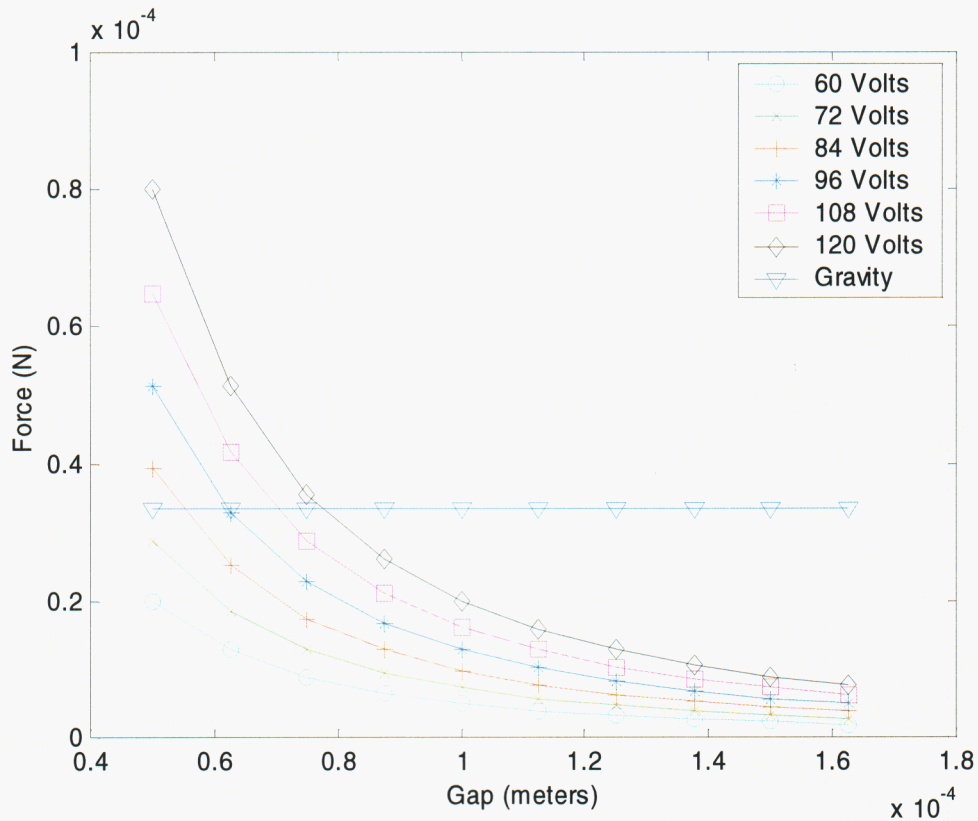


Figure 16. Theoretical electrostatic force of attraction.

Unfortunately, when the voltage on the electrostatic pads was returned to zero, the copper plate did not release 92.2% of the time. This sticking effect is believed to be caused by unmodeled residual electrostatic forces, van der Waals forces, and surface tension. The part could be jarred loose with a slight vertical acceleration along the robot's z-axis. To reduce this sticking, we designed the combined electrostatic/ electromagnetic grippers discussed in the next section.

3.2 Combined Electrostatic/Electromagnetic Gripper

During the second six months of the project, we designed three new stators that were fabricated at Sandia's Compound Semiconductor Research Laboratory. The first design is similar to the micro-Gyro stator except coils were added (see Figure 17) to create an electromagnetic repulsive force. Combining this repulsive force with the attractive electrostatic force, we had hoped to be able to levitate the 4 mm copper plate. The second and third design created an array of electrostatic pads and electromagnetic coils (see Figure 18). With this array, we planned to pick up a nonsymmetric part such as a 480 micron diameter pin.

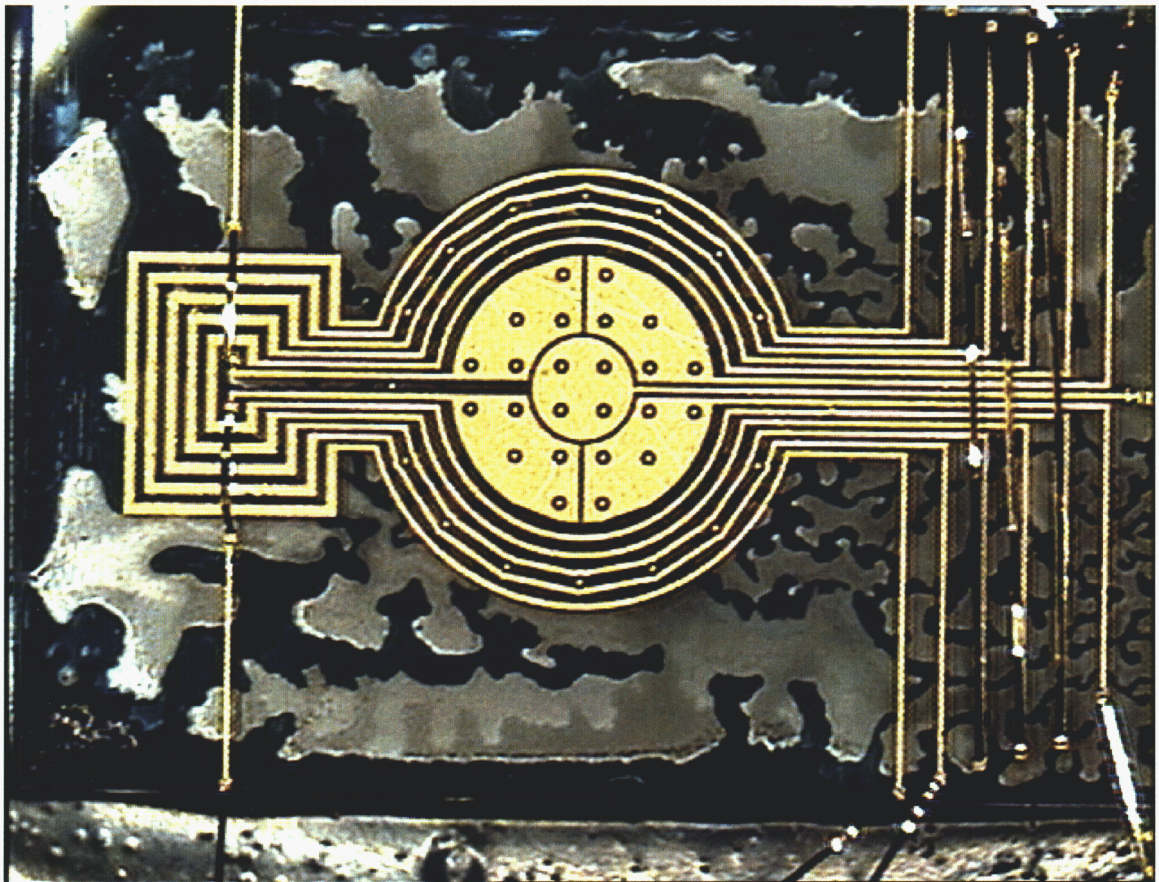
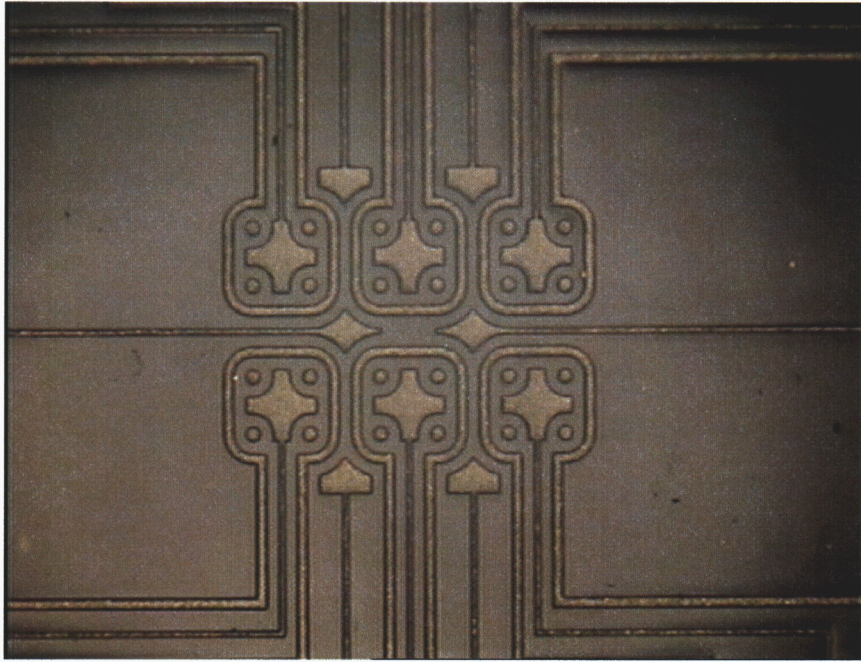
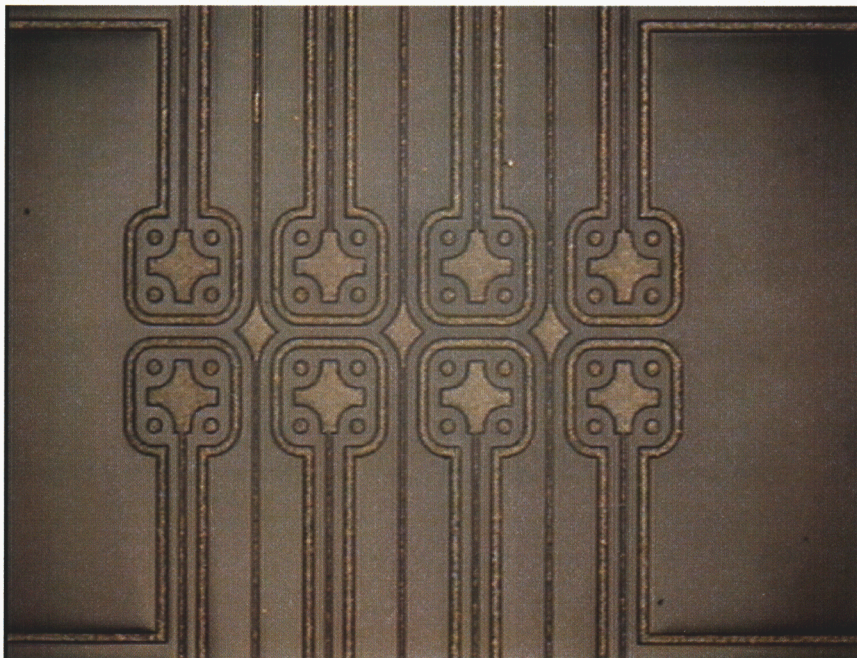


Figure 17. Combined electrostatic/electromagnetic stator. The electrostatic force of attraction is created by applying up to 150 volts to the four inner pads. The electromagnetic force of repulsion is created by applying up to 1 Amp of current to the coils surrounding the inner pads. The center circle is used to sense the stand-off distance between the part and the stator.



(a)



(b)

Figure 18. Two array designs for nonsymmetric parts. The cross-shaped pads in the middle of each coil are individually addressable electrostatic pads. The coils are individually addressable electromagnetic coils. The diamond-shaped pads are capacitive sensors.

The purpose of the first set of tests was to determine the probability of sticking for the structure in Figure 17. Since the electrostatic pads on this structure were smaller than the electrostatic gripper described in the previous section, this new probability of sticking statistic was believed to be different than the previous determined probability of sticking.

Figure 19 shows the measured probability that the copper plate would not be released when the voltage was returned to zero. A total of 500 trials were performed over several days. Each batch number consists of 10 trials. The gap between the electrostatic pads and the rotor was the maximum distance at which the structure was able to pick up the rotor. This distance varied on a daily basis from approximately 30 to 40 microns. For each trial, 150 Volts was applied to the pads for 5 seconds. If the copper plate did not immediately fall off, it was counted as being “stuck” to the gripper. The average probability of sticking was calculated as 38% from these 50 data points (as indicated by the pink line on the graph.) With such a large deviation from batch to batch and no time dependent trends, the probability of sticking appears to be quite random.

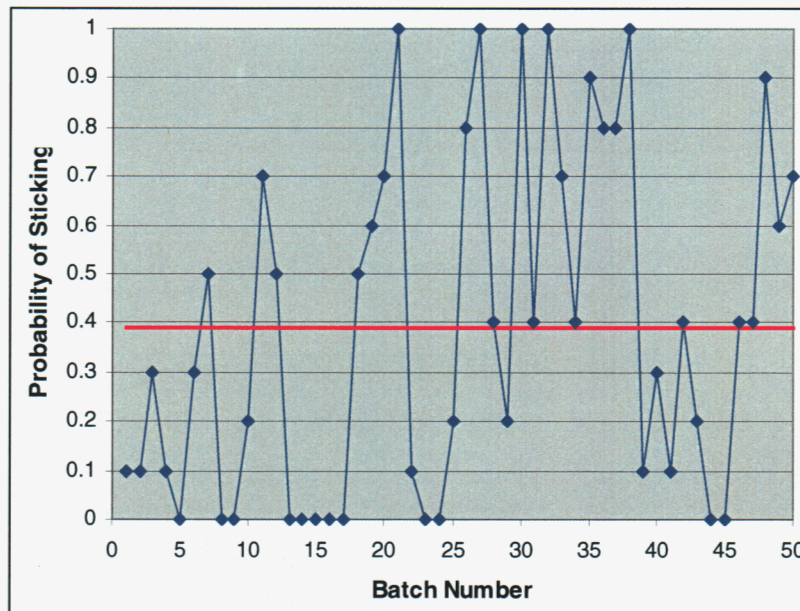


Figure 19. The measured probability that the copper plate would stick to the gripper after the voltage is returned to zero.

These tests were repeated with a 10MHz, 1A current applied to the electromagnetic coil after the electrostatic voltage was returned to zero. Similar to [6], the alternating current should create localized eddy currents on the part with a

resultant magnetic field that repels the part away from gripper. Figure 20 shows that, on a consistent basis, the copper plate either fell off immediately or fell off when the electromagnetic coils were shut-off. The electromagnetic coils were only allowed to be on for 1 second. Significant heating occurred if the coils were allowed to be on for more than a few seconds. Figure 20 shows the probability of sticking over 15 batches of 10 trials each. Due to the consistent nature of the data during this portion of the testing, it was believed that only 150 trials were necessary. In Figure 20, one can see that the use of the electromagnetic coils resulted in a probability of sticking of either 0 or 10% for every batch. The average probability of sticking was 6.0% with a standard deviation of 5%.

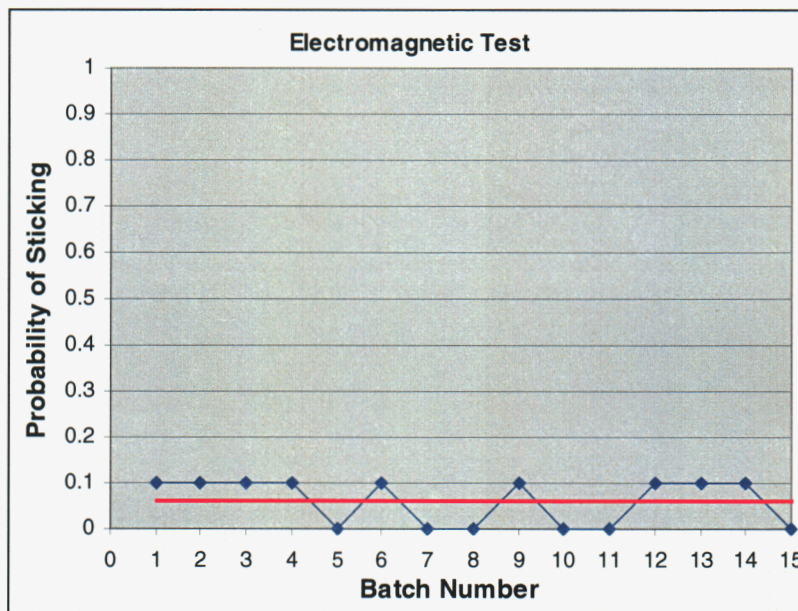


Figure 20. Probability of sticking when a 10MHz, 1A current is applied to the electromagnetic coil.

The last experiment involved connecting the electromagnetic coils to a DC voltage supply to simply heat the structure. This test was to assure that the AC current applied in the previous test wasn't just heating the structure, removing moisture, and thus, reducing surface tension effects. Since it was not certain this method should work for releasing the copper plate, the structure was heated only when the plate seemed to be stuck. Figure 21 shows that the heating of the structure was not as consistent in releasing the part as in the electromagnetic tests, and the probability of sticking varied considerably. The average probability of sticking was 15%.

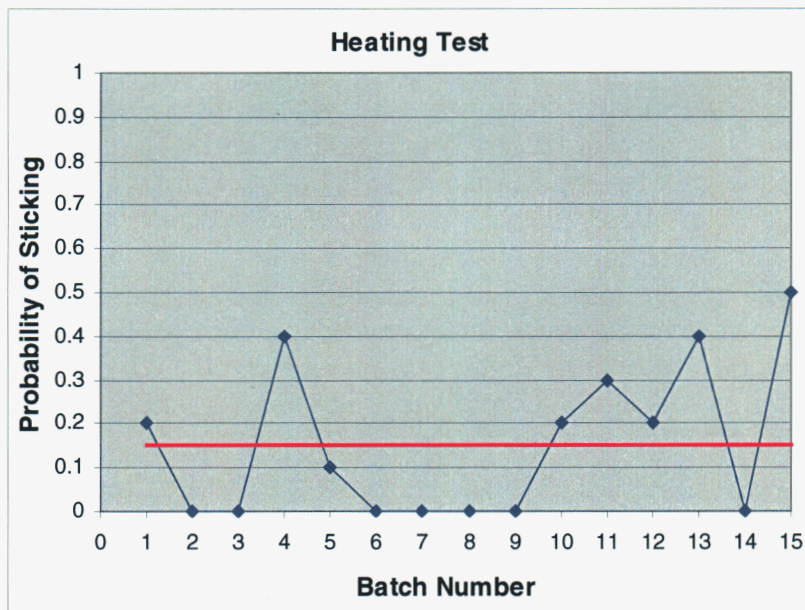


Figure 21. Probability of sticking when a 1A DC current is applied to the coil.

4.0 Conclusions and Future Directions

The experimental results show that electrostatic fields can be used to reliably pick up a LIGA part while electromagnetic fields can be used to release this part. The electromagnetic coils significantly reduce the sticking effect caused by residual electrostatic, van der Waal, and surface tension forces. The experimental results show that we can reliably pick up the 4mm diameter, 100 micron thick part when the gripper is within 80 microns of the part and a 120 volt potential is applied to the electrostatic pads. Unfortunately, there was 38 percent probability that the part will stick to the gripper when the voltage was turned off. To eliminate this sticking problem, the electromagnetic coils were added to the gripper design. Driving the coils with a 1 A, 10 MHz sine wave reduces the probability of sticking to 6 percent. Other tests show that simply heating the surface by applying a DC current through the coils reduces the probability of sticking to 15 percent.

Experimental tests and the lateral stability analysis discussed in the Appendix suggest that it is difficult to stably levitate a part with the current planar gripper designs. Any small lateral disturbance or initial displacement can cause the part to jump out of the electrostatic/electromagnetic fields. Further research is needed to design a true levitation device. However, the current design is still a possible solution for reliably picking up and releasing metal LIGA parts that are less than 1 mm³ in size.

References

1. J.T. Feddema, Ron Simon, Marc Polosky, Todd Christenson, "Ultra-Precise Assembly of Micro-Electromechanical Systems (MEMS) Components," Sand Report SAND99-0746, April 1999.
2. J.T. Feddema, R.W. Simon, "Visual Servoing and CAD Driven Microassembly," *IEEE Robotics and Automation Magazine*, pp. 18-24, December 1998.
3. J.T. Feddema, P. Xavier, R. Brown, "Assembly Planning Using Van Der Waals Force," *Journal of Micromechatronics*, Vol. 1, No. 2, pp. 139-153, 2001..
4. R. Arai, D. Ando, T. Fukuda, Y. Nonoda, T. Oota, "Micro Manipulation Based on Micro Physics - Strategy Based on Attractive Force Reduction and Stress Measurement," *Proc. of ICRA 1995*, pp. 236-241.
5. R.S. Fearing, "Survey of Sticking Effects for Micro Parts Handling," *Proc. of IROS '95*, Pittsburgh, PA, August 1995, Vol. 2, pp. 212-217.
6. C.B. Williams, C. Shearwood, P.H. Mellor, R.B. Yates, "Modelling and Testing of a Frictionless Levitated Micromotor," *Sensors and Actuators A*, 61, pp. 469-473, 1997.
7. A.J. Rulison, J.L. Watkins, and B. Zambrano, "Electrostatic Containerless Processing System," *Rev. Sci. Instrum.*, 68 (7), pp. 2856-2863, July 1997.
8. E.E. Allison, B.R.F. Kendall, "Cubic Electrodynamic Levitation Trap with Transparent Electrodes," *Rev. Sci. Instrum.*, 67(11), pp. 3806-3812, November 1996.
9. Cell Robotics International, Inc., <http://www.cellrobotics.com/cell/>.
10. Roger F. Harrington, *Field Computation by Moment Methods*, Rober E. Krieger Publishing CO., Malabar, Florida, original 1968, reprinted 1982, 1983.
11. J.N Israelachvili, "The Nature of van der Waals Forces," *Contemporary Physics*, Vol. 15, No. 2, pp. 159-177, 1974.
12. H.C. Hamaker, "The London-van der Waals Attraction Between Spherical Particles," *Physica IV*, No. 10, pp. 1058-1072, November 1937.

Intentionally Left Blank

Appendix A

Derivation of van der Waals Force

Intentionally Left Blank

Van der Waals (sometimes called London's or dispersion) force is caused by a momentary dipole moment between atoms resulting from interaction between electrons in the outermost bands rotating around the nucleus. This moment exists even for atoms which do not contain a permanent polarization. While the average distribution of electrons is uniformly distributed about the nucleus, the outermost electrons of one atom are inducing a dipole on the other atoms which in turn induce a dipole on still more atoms. An easy-to-read overview of van der Waals forces is given in [11].

The end result is that the non-retarded interaction energy between two atoms or molecules is proportional to the inverse of the sixth power of distance between the molecules.

$$E_i = -\frac{\lambda}{r^6} \quad (\text{A.1})$$

where r is the distance between the molecule centers and λ is a constant. This constant depends on temperature and material properties such as the distortion polarization, permanent dipole moment, and ionization energy.

The derivation of energy between a disk and a plane (modeled as an infinite half space) follows that of Hamaker [12]. The energy of interaction between two particles containing n atoms per cm^3 is given by

$$E = -\int_{V_1} \int_{V_2} \frac{n^2 \lambda}{r^6} dv_2 dv_1 \quad (\text{A.2})$$

where V_1 and V_2 are the volumes of the first and second particles. The energy of a particle p outside of the infinite half space is determined by integrating van der Waals energy inside the volume of the plane with respect to the coordinates of p (see Figure A.1(a)).

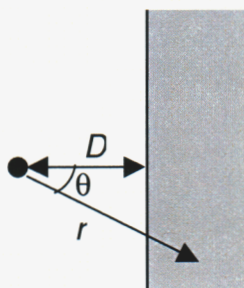
$$E_p = -\int_D \int_0^{2\pi} \int_0^{\theta_0} \frac{\lambda n}{r^6} r^2 \sin \theta d\theta d\phi dr = \frac{\pi \lambda n}{6D^3} \quad (\text{A.3})$$

where D is the distance from the particle p to the plane, and $\cos \theta_0 = \frac{D}{r}$. The total energy between the disk and the plane is determined by integrating E_p inside the disks's cylindrical volume (see Figure A.1(b)).

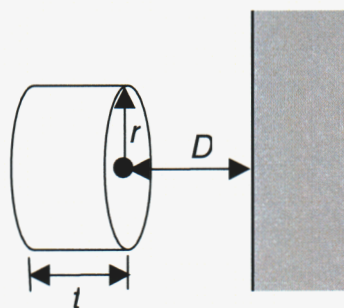
$$E = \int_D^{D+t} \int_0^{2\pi} \int_0^R E_p n dx dy dz = \frac{HR^2}{12} \left[\frac{1}{D^2} - \frac{1}{(D+t)^2} \right] \quad (\text{A.4})$$

where $H = \pi^2 n^2 \lambda$ is the Hamaker constant, t is the thickness of the disk, and R is the radius of the disk. The non-retarded van der Waals force along the z axis is given by

$$F_z = \frac{\partial E}{\partial D} = \frac{HR^2}{6} \left[\frac{1}{(D+t)^3} - \frac{1}{D^3} \right]. \quad (\text{A.5})$$



(a)



(b)

Figure A.1. Notation for computing van der Waals energy between (a) A particle p and an infinite half space, and (b) A disk and an infinite half space.

Appendix B

Larry Warne

Stability Analysis Report for Magnetically Levitated Disc

Intentionally Left Blank




Sandia National Laboratories

Operated for the U.S. Department of Energy by
Sandia Corporation

Albuquerque, New Mexico 87185-0329

date: September 20, 2001

to: John T. Feddema, MS-1003 (15211)

from: 
Larry K. Warne, MS-1152 (1642)

subject: Stability analysis report for magnetically levitated disc

Enclosed are the report and associated viewgraphs for the stability analysis that was conducted on a magnetically levitated disc. If you have any questions contact Larry Warne at 844-5683.

CC: Frank J. Peter, MS-0329 (2614)
Mark L. Kiefer, MS-1152 (1642)
William A. Johnson, MS-1152 (1642)
Roy E. Jorgenson, MS-1152 (1642)
L.K. Warne, MS-1152 (1642)

Levitation and Stability of a Conducting Disc Above a Coil of Electric Current

Larry K. Warne

September 19, 2001

Abstract

The problem of a conducting disc above a loop of electric current is analyzed to examine levitation and stability criteria. Experiments with microstructures demonstrated that oppositely directed stability coil and levitation coil currents were required (which was consistent with experiments discussed in the literature). This report constructs simple models of the structure that explain why such an arrangement leads to stability.

Acknowledgement 1 I would like to thank John Feddema and Frank Peter for including me on the design team for these structures, for many helpful discussions with regard to their operation, and for funding. I would also like to thank William Derr for many suggestions and discussions about operation of the device. Finally I would like thank Roy Jorgenson and William Johnson for many discussions on modeling of these devices.

1 INTRODUCTION

This report addresses the levitation and stability issues of a disc conductor above a current carrying coil (consisting of several current loops). Experiments were performed several years ago on these structures and were also conducted elsewhere [1], [2]. Although actual discs have finite conductivity, and thus nonzero skin depths δ and thicknesses Δ , we use a perfectly conducting thin disc model in this report.

We first look at two models for the lateral restoring forces predicted from the disc edge alone. The first, which is the simplest, consists of a perfectly conducting half plane (the edge of the disc) above a perfectly conducting plane (the stator coils), with magnetic fields induced by magnetic line charges representing the gaps between the stator coils as shown in Figure 1. This first model illustrates the criterion for stable lateral restoring forces. Because previous experiments used very thin stator coils, for which uniform current densities were present, a second model is considered that is a perfectly conducting half plane above thin uniform current density levitation and stability coils as shown in Figure 2. This second problem allows the choice of current densities on the drive coils to be made directly corresponding to the experiments. Conformal mapping is used to solve both these two dimensional models.

Oblate spheroidal coordinates is used to solve the actual three dimensional geometry of the disc above stator coils shown in Figure 3. Again uniform current density is assumed on the stator coils. Perturbation theory is used to simplify the eddy currents in the circular disc when it is displaced slightly off center from the stator center. The forces are estimated to investigate whether stable restoring forces are then experienced by the disc.

References for the physical models, conformal mapping, and oblate spheroidal coordinates are found in [3] and [4], and for the mathematics are found in [5], [6], and [7].

2 EDGE MODEL - MAGNETIC CHARGE SOURCE EXCITATION

To obtain a feel for the conditions required for lateral stability we consider a simpler problem consisting of a single edge of the disc. This edge is taken as a half plane conductor at $-\infty < x < d$ and $y = h$. Below this half plane conductor is a conducting plane. The magnetic field is induced by a two dimensional magnetic line charge $-q_m$ at the origin. Because we desire some of the magnetic flux to emerge between the disc half plane and the exciting coil ground plane we also need a magnetic line charge $+q_m/\alpha$ at $x \rightarrow -\infty$ and $0 < y < h$. First we include only the left two line charges in Figure 1a, then the third is also included.

2.1 Conformal Transformation

The conformal transformation to map the upper half of a $z_1 = x_1 + jy_1$ plane of Figure 1b into the region above the ground plane in the $z = x + jy$ plane of Figure 1b is

$$\frac{dz}{dz_1} = C_1 (z_1 + 1)^{2\pi/\pi-1} z_1^{0/\pi-1} = C_1 (1 + 1/z_1)$$

The z and z_1 plane geometries are shown in Figure 1. We are placing the point $x \rightarrow -\infty, y > h$ at $z_1 \rightarrow -\infty$. The edge of the half plane $z = d + jh$ maps to $z_1 = -1$. The point $x \rightarrow -\infty, 0 < y < h$ maps to $z_1 \rightarrow 0$. The point $x \rightarrow +\infty, y > 0$ maps to $z_1 \rightarrow +\infty$. Thus as we approach the point $z_1 = 0$ we let $z_1 = \varepsilon_1 e^{j\varphi}$, with $\varepsilon_1 \rightarrow 0$, or $dz_1/z_1 = j d\varphi$

$$dz \sim C_1 j d\varphi$$

Noting that z varies between $-R + j0$ and $-R + jh$ when φ varies between 0 and π we find that

$$C_1 = h/\pi$$

Integrating the transformation with respect to z_1 , and using the condition that $z = d + jh$ when $z_1 = -1$ to evaluate the integration constant, gives

$$z = \frac{h}{\pi} (z_1 + \ln z_1) + d + \frac{h}{\pi}$$

2.2 Magnetic Field Solution

At low frequencies, the magnetic field intensity \underline{H} obeys the equation

$$\nabla \times \underline{H} = \underline{J}$$

where \underline{J} is the electric current density. In nonmagnetic media, the magnetic flux density (or magnetic induction) \underline{B} is related to the field intensity through the constitutive relation

$$\underline{B} = \mu_0 \underline{H}$$

where $\mu_0 = 4\pi \times 10^{-7}$ H/m is the magnetic permeability of free space. The magnetic induction obeys the equation

$$\nabla \cdot \underline{B} = \rho_m$$

where ρ_m is the magnetic charge density. Although true magnetic charges have not yet been observed this is a convenient source quantity that can be used to mimic certain current source field distributions. In regions free of electric current we can determine the magnetic field intensity from the scalar potential ϕ_m by means of

$$\underline{H} = -\nabla\phi_m$$

The scalar potential satisfies

$$\nabla^2\phi_m = -\rho_m/\mu_0$$

Thus, in charge free regions it obeys Laplace's equation. Using the fact that the real and imaginary parts of an analytic function W are harmonic, we can take

$$\phi_m = \text{Re}(W)$$

where W is known as the complex potential.

We assume we have a two dimensional magnetic line charge q_m at location $\underline{\rho}'$

$$\nabla^2\phi_m = -q_m\delta(\underline{\rho} - \underline{\rho}')/\mu_0$$

In complex notation the two dimensional position vector $\underline{\rho}'$ is the location z' , which maps to location z'_1 by means of the conformal transformation. Because we intend to take the line charge q_m (as well as the line charge $-q_m/\alpha$) on the ground plane in the z_1 plane, the strengths of these line charges double as a result of images in the ground plane giving complex potential

$$W = -\frac{q_m}{\pi\mu_0} \ln(z_1 - z'_1) + \frac{q_m/\alpha}{\pi\mu_0} \ln z_1$$

The source location $z' = 0$ maps to $z'_1 = x'_1$ where

$$0 = x'_1 + \ln x'_1 + 1 + \pi d/h$$

Let us denote the value of x'_1 when $d = 0$ by x'_0

$$0 = x'_0 + \ln x'_0 + 1$$

The value is

$$x'_0 \approx 0.278464543$$

Now to first order in d we have

$$x'_1 \sim x'_0 \left(1 - \frac{\pi d/h}{1 + x'_0}\right)$$

The magnetic field can now be determined from

$$H_x = -\frac{\partial\phi_m}{\partial x} = -\text{Re}\left(\frac{dW}{dz}\right) = -\text{Re}\left(\frac{dW}{dz_1} \frac{dz_1}{dz}\right)$$

$$H_y = -\frac{\partial\phi_m}{\partial y} = -\text{Re}\left(\frac{dW}{dz} j\right) = \text{Im}\left(\frac{dW}{dz}\right) = \text{Im}\left(\frac{dW}{dz} \frac{dz_1}{dz}\right)$$

$$\frac{dW}{dz_1} = -\frac{q_m}{\pi\mu_0(z_1 - z'_1)} + \frac{q_m/\alpha}{\pi\mu_0 z_1}$$

$$\frac{dz}{dz_1} = \frac{h}{\pi}(1 + z_1)/z_1$$

2.3 Lateral Force

The lateral or x directed force can be easily found by means of the Maxwell stress tensor

$$\underline{F} = \oint_S \left[\mu_0 \underline{H} (\underline{H} \cdot \underline{n}) - \frac{1}{2} \mu_0 H^2 \underline{n} \right] dS = \oint_C \left[\mu_0 \underline{H} (\underline{H} \cdot \underline{n}) - \frac{1}{2} \mu_0 H^2 \underline{n} \right] d\ell$$

where S encloses the object on which the force is desired and \underline{n} is the unit outward normal to S . The surface S is replaced with a cross sectional contour C and the force per unit length is found in this two dimensional problem. The contour C is taken as: the bottom of the half plane $-R < x < d - \varepsilon$ and $y = h - 0$; a small circle C_ε of radius ε at the edge of the half plane; the top of the half plane $-R < x < d - \varepsilon$ and $y = h + 0$. The lateral force F_x is determined all from the tip of the half plane on the contour C_ε where we take $z = d + jh + \varepsilon e^{j\varphi}$ and $d\ell = \varepsilon d\varphi$

$$F_x = \mu_0 \int_{-\pi}^{\pi} \left[\frac{1}{2} (H_x^2 - H_y^2) \cos \varphi + H_x H_y \sin \varphi \right] \varepsilon d\varphi$$

Letting $z = d + jh + \varepsilon e^{j\varphi}$, with $-\pi < \varphi < \pi$, and $z_1 = -1 + \eta_1$, with $\varepsilon, |\eta_1| \ll 1$, the transformation can be expanded as

$$\frac{\pi}{h} \varepsilon e^{j\varphi} = \eta_1 + \ln(1 - \eta_1) \sim -\frac{1}{2} \eta_1^2$$

or

$$\eta_1 \sim \sqrt{2\pi\varepsilon/h} e^{j(\varphi+\pi)/2}$$

so that $0 < \arg(\eta_1) < \pi$. The derivative of the potential is therefore

$$\begin{aligned} \frac{dW}{dz} &= -\frac{q_m}{\mu_0 h} \left(\frac{z_1}{z_1 - z'_1} - 1/\alpha \right) \frac{1}{(1 + z_1)} \sim -\frac{q_m}{\mu_0 h} \left(\frac{1}{1 + x'_1} - 1/\alpha \right) \frac{1}{\eta_1} \\ &\sim -\frac{q_m}{\mu_0 \sqrt{2\pi h \varepsilon}} \left(\frac{1}{1 + x'_1} - 1/\alpha \right) e^{-j(\varphi+\pi)/2} \end{aligned}$$

The fields are therefore

$$\begin{aligned} H_x &\sim -\frac{q_m}{\mu_0 \sqrt{2\pi h \varepsilon}} \left(\frac{1}{1 + x'_1} - 1/\alpha \right) \sin(\varphi/2) \\ H_y &\sim \frac{q_m}{\mu_0 \sqrt{2\pi h \varepsilon}} \left(\frac{1}{1 + x'_1} - 1/\alpha \right) \cos(\varphi/2) \end{aligned}$$

The force per unit length is thus

$$F_x = -\frac{q_m^2}{2\mu_0 h} \left(\frac{1}{1 + x'_1} - 1/\alpha \right)^2$$

2.3.1 small d expansion

The small displacement expansion of the force is

$$F_x \sim -\frac{q_m^2}{2\mu_0 h} \left(\frac{1}{1+x'_0} - 1/\alpha \right)^2 - \frac{q_m^2}{\mu_0 h} \left(\frac{1}{1+x'_0} - 1/\alpha \right) \frac{x'_0 \pi d/h}{(1+x'_0)^3}$$

2.4 Lateral Stability

The total force on the two dimensional model for the disc consists of the above force for the positive x edge minus the above formula with $d \rightarrow -d$ for the negative x edge times a length dimension ℓ_x

$$\begin{aligned} F_x^{tot} &= -\frac{q_m^2 \ell_x}{2\mu_0 h} \left[\left\{ \frac{1}{1+x'_1(d)} - 1/\alpha \right\}^2 - \left\{ \frac{1}{1+x'_1(-d)} - 1/\alpha \right\}^2 \right] \\ &= -\frac{q_m^2 \ell_x}{2\mu_0 h} \left[\frac{1}{1+x'_1(d)} - \frac{1}{1+x'_1(-d)} \right] \left[\frac{1}{1+x'_1(d)} + \frac{1}{1+x'_1(-d)} - 2/\alpha \right] \end{aligned}$$

Using the small d expansion gives

$$F_x^{tot} \sim -\frac{2q_m^2 \ell_x}{\mu_0 h} \left(\frac{1}{1+x'_0} - 1/\alpha \right) \frac{x'_0 \pi d/h}{(1+x'_0)^3}$$

A restoring force is obtained (that leads to lateral stability) if $F_x^{tot} < 0$ for $d > 0$. Thus we must have

$$\alpha > 1 + x'_0 \approx 1.278464543$$

or

$$\alpha < 0$$

for stability.

2.5 Choice of Length Parameter

The length parameter ℓ_x can be chosen from the global geometry of the disc problem. Suppose the disc has radius a . Then because the lateral edge force is radially directed F_ρ there will be a $\cos \varphi$ factor applied around the disc to determine the x directed component. Furthermore because the radial force is proportional to the small displacement d , and because this displacement is proportional to $\cos \varphi$ around the disc we take

$$F_x^{disc} \approx \int_{-\pi}^{\pi} F_\rho \cos^2 \varphi a d\varphi \approx F_x^{tot}$$

where

$$\ell_x \approx \int_{-\pi/2}^{\pi/2} \cos^2 \varphi a d\varphi = \pi a/2$$

2.6 Current Density On Stator Electrodes

We now look at the meaning of the choices of q_m and α in terms of current density on the stator electrodes. The current densities are taken positive when in the positive z direction.

The levitation electrode is taken to be $-\infty < x < 0$ and $y = 0$. The asymptotic form of the magnetic field between the half plane and the stator electrode is the same as the current density

$$K_\ell = -H_x(x, 0) \sim \frac{q_m/\alpha}{\mu_0 h}$$

Thus for a positive levitation current density we want $q_m/\alpha > 0$.

The stability electrode is taken to be $0 < x < \infty$ and $y = 0$. However, because the field is decaying in this region, the stability current density is decaying also. Suppose we take the width of the stability electrode to be b_s . Then we could take the value of the field at $x = b_s/2$ as a rough estimate for the stability electrode current density

$$K_s \approx -H_x(b_s/2, 0)$$

Because we are only interested in an approximate value we take $d = 0$ in the transformation

$$\pi b_s / (2h) - 1 \approx x_{1s} + \ln x_{1s}$$

where $x_{1s} > x'_0$. Suppose we take $b_s \approx 50 \mu\text{m}$ and $h \approx 20 \mu\text{m}$, which gives $x_{1s} \approx 2.15787$. Then

$$K_s \approx -\frac{q_m}{\mu_0 h} \left(\frac{x_{1s}}{x_{1s} - x'_0} - 1/\alpha \right) \frac{1}{(1 + x_{1s})}$$

The ratio of stability to levitation current densities is thus

$$K_s/K_\ell \approx \left(1 - \frac{\alpha}{1 - x'_0/x_{1s}} \right) \frac{1}{(1 + x_{1s})}$$

Thus the two currents have the same sign for

$$\alpha < 1 - x'_0/x_{1s} \approx 0.871$$

otherwise they have opposite signs. The region of stability $\alpha > 1 + x'_0 \approx 1.2785$ thus has opposite signs for the stability and levitation currents. The region of stability $\alpha < 0$ has the same sign for the two currents. The magnitude of the current ratio near the stability threshold $\alpha \approx 1.2785$ is smaller $K_s/K_\ell \approx -0.468/(1 + x_{1s})$ than the magnitude at the other threshold of stability $\alpha \approx 0$ where $K_s/K_\ell \approx 1/(1 + x_{1s})$.

2.7 Current Density Near Edge of Half Plane

The total current density on the half plane is

$$K_z = H_x(x, h - 0) - H_x(x, h + 0)$$

Far from the edge of the half plane, this current has the opposite direction from that of the current on the levitation electrode beneath (the resulting repulsion leads to a vertical levitation force on the half plane). Near the edge $x = d - \varepsilon$, however this current density becomes

$$K_z \sim \frac{2q_m}{\mu_0 \sqrt{2\pi h \varepsilon}} \left(\frac{1}{1 + x'_1} - 1/\alpha \right)$$

and for $d = 0$

$$K_z \sim \frac{2q_m}{\mu_0 \sqrt{2\pi h \epsilon}} \left(\frac{1}{1+x'_0} - 1/\alpha \right)$$

In the case where $q_m > 0$ and $\alpha > 0$ we see that the sign of the current near the half plane edge follows the opposite sign of the lateral force. A restoring (stable) force means that the current near the edge is positively directed (the same direction as the levitation current density below the half plane). This current is oppositely directed from the stability electrode current in this case. The repulsive force (between oppositely directed currents) with respect to the stability electrode is thus thought to be responsible for the stability in this region; without the positively directed sign of the current near the edge we would not expect a restoring force. Figure 1c illustrates the current sign reversal near the edge of the half plane. This sign reversal (which is also a sign reversal in the tangential magnetic field on the half plane) is not surprising from the point of view of the magnetic field emanating from the source below the edge of the half plane.

If we take $q_m < 0$ and $\alpha < 0$ the half plane current is always negatively directed (the opposite of the levitation electrode current and opposite of the stability electrode current) and repulsive forces apply to both electrodes.

2.8 Vertical Force

The energy per unit length is

$$\begin{aligned} W &= \int_S \frac{1}{2} \mu_0 H^2 dS = \frac{1}{2} \mu_0 \int_S \nabla \phi_m \cdot \nabla \phi_m dS = \frac{1}{2} \mu_0 \int_S [\nabla \cdot (\phi_m \nabla \phi_m) - \phi_m \nabla^2 \phi_m] dS \\ &= \frac{1}{2} \mu_0 \oint_C \phi_m \frac{\partial \phi_m}{\partial n} d\ell \end{aligned}$$

where here \underline{n} points out of the free space region. We have taken the region S to be indented just above the magnetic charge at the origin; thus the Laplace operator vanishes in S . Note that the normal derivative vanishes on the perfectly conducting surfaces. Thus

$$W = \frac{1}{2} \mu_0 \int_0^\pi \phi_m \frac{\partial \phi_m}{\partial \rho} \rho d\varphi - \frac{1}{2} \mu_0 \int_0^h \phi_m \frac{\partial \phi_m}{\partial x} dy + \frac{1}{2} q_m \phi_m(\rho_0)$$

where ρ is large in the first integral, $-x$ is large in the second integral, and $\rho_0 \rightarrow 0$ in the final integral. Required asymptotic forms of the transformation and potential are (in this subsection the energy is computed for $d = 0$):

Near the origin

$$\rho_0 e^{j\varphi} \sim \frac{h}{\pi} (1 + 1/x'_1) (z_1 - x'_1)$$

$$\phi_m(\rho_0) \sim -\frac{q_m}{\pi \mu_0} \ln \left(\frac{\pi \rho_0 / h}{1 + 1/x'_1} \right) + \frac{q_m / \alpha}{\pi \mu_0} \ln x'_1$$

$$\phi_m(\rho_0) \sim -\frac{q_m}{\pi \mu_0} \ln \left(\frac{\pi \rho_0 / h}{1 + 1/x'_0} \right) + \frac{q_m / \alpha}{\pi \mu_0} \ln x'_0, \quad d = 0$$

For $-x$ large

$$-\frac{\partial \phi_m}{\partial x} \sim -\frac{q_m / \alpha}{\mu_0 h}$$

$$e^{\pi(x-d)/h-1} \sim x_1$$

$$\phi_m \sim -\frac{q_m}{\pi\mu_0} \ln x'_1 + \frac{q_m/\alpha}{\pi\mu_0} \{\pi(d-x)/h+1\}$$

$$\phi_m \sim -\frac{q_m}{\pi\mu_0} \ln x'_0 + \frac{q_m/\alpha}{\pi\mu_0} \{\pi(-x)/h+1\}, d=0$$

For ρ large

$$-\frac{\partial\phi_m}{\partial\rho} \sim \frac{q_m}{\pi\mu_0\rho} (1-1/\alpha)$$

$$\pi(z-d)/h-1-\ln(\pi z/h) \sim z_1$$

$$\phi_m \sim -\frac{q_m}{\pi\mu_0} (1-1/\alpha) \ln(\pi\rho/h)$$

The energy is thus

$$W \sim \frac{q_m^2}{2\pi\mu_0} \ln(\pi\rho/h) (1-1/\alpha)^2 + \frac{q_m^2/\alpha}{2\pi\mu_0} [(1-\pi x/h)/\alpha - \ln x'_0] + \frac{q_m^2}{2\pi\mu_0} \left[\frac{1}{\alpha} \ln x'_0 - \ln \left(\frac{\pi\rho_0/h}{1+1/x'_0} \right) \right]$$

The vertical force per unit length is thus

$$\begin{aligned} F_y &= -\frac{\partial W}{\partial h} = \frac{q_m^2}{2\mu_0 h} (1-1/\alpha)^2 - \frac{xq_m^2/\alpha^2}{2\mu_0 h^2} - \frac{q_m^2}{2\pi\mu_0} \frac{1}{h} \\ &= \frac{q_m^2}{2\mu_0 h} \left[\left\{ (1-1/\alpha)^2 - 1 \right\} / \pi - x/(\alpha^2 h) \right] \end{aligned}$$

The total vertical force is twice this quantity (for both edges) times a length parameter ℓ_y

$$F_y^{tot} \approx 2\ell_y F_y = \frac{q_m^2 \ell_y}{\alpha^2 \mu_0 h} [(1-2\alpha)/\pi + b_\ell/h] \sim \ell_y \mu_0 K_\ell^2 [(1-2\alpha)h/\pi + b_\ell]$$

where we have taken $-x = b_\ell$ the total width of the levitation electrodes and $K_\ell \sim q_m/(\alpha\mu_0 h)$ has been used. Here we can take the length parameter to be the mean length of the levitation electrodes

$$\ell_y \approx 2\pi(a - b_\ell/2)$$

Notice that the first term in the force formula is negative for $\alpha > 1/2$, and thus reduces the vertical force (this includes the region of negative stability current). When $\alpha < 1/2$ the first term adds to the levitation force.

2.9 Second Magnetic Line Charge

A slightly better representation of a stability electrode can be introduced by placing another magnetic line charge $-q_m(1 - 1/\alpha)$ at $x = b_s$,

$$W = -\frac{q_m}{\pi\mu_0} \ln(z_1 - z'_1) + \frac{q_m/\alpha}{\pi\mu_0} \ln z_1 + \frac{q_m}{\pi\mu_0} (1 - 1/\alpha) \ln(z_1 - z''_1)$$

This line charge thus absorbs all magnetic flux leaving from between the half plane and conducting plane at a finite distance from the half plane edge. The position of the line charge is taken to map to $z''_1 = x''_1$ where

$$x''_1 + \ln x''_1 + 1 + \frac{\pi}{h} (d - b_s) = 0$$

We denote by x''_0 the value of x''_1 when $d = 0$

$$x''_0 + \ln x''_0 = \pi b_s/h - 1$$

Now for $b_s \approx 50 \mu\text{m}$ and $h \approx 20 \mu\text{m}$ we have $x''_0 \approx 5.2044646$. To first order in d we have

$$x''_1 \sim x''_0 \left(1 - \frac{\pi d/h}{1 + x''_0} \right)$$

The field components are found from the derivative

$$\frac{dW}{dz} = -\frac{q_m}{\mu_0 h} \left\{ \frac{z_1}{z_1 - x'_1} - 1/\alpha - (1 - 1/\alpha) \frac{z_1}{z_1 - x''_1} \right\} \frac{1}{(1 + z_1)}$$

The lateral force per unit length is thus

$$F_x = -\frac{q_m^2}{2\mu_0 h} \left(\frac{1}{1 + x'_1} - 1/\alpha - \frac{1 - 1/\alpha}{1 + x''_1} \right)^2$$

2.9.1 small d expansion

now for small d we find

$$F_x \sim -\frac{q_m^2}{2\mu_0 h} \left(\frac{1}{1 + x'_0} - 1/\alpha - \frac{1 - 1/\alpha}{1 + x''_0} \right)^2 - \frac{q_m^2}{\mu_0 h} \left(\frac{1}{1 + x'_0} - 1/\alpha - \frac{1 - 1/\alpha}{1 + x''_0} \right) \left\{ \frac{x'_0}{(1 + x'_0)^3} - \frac{(1 - 1/\alpha)x''_0}{(1 + x''_0)^3} \right\} \pi d/h$$

2.9.2 lateral stability

The total lateral force in the small d limit is thus

$$F_x^{tot} \sim -\frac{2q_m^2 \ell_x}{\mu_0 h} \left(\frac{1}{1 + x'_0} - 1/\alpha - \frac{1 - 1/\alpha}{1 + x''_0} \right) \left\{ \frac{x'_0}{(1 + x'_0)^3} - \frac{(1 - 1/\alpha)x''_0}{(1 + x''_0)^3} \right\} \pi d/h$$

Inserting the geometrical parameters gives

$$F_x^{tot} \sim -\frac{2q_m^2 \ell_x}{\mu_0 h} \left\{ \frac{1}{1.2785} - 1/\alpha - \frac{(1 - 1/\alpha)}{6.2045} \right\} \{0.13326 - 0.02179(1 - 1/\alpha)\} \pi d/h$$

The previous result ignored the final term in both sets of braces. The zero of the first brace now occurs at $\alpha \approx 1.35074$ instead of 1.2785. (The final brace can now be negative for $0 > \alpha > -0.19548$ creating an unstable region.)

2.9.3 stability current density

If we again take the midpoint location $x = b/2$ and $y = 0$ as an estimate of the stability current density for ($d = 0$) with $x_0'' > x_{1s}$

$$K_s \sim -\frac{q_m}{\mu_0 h} \left(\frac{1}{1 - x_0'/x_{1s}} - 1/\alpha + \frac{1 - 1/\alpha}{x_0''/x_{1s} - 1} \right) \frac{1}{(1 + x_{1s})}$$

The levitation current density is the same value as before and thus

$$K_s/K_\ell \sim \left(1 - \frac{\alpha}{1 - x_0'/x_{1s}} - \frac{\alpha - 1}{x_0''/x_{1s} - 1} \right) \frac{1}{(1 + x_{1s})}$$

where for the previous dimensions $1 - x_0'/x_{1s} \approx 0.870954$ and $x_0''/x_{1s} - 1 \approx 1.411853$. At the stability threshold $\alpha \approx 1.35074$ this gives $K_s/K_\ell \approx -0.80/(1 + x_{1s})$. At the stability threshold $\alpha \approx -0.19548$ this gives $K_s/K_\ell \approx 2.1/(1 + x_{1s})$.

2.9.4 current density near edge of half plane

The current density near the edge of the half plane in this case ($d = 0$) is

$$K_z \sim \frac{2q_m}{\mu_0 \sqrt{2\pi h \epsilon}} \left(\frac{1}{1 + x_0'} - 1/\alpha - \frac{1 - 1/\alpha}{1 + x_0''} \right)$$

Thus again for $q_m > 0$ and $\alpha > 0$ the sign of the current near the half plane edge is positive when there is a restoring force.

This case with the additional line source adds nothing qualitative new to the results even though it better represents the finite nature of the stability electrode. The next section introduces a better representation of the current density on the electrodes when the electrode conductors are electrically thin (uniform current density).

3 EDGE MODEL- UNIFORM DENSITY CURRENT STRIP EXCITATION

The stator electrodes that were used in the original experiments on the levitated disc were much thinner than the skin depth at the excitation frequency $\Delta_s \ll \delta = \sqrt{2/(\omega\mu_0\sigma)}$, where ω is the radian frequency of the applied current and σ is the electrical conductivity of the metal. Furthermore the width of the stator electrodes b were much less than the electrical impedance length parameter $b \ll Z_s/(\omega\mu_0) = 1/(\omega\mu_0\sigma\Delta_s/2)$. Under these conditions the current density in the stator electrodes was uniform across the width and thickness. A more accurate model is therefore to treat the stator electrodes as uniform current density strips. This approach is used in the present section (half plane edge treatment above strips) and in the next section (three dimensional disc above circular strips).

It is convenient here to consider a half plane along the positive x axis. The mapping uses the transformation

$$z_1 = \sqrt{z}$$

where $0 < \arg(z) < 2\pi$ and $0 < \arg(z_1) < \pi$ as shown in Figures 2a and 2b. Because we are considering electric current excitation instead of magnetic line charges here it is appropriate to take the magnetic scalar potential (outside of the electric current) to be

$$\phi_m = \text{Im}(W)$$

Consider first an electric line current source I at

$$z' = -d - jh$$

This maps to

$$z'_1 = \sqrt{-d - jh} = j\sqrt{d + jh}$$

where the principal branch of the square root $-\pi < \arg(d + jh) \leq \pi$ is used in the final form. We can take the complex potential to be

$$\begin{aligned} W &= -\frac{I}{2\pi} [\ln(z_1 - z'_1) - \ln(z_1 - z'_1^*)] = -\frac{I}{2\pi} \left[\ln(\sqrt{z} - \sqrt{z'}) - \ln(\sqrt{z} - \sqrt{z'}^*) \right] \\ &= -\frac{I}{2\pi} \left[\ln(\sqrt{z} - j\sqrt{d + jh}) - \ln(\sqrt{z} + j\sqrt{d - jh}) \right] \end{aligned}$$

where the square roots of $d \pm jh$ in this expression are taken as the principal branches, but we remember that $0 < \arg(z) < 2\pi$. The logarithms are taken as the principal branch $-\pi < \arg(\sqrt{z} \mp j\sqrt{d \pm jh}) \leq \pi$.

3.1 Strip Current Drive

Now we replace current I by K and integrate with respect to z' or d to construct strip current solutions. Thus we can write

$$\begin{aligned} W_{st} &= -\frac{K}{2\pi} \int_d^{d+b} \left[\ln(\sqrt{z} - j\sqrt{u + jh}) - \ln(\sqrt{z} + j\sqrt{u - jh}) \right] du \\ &= -\frac{K}{2\pi} \int_{d+jh}^{d+b+jh} \ln(\sqrt{z} - j\sqrt{u}) du + \frac{K}{2\pi} \int_{d-jh}^{d+b-jh} \ln(\sqrt{z} + j\sqrt{u}) du \\ &= -\frac{K}{\pi} \int_{\sqrt{d+jh}}^{\sqrt{d+b+jh}} \ln(\sqrt{z} - ju) du + \frac{K}{\pi} \int_{\sqrt{d-jh}}^{\sqrt{d+b-jh}} \ln(\sqrt{z} + ju) u du \\ &= -\frac{K}{\pi} \int_{\sqrt{d+jh}}^{\sqrt{d+b+jh}} [\ln(\sqrt{z} - ju) - \ln(\sqrt{z} + ju)] u du \end{aligned}$$

Using the identity

$$\begin{aligned} \int \ln(v \pm ju) u du &= -\frac{1}{2} (v \pm ju)^2 \left[\ln(v \pm ju) - \frac{1}{2} \right] + v(v \pm ju) [\ln(v \pm ju) - 1] \\ &= (v \pm ju) \left\{ -\frac{1}{2} (v \pm ju) \left[\ln(v \pm ju) - \frac{1}{2} \right] + v [\ln(v \pm ju) - 1] \right\} \\ &= (v \pm ju) \left\{ \frac{1}{2} (v \mp ju) \left[\ln(v \pm ju) - \frac{1}{2} \right] - v/2 \right\} \end{aligned}$$

we find the strip current complex potential

$$\begin{aligned}
W_{st} = & -\frac{K}{\pi} \left[\left(\sqrt{z} - j\sqrt{d+b+jh} \right) \left\{ \frac{1}{2} \left(\sqrt{z} + j\sqrt{d+b+jh} \right) \left[\ln \left(\sqrt{z} - j\sqrt{d+b+jh} \right) - \frac{1}{2} \right] - \sqrt{z}/2 \right\} \right. \\
& - \left(\sqrt{z} + j\sqrt{d+b-jh} \right) \left\{ \frac{1}{2} \left(\sqrt{z} - j\sqrt{d+b-jh} \right) \left[\ln \left(\sqrt{z} + j\sqrt{d+b-jh} \right) - \frac{1}{2} \right] - \sqrt{z}/2 \right\} \Big] \\
& + \frac{K}{\pi} \left[\left(\sqrt{z} - j\sqrt{d+jh} \right) \left\{ \frac{1}{2} \left(\sqrt{z} + j\sqrt{d+jh} \right) \left[\ln \left(\sqrt{z} - j\sqrt{d+jh} \right) - \frac{1}{2} \right] - \sqrt{z}/2 \right\} \right. \\
& - \left(\sqrt{z} + j\sqrt{d-jh} \right) \left\{ \frac{1}{2} \left(\sqrt{z} - j\sqrt{d-jh} \right) \left[\ln \left(\sqrt{z} + j\sqrt{d-jh} \right) - \frac{1}{2} \right] - \sqrt{z}/2 \right\} \Big] \\
= & -\frac{K}{\pi} \left[\frac{1}{2} (z+d+b+jh) \left\{ \ln \left(\sqrt{z} - j\sqrt{d+b+jh} \right) - \frac{1}{2} \right\} - \left(\sqrt{z} - j\sqrt{d+b+jh} \right) \sqrt{z}/2 \right. \\
& - \frac{1}{2} (z+d+b-jh) \left\{ \ln \left(\sqrt{z} + j\sqrt{d+b-jh} \right) - \frac{1}{2} \right\} + \left(\sqrt{z} + j\sqrt{d+b-jh} \right) \sqrt{z}/2 \Big] \\
& + \frac{K}{\pi} \left[\frac{1}{2} (z+d+jh) \left\{ \ln \left(\sqrt{z} - j\sqrt{d+jh} \right) - \frac{1}{2} \right\} - \left(\sqrt{z} - j\sqrt{d+jh} \right) \sqrt{z}/2 \right. \\
& - \frac{1}{2} (z+d-jh) \left\{ \ln \left(\sqrt{z} + j\sqrt{d-jh} \right) - \frac{1}{2} \right\} + \left(\sqrt{z} + j\sqrt{d-jh} \right) \sqrt{z}/2 \Big]
\end{aligned}$$

or

$$\begin{aligned}
W_{st} = & \frac{K}{2\pi} \left[(z+d+b-jh) \ln \left(\sqrt{z} + j\sqrt{d+b-jh} \right) - (z+d+b+jh) \ln \left(\sqrt{z} - j\sqrt{d+b+jh} \right) \right. \\
& - j \left(\sqrt{d+b+jh} + \sqrt{d+b-jh} \right) \sqrt{z} \\
& - (z+d-jh) \ln \left(\sqrt{z} + j\sqrt{d-jh} \right) + (z+d+jh) \ln \left(\sqrt{z} - j\sqrt{d+jh} \right) + j \left(\sqrt{d+jh} + \sqrt{d-jh} \right) \sqrt{z} \Big]
\end{aligned}$$

3.2 Levitation and Stability Currents

Now we take the stability strip to have uniform current density K_s over $-b_s - d < x < -d$ and $y = -jh$ ($b \rightarrow b_s$). The levitation strip has uniform current density K_ℓ over $-d < x < b_\ell - d$ and $y = -jh$ ($b \rightarrow -b_\ell$). The geometry is shown in Figure 2c. The total complex potential for both stability and levitation currents is thus (note that for $b = -b_\ell < 0$ we must reverse the sign of K_ℓ , because the integration limits should have been reversed since the incremental length along the strip should be positive)

$$\begin{aligned}
W_{tot} = & \frac{K_s}{2\pi} \left[(z+d+b_s-jh) \ln \left(\sqrt{z} + j\sqrt{d+b_s-jh} \right) - (z+d+b_s+jh) \ln \left(\sqrt{z} - j\sqrt{d+b_s+jh} \right) \right. \\
& - j \left(\sqrt{d+b_s+jh} + \sqrt{d+b_s-jh} \right) \sqrt{z}
\end{aligned}$$

$$-(z+d-jh)\ln(\sqrt{z}+j\sqrt{d-jh})+(z+d+jh)\ln(\sqrt{z}-j\sqrt{d+jh})+j(\sqrt{d+jh}+\sqrt{d-jh})\sqrt{z}]$$

$$-\frac{K_\ell}{2\pi}\left[(z+d-b_\ell-jh)\ln(\sqrt{z}+j\sqrt{d-b_\ell-jh})-(z+d-b_\ell+jh)\ln(\sqrt{z}-j\sqrt{d-b_\ell+jh})\right.$$

$$\left.-j(\sqrt{d-b_\ell+jh}+\sqrt{d-b_\ell-jh})\sqrt{z}\right]$$

$$-(z+d-jh)\ln(\sqrt{z}+j\sqrt{d-jh})+(z+d+jh)\ln(\sqrt{z}-j\sqrt{d+jh})+j(\sqrt{d+jh}+\sqrt{d-jh})\sqrt{z}]$$

Using the fact that

$$H_x = -\frac{\partial\phi_m}{\partial x} = -\text{Im}\left(\frac{dW}{dz}\right)$$

$$H_y = -\frac{\partial\phi_m}{\partial y} = -\text{Im}\left(\frac{dW}{dz}j\right) = -\text{Re}\left(\frac{dW}{dz}\right)$$

we need the quantity dW_{tot}/dz

$$\frac{dW_{tot}}{dz} = \frac{K_s}{2\pi}\left[\ln\left(\frac{\sqrt{z}+j\sqrt{d+b_s-jh}}{\sqrt{z}-j\sqrt{d+b_s+jh}}\right) + \frac{(z+d+b_s-jh)}{\sqrt{z}+j\sqrt{d+b_s-jh}}\frac{1}{2\sqrt{z}} - \frac{(z+d+b_s-jh)}{\sqrt{z}-j\sqrt{d+b_s-jh}}\frac{1}{2\sqrt{z}}\right.$$

$$\left.-j(\sqrt{d+b_s+jh}+\sqrt{d+b_s-jh})\frac{1}{2\sqrt{z}}\right]$$

$$-\ln\left(\frac{\sqrt{z}+j\sqrt{d-jh}}{\sqrt{z}-j\sqrt{d+jh}}\right) - \frac{(z+d-jh)}{\sqrt{z}+j\sqrt{d-jh}}\frac{1}{2\sqrt{z}} + \frac{(z+d+jh)}{\sqrt{z}-j\sqrt{d+jh}}\frac{1}{2\sqrt{z}} + j(\sqrt{d+jh}+\sqrt{d-jh})\frac{1}{2\sqrt{z}}]$$

$$-\frac{K_\ell}{2\pi}\left[\ln\left(\frac{\sqrt{z}+j\sqrt{d-b_\ell-jh}}{\sqrt{z}-j\sqrt{d-b_\ell+jh}}\right) + \frac{(z+d-b_\ell-jh)}{\sqrt{z}+j\sqrt{d-b_\ell-jh}}\frac{1}{2\sqrt{z}} - \frac{(z+d-b_\ell+jh)}{\sqrt{z}-j\sqrt{d-b_\ell+jh}}\frac{1}{2\sqrt{z}}\right.$$

$$\left.-j(\sqrt{d-b_\ell+jh}+\sqrt{d-b_\ell-jh})\frac{1}{2\sqrt{z}}\right]$$

$$-\ln\left(\frac{\sqrt{z}+j\sqrt{d-jh}}{\sqrt{z}-j\sqrt{d+jh}}\right) - \frac{(z+d-jh)}{\sqrt{z}+j\sqrt{d-jh}}\frac{1}{2\sqrt{z}} + \frac{(z+d+jh)}{\sqrt{z}-j\sqrt{d+jh}}\frac{1}{2\sqrt{z}} + j(\sqrt{d+jh}+\sqrt{d-jh})\frac{1}{2\sqrt{z}}]$$

$$= \frac{K_s}{2\pi}\left[\ln\left(\frac{\sqrt{z}+j\sqrt{d+b_s-jh}}{\sqrt{z}-j\sqrt{d+b_s+jh}}\right) - j(\sqrt{d+b_s+jh}+\sqrt{d+b_s-jh})\frac{1}{\sqrt{z}}\right.$$

$$\left.-\ln\left(\frac{\sqrt{z}+j\sqrt{d-jh}}{\sqrt{z}-j\sqrt{d+jh}}\right) + j(\sqrt{d+jh}+\sqrt{d-jh})\frac{1}{\sqrt{z}}\right]$$

$$-\frac{K_\ell}{2\pi} \left[\ln \left(\frac{\sqrt{z} + j\sqrt{d-b_\ell-jh}}{\sqrt{z} - j\sqrt{d-b_\ell+jh}} \right) - j \left(\sqrt{d-b_\ell+jh} + \sqrt{d-b_\ell-jh} \right) \frac{1}{\sqrt{z}} \right. \\ \left. - \ln \left(\frac{\sqrt{z} + j\sqrt{d-jh}}{\sqrt{z} - j\sqrt{d+jh}} \right) + j \left(\sqrt{d+jh} + \sqrt{d-jh} \right) \frac{1}{\sqrt{z}} \right]$$

Thus in the limit $z \rightarrow 0$

$$\frac{dW_{tot}}{dz} \sim \frac{K_s}{2\pi} \left[\left(\sqrt{d+jh} + \sqrt{d-jh} \right) - \left(\sqrt{d+b_s+jh} + \sqrt{d+b_s-jh} \right) \right] \frac{j}{\sqrt{z}} \\ - \frac{K_\ell}{2\pi} \left[\left(\sqrt{d+jh} + \sqrt{d-jh} \right) - \left(\sqrt{d-b_\ell+jh} + \sqrt{d-b_\ell-jh} \right) \right] \frac{j}{\sqrt{z}}$$

The fields are thus

$$H_x \sim \left[-K_s \left\{ \left(\sqrt{d+jh} + \sqrt{d-jh} \right) - \left(\sqrt{d+b_s+jh} + \sqrt{d+b_s-jh} \right) \right\} \right. \\ \left. + K_\ell \left\{ \left(\sqrt{d+jh} + \sqrt{d-jh} \right) - \left(\sqrt{d-b_\ell+jh} + \sqrt{d-b_\ell-jh} \right) \right\} \right] \frac{1}{2\pi\sqrt{\rho}} \cos(\varphi/2) \sim H_\rho \\ H \sim \left[-K_s \left\{ \left(\sqrt{d+jh} + \sqrt{d-jh} \right) - \left(\sqrt{d+b_s+jh} + \sqrt{d+b_s-jh} \right) \right\} \right. \\ \left. + K_\ell \left\{ \left(\sqrt{d+jh} + \sqrt{d-jh} \right) - \left(\sqrt{d-b_\ell+jh} + \sqrt{d-b_\ell-jh} \right) \right\} \right] \frac{1}{2\pi\sqrt{\rho}}$$

The stress tensor force per unit length is

$$\underline{F} = \oint_C \left[\mu_0 \underline{H} (\underline{H} \cdot \underline{n}) - \frac{1}{2} \mu_0 H^2 \underline{n} \right] d\ell$$

The contour C is here taken as: the bottom of the half plane $\varepsilon < x < R$ and $y = -0$; a small circle C_ε of radius ε at the edge of the half plane; the top of the half plane $\varepsilon < x < R$ and $y = +0$. The lateral force F_x is again determined all from the tip of the half plane on the contour C_ε where we take $z = \rho e^{j\varphi} \rightarrow \varepsilon e^{j\varphi}$ and $d\ell = \varepsilon d\varphi$. This yields the lateral force per unit length

$$F_x = \mu_0 \int_0^{2\pi} \left[H_x H_\rho - \frac{1}{2} H^2 \cos \varphi \right] \varepsilon d\varphi$$

Now using the fact that

$$\int_0^{2\pi} \cos \varphi d\varphi = 0 \\ \int_0^{2\pi} \cos^2(\varphi/2) d\varphi = \frac{1}{2} \int_0^{2\pi} \{1 + \cos \varphi\} d\varphi = \pi \\ \int_0^{2\pi} \sin^2(\varphi/2) d\varphi = \frac{1}{2} \int_0^{2\pi} \{1 - \cos \varphi\} d\varphi = \pi \\ \int_0^{2\pi} \sin(\varphi/2) \cos(\varphi/2) d\varphi = \frac{1}{2} \int_0^{2\pi} \sin \varphi d\varphi = 0$$

gives

$$F_x = \frac{\mu_0}{4\pi} \left[-K_s \left\{ \left(\sqrt{d+jh} + \sqrt{d-jh} \right) - \left(\sqrt{d+b_s+jh} + \sqrt{d+b_s-jh} \right) \right\} \right. \\ \left. + K_\ell \left\{ \left(\sqrt{d+jh} + \sqrt{d-jh} \right) - \left(\sqrt{d-b_\ell+jh} + \sqrt{d-b_\ell-jh} \right) \right\} \right]^2$$

where the roots are defined via their principal values and the expression is thus real. Figure 2d shows the total force

$$F_x^{tot} = \ell_x [F_x(d) - F_x(-d)]$$

derived from this formula for a typical set of parameters where $I_s = b_s K_s$ and $I_\ell = b_\ell K_\ell / n_\ell$. Notice that linearity of the result only fails for $d = O(h/2)$. The next two subsections simplify this result.

3.3 Semi-infinite Levitation Electrode

To simplify the force formula a bit further we can take the limit of a wide levitation electrode $b_\ell \rightarrow \infty$, because in the experiment the three levitation electrodes together were three times the width of the single stability electrode. Noting that the branches must be taken as $-\pi < \arg(d - b_\ell \pm jh) < \pi$ or $0 < \arg(b_\ell - d \mp jh) < 2\pi$ with $\arg(d - b_\ell \pm jh) = \arg(b_\ell - d \mp jh) - \pi$

$$\sqrt{d - b_\ell + jh} = -j\sqrt{b_\ell - d - jh} \rightarrow j\sqrt{b_\ell}$$

$$\sqrt{d - b_\ell - jh} = -j\sqrt{b_\ell - d + jh} \rightarrow -j\sqrt{b_\ell}$$

Thus in the $b_\ell \rightarrow \infty$ limit we have

$$\frac{dW_{tot}}{dz} = \frac{K_s}{2\pi} \left[\ln \left(\frac{\sqrt{z} + j\sqrt{d+b_s-jh}}{\sqrt{z} - j\sqrt{d+b_s+jh}} \right) - j \left(\sqrt{d+b_s+jh} + \sqrt{d+b_s-jh} \right) \frac{1}{\sqrt{z}} \right] \\ + \frac{K_s - K_\ell}{2\pi} \left[-\ln \left(\frac{\sqrt{z} + j\sqrt{d-jh}}{\sqrt{z} - j\sqrt{d+jh}} \right) + j \left(\sqrt{d+jh} + \sqrt{d-jh} \right) \frac{1}{\sqrt{z}} \right]$$

or as the edge of the half plane is approached $z \rightarrow 0$

$$\frac{dW_{tot}}{dz} \sim \frac{K_s}{2\pi} \left[\ln \left(\frac{j\sqrt{d+b_s-jh}}{-j\sqrt{d+b_s+jh}} \right) - j \left(\sqrt{d+b_s+jh} + \sqrt{d+b_s-jh} \right) \frac{1}{\sqrt{z}} \right] \\ + \frac{K_s - K_\ell}{2\pi} \left[-\ln \left(\frac{j\sqrt{d-jh}}{-j\sqrt{d+jh}} \right) + j \left(\sqrt{d+jh} + \sqrt{d-jh} \right) \frac{1}{\sqrt{z}} \right] \\ \sim \frac{1}{2\pi} \left[(K_s - K_\ell) \left(\sqrt{d+jh} + \sqrt{d-jh} \right) - K_s \left(\sqrt{d+b_s+jh} + \sqrt{d+b_s-jh} \right) \right] \frac{j}{\sqrt{z}}$$

Letting $z = \rho e^{j\varphi}$ gives

$$\frac{dW_{tot}}{dz} \sim \left[(K_s - K_\ell) \left(\sqrt{d+jh} + \sqrt{d-jh} \right) - K_s \left(\sqrt{d+b_s+jh} + \sqrt{d+b_s-jh} \right) \right] \frac{1}{2\pi\sqrt{\rho}} j e^{-j\varphi/2}$$

$$\sim \left[(K_s - K_\ell) \left(\sqrt{d+jh} + \sqrt{d-jh} \right) - K_s \left(\sqrt{d+b_s+jh} + \sqrt{d+b_s-jh} \right) \right] \frac{1}{2\pi\sqrt{\rho}} [\sin(\varphi/2) + j \cos(\varphi/2)]$$

and thus

$$H_x \sim - \left[(K_s - K_\ell) \left(\sqrt{d+jh} + \sqrt{d-jh} \right) - K_s \left(\sqrt{d+b_s+jh} + \sqrt{d+b_s-jh} \right) \right] \frac{1}{2\pi\sqrt{\rho}} \cos(\varphi/2)$$

$$H_y \sim - \left[(K_s - K_\ell) \left(\sqrt{d+jh} + \sqrt{d-jh} \right) - K_s \left(\sqrt{d+b_s+jh} + \sqrt{d+b_s-jh} \right) \right] \frac{1}{2\pi\sqrt{\rho}} \sin(\varphi/2)$$

$$H_\rho = -\frac{\partial \phi_m}{\partial \rho} = -\text{Im} \left(\frac{\partial z}{\partial \rho} \frac{dW}{dz} \right) = -\text{Im} \left(e^{j\varphi} \frac{dW}{dz} \right)$$

$$\sim - \left[(K_s - K_\ell) \left(\sqrt{d+jh} + \sqrt{d-jh} \right) - K_s \left(\sqrt{d+b_s+jh} + \sqrt{d+b_s-jh} \right) \right] \frac{1}{2\pi\sqrt{\rho}} \cos(\varphi/2)$$

and

$$H = \left| (K_s - K_\ell) \left(\sqrt{d+jh} + \sqrt{d-jh} \right) - K_s \left(\sqrt{d+b_s+jh} + \sqrt{d+b_s-jh} \right) \right| \frac{1}{2\pi\sqrt{\rho}}$$

Now

$$\begin{aligned} H_x H_\rho &\sim \\ &\sim \left[(K_s - K_\ell) \left(\sqrt{d+jh} + \sqrt{d-jh} \right) - K_s \left(\sqrt{d+b_s+jh} + \sqrt{d+b_s-jh} \right) \right]^2 \frac{1}{4\pi^2 \rho} \cos^2(\varphi/2) \\ H^2 &\sim \left[(K_s - K_\ell) \left(\sqrt{d+jh} + \sqrt{d-jh} \right) - K_s \left(\sqrt{d+b_s+jh} + \sqrt{d+b_s-jh} \right) \right]^2 \frac{1}{4\pi^2 \rho} \end{aligned}$$

The force per unit length is thus

$$F_x = \frac{\mu_0}{4\pi} \left[(K_s - K_\ell) \left(\sqrt{d+jh} + \sqrt{d-jh} \right) - K_s \left(\sqrt{d+b_s+jh} + \sqrt{d+b_s-jh} \right) \right]^2$$

3.3.1 small d expansion

Now expand for small d

$$\begin{aligned} &(K_s - K_\ell) \left(\sqrt{d+jh} + \sqrt{d-jh} \right) - K_s \left(\sqrt{d+b_s+jh} + \sqrt{d+b_s-jh} \right) \\ &\sim (K_s - K_\ell) \sqrt{h/2} \left\{ (1+j) \left(1 + \frac{d}{2jh} \right) + (1-j) \left(1 - \frac{d}{2jh} \right) \right\} \\ &\quad - K_s \left\{ \sqrt{b_s+jh} \left(1 + \frac{d/2}{b_s+jh} \right) + \sqrt{b_s-jh} \left(1 + \frac{d/2}{b_s-jh} \right) \right\} \end{aligned}$$

$$\begin{aligned} & \sim (K_s - K_\ell) \sqrt{2h} - K_s \left(\sqrt{b_s + jh} + \sqrt{b_s - jh} \right) \\ & + (K_s - K_\ell) \frac{d}{\sqrt{2h}} - K_s \left(1/\sqrt{b_s + jh} + 1/\sqrt{b_s - jh} \right) \frac{d}{2} \end{aligned}$$

Thus we have

$$\begin{aligned} F_x & \sim \frac{\mu_0}{4\pi} \left[(K_s - K_\ell) \sqrt{2h} - K_s \left(\sqrt{b_s + jh} + \sqrt{b_s - jh} \right) + (K_s - K_\ell) \frac{d}{\sqrt{2h}} - K_s \left(1/\sqrt{b_s + jh} + 1/\sqrt{b_s - jh} \right) \frac{d}{2} \right]^2 \\ & \sim \frac{\mu_0}{4\pi} \left[\left\{ (K_s - K_\ell) \sqrt{2h} - K_s \left(\sqrt{b_s + jh} + \sqrt{b_s - jh} \right) \right\}^2 \right. \\ & \left. + 2 \left\{ (K_s - K_\ell) \sqrt{2h} - K_s \left(\sqrt{b_s + jh} + \sqrt{b_s - jh} \right) \right\} \left\{ (K_s - K_\ell) \frac{1}{\sqrt{2h}} - K_s \left(1/\sqrt{b_s + jh} + 1/\sqrt{b_s - jh} \right) \frac{1}{2} \right\} d \right] \end{aligned}$$

3.3.2 total force and stability

The total force is thus

$$\begin{aligned} F_x^{tot} & \sim \frac{\mu_0 \ell_x d}{\pi} \left\{ (K_s - K_\ell) \sqrt{2h} - K_s \left(\sqrt{b_s + jh} + \sqrt{b_s - jh} \right) \right\} \\ & \left\{ (K_s - K_\ell) \frac{1}{\sqrt{2h}} - K_s \left(1/\sqrt{b_s + jh} + 1/\sqrt{b_s - jh} \right) \frac{1}{2} \right\} \end{aligned}$$

Using the identities

$$\begin{aligned} \sqrt{b_s + jh} + \sqrt{b_s - jh} & = 2 (b_s^2 + h^2)^{1/4} \cos \left\{ \frac{1}{2} \arctan (h/b_s) \right\} = \sqrt{2} \sqrt{b_s + \sqrt{b_s^2 + h^2}} \\ 1/\sqrt{b_s + jh} + 1/\sqrt{b_s - jh} & = \frac{\sqrt{b_s + jh} + \sqrt{b_s - jh}}{\sqrt{b_s^2 + h^2}} \end{aligned}$$

gives

$$F_x^{tot} \sim \frac{\mu_0 \ell_x d}{\pi} \left(K_s - K_\ell - K_s \sqrt{b_s/h + \sqrt{1 + b_s^2/h^2}} \right) \left(K_s - K_\ell - K_s \frac{\sqrt{b_s/h + \sqrt{1 + b_s^2/h^2}}}{\sqrt{1 + b_s^2/h^2}} \right)$$

Let us write this as

$$F_x^{tot} \approx F_0 (c_1 I_s + I_\ell) (c_2 I_s + I_\ell)$$

where

$$F_0 = \frac{\mu_0 \ell_x d}{\pi b_s^2}$$

$$c_1 = \sqrt{b_s/h + \sqrt{1 + b_s^2/h^2}} - 1 > 0$$

$$c_2 = \frac{\sqrt{b_s/h + \sqrt{1 + b_s^2/h^2}}}{\sqrt{1 + b_s^2/h^2}} - 1$$

and where $K_s = I_s/b_s$ and $K_\ell = I_\ell/b_s$, the quantities I_s and I_ℓ are the coil currents.

Now taking $h \approx 20 \mu\text{m}$, $b_s \approx 50 \mu\text{m}$, $a \approx 250 \mu\text{m}$, $d \approx 1 \mu\text{m}$, and $\ell_x \approx \pi a/2$ gives

$$F_x^{tot} \approx (1.278724I_s + I_\ell) (-0.1537032I_s + I_\ell) 62.83\text{nN/A}^2$$

Suppose, as in the test, we let $I_\ell \approx 0.9\text{A}$ and $I_s \approx -1.2\text{A}$

$$F_x^{tot} \approx -43.23\text{nN}$$

a restoring force. Alternatively if we assume that $I_\ell \approx 0.9\text{A}$ and $I_s \approx 1.2\text{A}$

$$F_x^{tot} \approx 109.45\text{nN}$$

an unstable force.

3.3.3 quadratic equation for stability limits

The force is

$$F_x^{tot} \approx F_0 (c_1 I_s + I_\ell) (c_2 I_s + I_\ell)$$

The zeros are

$$I_s/I_\ell = K_s/K_\ell \approx -1/c_1, -1/c_2$$

In the preceding example

$$I_s/I_\ell \approx -0.78203, 6.50605$$

Thus there is a lateral restoring force for

$$I_s/I_\ell < -0.78203$$

$$I_s/I_\ell > 6.50605$$

3.3.4 current density near edge

The current density on the half plane is

$$K_z = H_x(x, -0) - H_x(x, +0) = H_x(\rho, \varphi = 2\pi) - H_x(\rho, \varphi = 0)$$

We use the $b_\ell \rightarrow \infty$ result to determine the current density near the edge

$$K_z \sim \left[(K_s - K_\ell) \left(\sqrt{d + jh} + \sqrt{d - jh} \right) - K_s \left(\sqrt{d + b_s + jh} + \sqrt{d + b_s - jh} \right) \right] \frac{1}{\pi\sqrt{\rho}}$$

The current density near the edge when $d \rightarrow 0$ is

$$K_z \sim \left(K_s - K_\ell - K_s \sqrt{b_s/h + \sqrt{1 + b_s^2/h^2}} \right) \frac{1}{\pi} \sqrt{2h/\rho}$$

$$\sim - (c_1 K_s + K_\ell) \frac{1}{\pi} \sqrt{2h/\rho}$$

Noting that $c_1 > 0$, if $K_s/K_\ell < -1/c_1$, this current is positive, otherwise it is negative. Both regions of stability $K_s/K_\ell < -0.78203$ and $K_s/K_\ell > 6.50605$ lead to repulsion between the edge current and the stability coil.

3.4 Vertical Force

We now sketch how the vertical force when $d \rightarrow 0$ can be found. Here we use the form with b_ℓ retained

$$\begin{aligned} \frac{dW_{tot}}{dz} \rightarrow & \frac{K_s}{2\pi} \left[\ln \left(\frac{\sqrt{z} + j\sqrt{b_s - jh}}{\sqrt{z} - j\sqrt{b_s + jh}} \right) - j \left(\sqrt{b_s + jh} + \sqrt{b_s - jh} \right) \frac{1}{\sqrt{z}} \right. \\ & \left. - \ln \left(\frac{\sqrt{z} + (1+j)\sqrt{h/2}}{\sqrt{z} + (1-j)\sqrt{h/2}} \right) + \sqrt{2h} \frac{j}{\sqrt{z}} \right] \\ & - \frac{K_\ell}{2\pi} \left[\ln \left(\frac{\sqrt{z} + j\sqrt{-b_\ell - jh}}{\sqrt{z} - j\sqrt{-b_\ell + jh}} \right) - j \left(\sqrt{-b_\ell + jh} + \sqrt{-b_\ell - jh} \right) \frac{1}{\sqrt{z}} \right. \\ & \left. - \ln \left(\frac{\sqrt{z} + (1+j)\sqrt{h/2}}{\sqrt{z} + (1-j)\sqrt{h/2}} \right) + \sqrt{2h} \frac{j}{\sqrt{z}} \right] \end{aligned}$$

The field is

$$\begin{aligned} H_x = & -\frac{K_s}{2\pi} \text{Im} \left[\ln \left(\frac{\sqrt{z} + j\sqrt{b_s - jh}}{\sqrt{z} - j\sqrt{b_s + jh}} \right) - j \left(\sqrt{b_s + jh} + \sqrt{b_s - jh} \right) \frac{1}{\sqrt{z}} \right. \\ & \left. - \ln \left(\frac{\sqrt{z} + (1+j)\sqrt{h/2}}{\sqrt{z} + (1-j)\sqrt{h/2}} \right) + \sqrt{2h} \frac{j}{\sqrt{z}} \right] \\ & + \frac{K_\ell}{2\pi} \text{Im} \left[\ln \left(\frac{\sqrt{z} + j\sqrt{-b_\ell - jh}}{\sqrt{z} - j\sqrt{-b_\ell + jh}} \right) - j \left(\sqrt{-b_\ell + jh} + \sqrt{-b_\ell - jh} \right) \frac{1}{\sqrt{z}} \right. \\ & \left. - \ln \left(\frac{\sqrt{z} + (1+j)\sqrt{h/2}}{\sqrt{z} + (1-j)\sqrt{h/2}} \right) + \sqrt{2h} \frac{j}{\sqrt{z}} \right] \end{aligned}$$

Thus

$$\begin{aligned} H_x(x, \pm 0) = & -\frac{K_s}{2\pi} \text{Im} \left[\ln \left(\frac{\pm\sqrt{x} + j\sqrt{b_s - jh}}{\pm\sqrt{x} - j\sqrt{b_s + jh}} \right) - j \left(\sqrt{b_s + jh} + \sqrt{b_s - jh} \right) \frac{1}{\pm\sqrt{x}} \right. \\ & \left. - \ln \left(\frac{\pm\sqrt{x} + (1+j)\sqrt{h/2}}{\pm\sqrt{x} + (1-j)\sqrt{h/2}} \right) + \sqrt{2h} \frac{j}{\pm\sqrt{x}} \right] \end{aligned}$$

$$\begin{aligned}
& + \frac{K_\ell}{2\pi} \operatorname{Im} \left[\ln \left(\frac{\pm\sqrt{x} + j\sqrt{-b_\ell - jh}}{\pm\sqrt{x} - j\sqrt{-b_\ell + jh}} \right) - j \left(\sqrt{-b_\ell + jh} + \sqrt{-b_\ell - jh} \right) \frac{1}{\pm\sqrt{x}} \right. \\
& \quad \left. - \ln \left(\frac{\pm\sqrt{x} + (1+j)\sqrt{h/2}}{\pm\sqrt{x} + (1-j)\sqrt{h/2}} \right) + \sqrt{2h} \frac{j}{\pm\sqrt{x}} \right]
\end{aligned}$$

The sum is

$$\begin{aligned}
H_x(x, +0) + H_x(x, -0) &= -\frac{K_s}{2\pi} \operatorname{Im} \left[\ln \left(\frac{\sqrt{x} + j\sqrt{b_s - jh}}{\sqrt{x} - j\sqrt{b_s + jh}} \right) + \ln \left(\frac{-\sqrt{x} + j\sqrt{b_s - jh}}{-\sqrt{x} - j\sqrt{b_s + jh}} \right) \right. \\
& \quad \left. - \ln \left(\frac{\sqrt{x} + (1+j)\sqrt{h/2}}{\sqrt{x} + (1-j)\sqrt{h/2}} \right) - \ln \left(\frac{-\sqrt{x} + (1+j)\sqrt{h/2}}{-\sqrt{x} + (1-j)\sqrt{h/2}} \right) \right] \\
& + \frac{K_\ell}{2\pi} \operatorname{Im} \left[\ln \left(\frac{\sqrt{x} + j\sqrt{-b_\ell - jh}}{\sqrt{x} - j\sqrt{-b_\ell + jh}} \right) + \ln \left(\frac{-\sqrt{x} + j\sqrt{-b_\ell - jh}}{-\sqrt{x} - j\sqrt{-b_\ell + jh}} \right) \right. \\
& \quad \left. - \ln \left(\frac{\sqrt{x} + (1+j)\sqrt{h/2}}{\sqrt{x} + (1-j)\sqrt{h/2}} \right) - \ln \left(\frac{-\sqrt{x} + (1+j)\sqrt{h/2}}{-\sqrt{x} + (1-j)\sqrt{h/2}} \right) \right] \\
& = -\frac{K_s}{2\pi} \operatorname{Im} \left[\ln \left(\frac{x + b_s - jh}{x + b_s + jh} \right) - \ln \left(\frac{x - jh}{x + jh} \right) \right] \\
& + \frac{K_\ell}{2\pi} \operatorname{Im} \left[\ln \left(\frac{x - b_\ell - jh}{x - b_\ell + jh} \right) - \ln \left(\frac{x - jh}{x + jh} \right) \right] \\
& = \frac{K_s}{\pi} \left[\arctan \left(\frac{h}{x + b_s} \right) - \arctan(h/x) \right] \\
& - \frac{K_\ell}{\pi} \left[\arctan \left(\frac{h}{x - b_\ell} \right) - \arctan(h/x) \right]
\end{aligned}$$

and the difference is

$$\begin{aligned}
H_x(x, +0) - H_x(x, -0) &= -\frac{K_s}{2\pi} \operatorname{Im} \left[\ln \left(\frac{\sqrt{x} + j\sqrt{b_s - jh}}{\sqrt{x} - j\sqrt{b_s + jh}} \right) - \ln \left(\frac{-\sqrt{x} + j\sqrt{b_s - jh}}{-\sqrt{x} - j\sqrt{b_s + jh}} \right) \right. \\
& \quad \left. - j \left(\sqrt{b_s + jh} + \sqrt{b_s - jh} \right) \frac{2}{\sqrt{x}} \right. \\
& \quad \left. - \ln \left(\frac{\sqrt{x} + (1+j)\sqrt{h/2}}{\sqrt{x} + (1-j)\sqrt{h/2}} \right) + \ln \left(\frac{-\sqrt{x} + (1+j)\sqrt{h/2}}{-\sqrt{x} + (1-j)\sqrt{h/2}} \right) + \sqrt{2h} \frac{j2}{\sqrt{x}} \right] \\
& + \frac{K_\ell}{2\pi} \operatorname{Im} \left[\ln \left(\frac{\sqrt{x} + j\sqrt{-b_\ell - jh}}{\sqrt{x} - j\sqrt{-b_\ell + jh}} \right) - \ln \left(\frac{-\sqrt{x} + j\sqrt{-b_\ell - jh}}{-\sqrt{x} - j\sqrt{-b_\ell + jh}} \right) - j \left(\sqrt{-b_\ell + jh} + \sqrt{-b_\ell - jh} \right) \frac{2}{\sqrt{x}} \right. \\
& \quad \left. - \ln \left(\frac{\sqrt{x} + (1+j)\sqrt{h/2}}{\sqrt{x} + (1-j)\sqrt{h/2}} \right) + \ln \left(\frac{-\sqrt{x} + (1+j)\sqrt{h/2}}{-\sqrt{x} + (1-j)\sqrt{h/2}} \right) + \sqrt{2h} \frac{j2}{\sqrt{x}} \right]
\end{aligned}$$

$$\begin{aligned}
&= -\frac{K_s}{2\pi} \text{Im} \left[\ln \left(\frac{(\sqrt{x} + j\sqrt{b_s - jh})(\sqrt{x} + j\sqrt{b_s + jh})}{(\sqrt{x} - j\sqrt{b_s - jh})(\sqrt{x} - j\sqrt{b_s + jh})} \right) - j \left(\sqrt{b_s + jh} + \sqrt{b_s - jh} \right) \frac{2}{\sqrt{x}} \right. \\
&\quad \left. - \ln \left(\frac{\sqrt{x} + (1+j)\sqrt{h/2}}{\sqrt{x} + (1-j)\sqrt{h/2}} \right) + \ln \left(\frac{\sqrt{x} - (1+j)\sqrt{h/2}}{\sqrt{x} - (1-j)\sqrt{h/2}} \right) + \sqrt{2h} \frac{j2}{\sqrt{x}} \right] \\
&+ \frac{K_\ell}{2\pi} \text{Im} \left[\ln \left(\frac{\sqrt{x} + j\sqrt{-b_\ell - jh}}{\sqrt{x} - j\sqrt{-b_\ell + jh}} \right) - \ln \left(\frac{\sqrt{x} - j\sqrt{-b_\ell - jh}}{\sqrt{x} + j\sqrt{-b_\ell + jh}} \right) - j \left(\sqrt{-b_\ell + jh} + \sqrt{-b_\ell - jh} \right) \frac{2}{\sqrt{x}} \right. \\
&\quad \left. - \ln \left(\frac{\sqrt{x} + (1+j)\sqrt{h/2}}{\sqrt{x} + (1-j)\sqrt{h/2}} \right) + \ln \left(\frac{\sqrt{x} - (1+j)\sqrt{h/2}}{\sqrt{x} - (1-j)\sqrt{h/2}} \right) + \sqrt{2h} \frac{j2}{\sqrt{x}} \right]
\end{aligned}$$

Near the edge the y directed field is

$$H_y = -\text{Re} \left(\frac{dW_{tot}}{dz} \right)$$

$$\sim - \left[K_s \left\{ \sqrt{2h} - \left(\sqrt{b_s + jh} + \sqrt{b_s - jh} \right) \right\} - K_\ell \left\{ \sqrt{2h} - \left(\sqrt{-b_\ell + jh} + \sqrt{-b_\ell - jh} \right) \right\} \right] \frac{1}{2\pi\sqrt{\rho}} \sin(\varphi/2)$$

and the ρ directed field is

$$H_\rho = -\text{Im} \left(e^{j\varphi} \frac{dW_{tot}}{dz} \right)$$

$$\sim - \left[K_s \left\{ \sqrt{2h} - \left(\sqrt{b_s + jh} + \sqrt{b_s - jh} \right) \right\} - K_\ell \left\{ \sqrt{2h} - \left(\sqrt{-b_\ell + jh} + \sqrt{-b_\ell - jh} \right) \right\} \right] \frac{1}{2\pi\sqrt{\rho}} \cos(\varphi/2)$$

From the stress tensor the vertical force per unit length can be written as

$$\begin{aligned}
F_y &= \mu_0 \int_0^{2\pi} H_y H_\rho \rho d\varphi + \frac{1}{2} \mu_0 \int_0^\infty \{H_x(x, +0) - H_x(x, -0)\} \{H_x(x, +0) + H_x(x, -0)\} dx \\
&= \frac{1}{2} \mu_0 \int_0^\infty \{H_x(x, +0) - H_x(x, -0)\} \{H_x(x, +0) + H_x(x, -0)\} dx
\end{aligned}$$

where the edge contribution vanishes. It appears that this integral must be evaluated numerically. The total vertical force is thus

$$F_y^{tot} \approx 2\ell_y F_y$$

4 COIL DRIVE FIELD

Here it is convenient to use the magnetic vector potential for the source field. The magnetic vector potential is found from

$$\underline{A}(\underline{r}) = \frac{\mu_0}{4\pi} \int_V \frac{\underline{J}(\underline{r}')}{|\underline{r} - \underline{r}'|} dV'$$

where \underline{r} is the position vector and the volume V contains the current density \underline{J} . The vector potential of a symmetric loop of current has only an azimuthal component φ . The magnetic vector potential produced by the exciting current loop of radius b , with azimuthal current I , is

$$A_\varphi^i(\rho, z) = \frac{\mu_0 I}{2\pi} \sqrt{\frac{b}{\rho}} k \left[\left(\frac{2}{k^2} - 1 \right) K(k) - \frac{2}{k^2} E(k) \right]$$

where $K(k) = \int_0^{\pi/2} d\theta / \sqrt{1 - k^2 \sin^2 \theta}$ and $E(k) = \int_0^{\pi/2} d\theta \sqrt{1 - k^2 \sin^2 \theta}$ are the complete elliptic integrals and

$$k = \frac{2\sqrt{\rho b}}{\sqrt{(b + \rho)^2 + z^2}}$$

The spherical coordinate expansion is

$$A_\varphi^i(r, \theta) = \mu_0 I \sum_{n=0}^{\infty} \frac{(-1)^{n+1} (2n-1)!!}{2^{n+2} (n+1)!} \frac{br_{<}^{2n+1}}{r_{>}^{2n+2}} P_{2n+1}^1(\cos \theta)$$

where $r_{<} = \min(r, b)$ and $r_{>} = \max(r, b)$. The cylindrical form is

$$A_\varphi^i(\rho, z) = \frac{1}{2} \mu_0 I b \int_0^\infty J_1(\alpha \rho) J_1(\alpha b) e^{-\alpha|z|} d\alpha$$

The corresponding fields are

$$\underline{B} = \mu_0 \underline{H} = \nabla \times \underline{A}$$

or

$$H_\rho^i = \frac{Iz}{8\pi\rho\sqrt{b\rho}} k \left[-2K(k) + \left(2 + \frac{k^2}{k'^2} \right) E(k) \right]$$

$$H_z^i = \frac{-I}{8\pi\sqrt{b\rho}} k \left[-2K(k) + \left\{ (1 + b/\rho) + \frac{1}{k'^2} (1 - b/\rho) \right\} E(k) \right]$$

where

$$k' = \sqrt{1 - k^2}$$

and the superscript i denotes the incident or exciting field.

The exciting fields from this single coil loop are later integrated with respect to the radius b to generate circular strip stator electrodes with uniform current density in cross section.

5 OBLATE SPHEROID PEC DISC SOLUTION

Using the oblate spheroidal coordinate system we can find a scattered potential from the induced disc currents which satisfies

$$\nabla^2 \phi_m = 0$$

and the field is found as

$$\underline{H} = -\nabla \phi_m$$

The coordinate system is centered now on the disc with the electric current loop excitation displaced as shown in Figure 3a. The boundary condition on the disc surface is

$$H_\zeta(0, \xi, \varphi) \operatorname{sgn}(\xi) = -\frac{1}{a|\xi|} \frac{\partial \phi_m}{\partial \zeta}(0, \xi, \varphi) \operatorname{sgn}(\xi) = -H_z^i, \quad -1 < \xi < 1, \quad -\pi < \varphi < \pi$$

The solution to Laplace's equation is

$$\phi_m = \sum_n \sum_m [A_{mn} P_n^m(\xi) + B_{mn} Q_n^m(\xi)] [C_{mn} P_n^m(j\zeta) + D_{mn} Q_n^m(j\zeta)] [E_{mn} \cos(m\varphi) + F_{mn} \sin(m\varphi)]$$

Finiteness on the $\xi = 1$ (z axis) makes $B_{mn} = 0$. Decay at infinity requires $C_{mn} = 0$. Finally, we can assume that movement of the exciting current loop relative to the perfectly conducting disc is restricted to the x axis, so that the problem is even in φ and $F_{mn} = 0$. Thus we obtain

$$\phi_m = \sum_{n=0}^{\infty} \sum_{m=0}^n A_{mn} P_n^m(\xi) Q_n^m(j\zeta) \cos(m\varphi)$$

where the fact that $P_n^m(\xi) = 0$ for $m > n$ has been used.

The incident field can be transformed to the oblate spheroidal system by using the relations

$$x = a\sqrt{1+\zeta^2}\sqrt{1-\xi^2}\cos\varphi$$

$$y = a\sqrt{1+\zeta^2}\sqrt{1-\xi^2}\sin\varphi$$

$$\rho = a\sqrt{1+\zeta^2}\sqrt{1-\xi^2}$$

$$z = a\zeta\xi$$

We take the incident field to be

$$H_z^i = \frac{-I}{8\pi\sqrt{b\hat{\rho}}} k \left[-2K(k) + \left\{ (1+b/\hat{\rho}) + \frac{1}{k'^2} (1-b/\hat{\rho}) \right\} E(k) \right]$$

$$\hat{\rho} = \sqrt{(x+d)^2 + y^2} = \sqrt{\rho^2 + d^2 + 2d\rho\cos\varphi}$$

$$\hat{z} = z + h$$

$$k = \frac{2\sqrt{\hat{\rho}b}}{\sqrt{(b+\hat{\rho})^2 + \hat{z}^2}}, \quad k' = \sqrt{1-k^2}$$

where the original coordinate system of the current loop has been shifted by d along the x axis and by h along the z axis.

Using the orthogonality relations

$$\int_{-1}^1 P_n^m(\xi) P_{n'}^m(\xi) d\xi = \frac{(n+m)!}{(n+\frac{1}{2})(n-m)!} \delta_{nn'}$$

$$\int_{-\pi}^{\pi} \cos(m\varphi) \cos(m'\varphi) d\varphi = \frac{2\pi}{\varepsilon_m} \delta_{mm'}$$

in the boundary condition we find

$$-\frac{1}{a} A_{mn} \frac{(n+m)!}{(n+\frac{1}{2})(n-m)!} j Q_n^{m'}(j0) \frac{2\pi}{\varepsilon_m} = - \int_{-1}^1 \int_{-\pi}^{\pi} H_z^i(\xi, \varphi, z=0) P_n^m(\xi) \xi d\xi \cos(m\varphi) d\varphi$$

where

$$H_z^i(\xi, \varphi, z=0) = \frac{-I}{8\pi\sqrt{b\hat{\rho}}} k \left[-2K(k) + \left\{ (1+b/\hat{\rho}) + \frac{1}{k'^2} (1-b/\hat{\rho}) \right\} E(k) \right]$$

$$\hat{\rho} = \sqrt{a^2(1-\xi^2) + d^2 + 2da\sqrt{1-\xi^2}\cos\varphi}$$

$$k = \frac{2\sqrt{\hat{\rho}b}}{\sqrt{(b+\hat{\rho})^2 + h^2}}, \quad k' = \sqrt{1-k^2}$$

Because the exciting field is even in ξ at $\zeta = 0$, only the terms $m+n$ odd contribute. This makes the scattered potential odd in ξ . The evenness of the exciting field in φ allows us to write

$$A_{mn} = \frac{a\varepsilon_m}{\pi} \frac{(n-m)!}{(n+m)!} \frac{(2n+1)}{j Q_n^{m'}(j0)} \int_0^1 \int_0^{\pi} H_z^i(\xi, \varphi, z=0) P_n^m(\xi) \xi d\xi \cos(m\varphi) d\varphi$$

Thus the boundary value problem has been solved in terms of these quadratures for the coefficients.

5.1 Zero Displacement Symmetric Result

The limit of zero displacement $d=0$ results in the symmetric exciting field

$$H_z^i(\xi, z=0) = \frac{-I}{8\pi\sqrt{b\rho}} k \left[-2K(k) + \left\{ (1+b/\rho) + \frac{1}{k'^2} (1-b/\rho) \right\} E(k) \right]$$

$$\rho = a\sqrt{1-\xi^2}$$

$$k = \frac{2\sqrt{\hat{\rho}b}}{\sqrt{(b+\rho)^2 + h^2}}, \quad k' = \sqrt{1-k^2}$$

All modal coefficients with $m \neq 0$ vanish. Thus

$$\phi_m = \sum_{n, \text{odd}}^{\infty} A_n P_n(\xi) Q_n(j\zeta)$$

$$A_n = a \frac{(2n+1)}{jQ'_n(j0)} \int_0^1 H_z^i(\xi, z=0) P_n(\xi) \xi d\xi$$

5.1.1 symmetric and far apart

The far limit $h \gg a$ we use

$$H_z^i \approx \frac{Ib^2/2}{(b^2 + h^2)^{3/2}}$$

$$A_n = a \frac{(2n+1)}{jQ'_n(j0)} H_z^i \int_0^1 P_n(\xi) \xi d\xi$$

$$= \frac{aH_z^i}{jQ'_1(j0)} \delta_{n1}$$

$$\phi_m \approx H_z^i a \xi Q_1(j\zeta) / [jQ'_1(j0)]$$

$$Q_1(j\zeta) = \zeta \operatorname{arccot} \zeta - 1$$

$$jQ'_1(j0) = \pi/2$$

$$\phi_m \approx H_z^i \frac{2}{\pi} a \xi (\zeta \operatorname{arccot} \zeta - 1)$$

Now for $\zeta = 0$

$$\phi_m \approx -H_z^i \frac{2}{\pi} a \xi = \mp H_z^i \frac{2}{\pi} \sqrt{a^2 - \rho^2}, \xi \begin{matrix} > \\ < \end{matrix} 0$$

or

$$H_\rho = -\frac{\partial \phi_m}{\partial \rho} = \mp H_z^i \frac{2}{\pi} \frac{\rho}{\sqrt{a^2 - \rho^2}}$$

$$K_\varphi = \pm H_\rho = -H_z^i \frac{2}{\pi} \frac{\rho}{\sqrt{a^2 - \rho^2}}$$

The case of zero displacement does not lead to net lateral forces. Thus we later consider small displacements.

5.2 Forces

The forces acting on the disc can be found from evaluating the integral

$$\underline{F} = \int_V \underline{J} \times \underline{B} dV$$

where we can take the volume V to be the disc and the magnetic field \underline{B} to be that resulting from the source current loops only. This ignores the self interaction of the disc currents, which is not important for rigid bodies. We can rewrite this as

$$\begin{aligned} \underline{F} &= \mu_0 \oint_S \underline{K} \times \underline{H}^i dS = -\mu_0 \oint_S (\underline{n} \times \nabla \phi_m) \times \underline{H}^i dS \\ &= -\mu_0 \int_{-1}^1 \frac{a|\xi|}{\sqrt{1-\xi^2}} d\xi \int_{-\pi}^{\pi} a\sqrt{1-\xi^2} d\varphi [\underline{e}_\zeta \times \nabla \phi_m(\zeta=0, \xi, \varphi)] \times \underline{H}^i \\ &= -\mu_0 a^2 \int_{-1}^1 |\xi| d\xi \int_{-\pi}^{\pi} d\varphi \left[\underline{e}_\zeta \times \underline{e}_\xi \frac{\sqrt{1-\xi^2}}{a|\xi|} \frac{\partial \phi_m}{\partial \xi}(\zeta=0, \xi, \varphi) + \underline{e}_\zeta \times \underline{e}_\varphi \frac{1}{a\sqrt{1-\xi^2}} \frac{\partial \phi_m}{\partial \varphi}(\zeta=0, \xi, \varphi) \right] \times \underline{H}^i \\ &= -\mu_0 a^2 \int_{-1}^1 |\xi| d\xi \int_{-\pi}^{\pi} d\varphi \left[-\underline{e}_\varphi \frac{\sqrt{1-\xi^2}}{a|\xi|} \frac{\partial \phi_m}{\partial \xi}(\zeta=0, \xi, \varphi) + \underline{e}_\xi \frac{1}{a\sqrt{1-\xi^2}} \frac{\partial \phi_m}{\partial \varphi}(\zeta=0, \xi, \varphi) \right] \\ &\quad \times (H_\zeta^i \underline{e}_\zeta + H_\xi^i \underline{e}_\xi + H_\varphi^i \underline{e}_\varphi) \\ &= -\mu_0 a^2 \int_{-1}^1 |\xi| d\xi \int_{-\pi}^{\pi} d\varphi \left[(H_\zeta^i \underline{e}_\xi - H_\xi^i \underline{e}_\zeta) \frac{\sqrt{1-\xi^2}}{a|\xi|} \frac{\partial \phi_m}{\partial \xi} + (H_\zeta^i \underline{e}_\varphi - H_\varphi^i \underline{e}_\zeta) \frac{1}{a\sqrt{1-\xi^2}} \frac{\partial \phi_m}{\partial \varphi} \right] \end{aligned}$$

where H_ζ^i is odd in ξ and even in φ , H_ξ^i is odd in ξ and even in φ , and H_φ^i is even in ξ but odd in φ at $\zeta=0$. Also $\frac{\partial \phi_m}{\partial \xi}$ is even in ξ and even in φ , and $\frac{\partial \phi_m}{\partial \varphi}$ is odd in ξ and odd in φ at $\zeta=0$. In addition \underline{e}_ξ is odd in ξ , \underline{e}_ζ is odd in ξ , and \underline{e}_φ is even in ξ at $\zeta=0$. Thus we can write

$$\underline{F} = -2\mu_0 a^2 \int_0^1 \xi d\xi \int_{-\pi}^{\pi} d\varphi \left[(H_\zeta^i \underline{e}_\xi - H_\xi^i \underline{e}_\zeta) \frac{\sqrt{1-\xi^2}}{a\xi} \frac{\partial \phi_m}{\partial \xi} + (H_\zeta^i \underline{e}_\varphi - H_\varphi^i \underline{e}_\zeta) \frac{1}{a\sqrt{1-\xi^2}} \frac{\partial \phi_m}{\partial \varphi} \right]$$

Now the unit vectors can be replaced first with cylindrical then with Cartesian quantities (see the appendix)

$$\begin{aligned} \underline{F} &= -2\mu_0 a^2 \int_0^1 \xi d\xi \int_{-\pi}^{\pi} d\varphi \left[(-H_\zeta^i \underline{e}_\rho - H_\xi^i \underline{e}_z) \frac{\sqrt{1-\xi^2}}{a\xi} \frac{\partial \phi_m}{\partial \xi} + (H_\zeta^i \underline{e}_\varphi - H_\varphi^i \underline{e}_z) \frac{1}{a\sqrt{1-\xi^2}} \frac{\partial \phi_m}{\partial \varphi} \right] \\ &= -2\mu_0 a^2 \int_0^1 \xi d\xi \int_{-\pi}^{\pi} d\varphi \left[(-H_z^i \underline{e}_\rho + H_\rho^i \underline{e}_z) \frac{\sqrt{1-\xi^2}}{a\xi} \frac{\partial \phi_m}{\partial \xi} + (H_z^i \underline{e}_\varphi - H_\varphi^i \underline{e}_z) \frac{1}{a\sqrt{1-\xi^2}} \frac{\partial \phi_m}{\partial \varphi} \right] \\ &= 2\mu_0 \int_0^a \rho d\rho \int_{-\pi}^{\pi} d\varphi \left[(H_z^i \underline{e}_\rho - H_\rho^i \underline{e}_z) \left(-\frac{\partial \phi_m}{\partial \rho} \right) + (H_z^i \underline{e}_\varphi - H_\varphi^i \underline{e}_z) \left(-\frac{1}{\rho} \frac{\partial \phi_m}{\partial \varphi} \right) \right] \end{aligned}$$

$$\begin{aligned}
&= 2\mu_0 \int_0^a \rho d\rho \int_{-\pi}^{\pi} d\varphi [(H_z^i \underline{e}_\rho - H_\rho^i \underline{e}_z) H_\rho + (H_z^i \underline{e}_\varphi - H_\varphi^i \underline{e}_z) H_\varphi] \\
&= 2\mu_0 \int_0^a \rho d\rho \int_{-\pi}^{\pi} d\varphi [\{H_z^i (\underline{e}_x \cos \varphi + \underline{e}_y \sin \varphi) - H_\rho^i \underline{e}_z\} H_\rho + \{H_z^i (-\underline{e}_x \sin \varphi + \underline{e}_y \cos \varphi) - H_\varphi^i \underline{e}_z\} H_\varphi]
\end{aligned}$$

Because H_z^i is even in φ , H_ρ^i is even and φ , H_ρ is even in φ , H_φ^i is odd in φ , and H_φ is odd in φ , we find

$$\underline{F} = 4\mu_0 \int_0^a \rho d\rho \int_0^\pi d\varphi [(H_z^i \underline{e}_x \cos \varphi - H_\rho^i \underline{e}_z) H_\rho + (-H_z^i \underline{e}_x \sin \varphi - H_\varphi^i \underline{e}_z) H_\varphi]$$

or

$$\begin{aligned}
F_x &= 4\mu_0 \int_0^a \rho d\rho \int_0^\pi d\varphi (H_z^i H_\rho \cos \varphi - H_z^i H_\varphi \sin \varphi) \\
&= -4\mu_0 a^2 \int_0^1 \xi d\xi \int_0^\pi d\varphi (H_z^i H_\xi \cos \varphi + H_z^i H_\varphi \sin \varphi) \\
F_z &= -4\mu_0 \int_0^a \rho d\rho \int_0^\pi d\varphi (H_\rho^i H_\rho + H_\varphi^i H_\varphi) \\
&= -4\mu_0 a^2 \int_0^1 \xi d\xi \int_0^\pi d\varphi (H_\xi^i H_\xi + H_\varphi^i H_\varphi)
\end{aligned}$$

where the fields H_ρ and H_φ are the disc current induced fields evaluated on top of the disc. They are found from the potential

$$\phi_m = \sum_{n=0}^{\infty} \sum_{m=0}^n A_{mn} P_n^m(\xi) Q_n^m(j\xi) \cos(m\varphi), \quad m+n \text{ odd}$$

or

$$H_\xi = - \sum_{n=0}^{\infty} \sum_{m=0}^n A_{mn} \frac{1}{a\xi} \sqrt{1-\xi^2} P_n^{m'}(\xi) Q_n^m(j0) \cos(m\varphi)$$

where identities for the derivative are

$$\begin{aligned}
-\sqrt{1-\xi^2} P_n^{m'}(\xi) &= P_n^{m+1}(\xi) + \frac{\xi}{\sqrt{1-\xi^2}} m P_n^m(\xi) \\
&= \frac{\xi}{\sqrt{1-\xi^2}} n P_n^m(\xi) - \frac{1}{\sqrt{1-\xi^2}} (n+m) P_{n-1}^m(\xi) \\
&= -(n-m+1)(n+m) P_n^{m-1}(\xi) - \frac{\xi}{\sqrt{1-\xi^2}} m P_n^m(\xi) \\
&= -\frac{\xi}{\sqrt{1-\xi^2}} (n+1) P_n^m(\xi) + \frac{\xi}{\sqrt{1-\xi^2}} (n-m+1) P_{n+1}^m(\xi)
\end{aligned}$$

and

$$H_\varphi = \sum_{n=0}^{\infty} \sum_{m=0}^n A_{mn} \frac{1}{a\sqrt{1-\xi^2}} P_n^m(\xi) Q_n^m(j0) m \sin(m\varphi)$$

5.3 Torques

Now we consider the torques on the disc. Because of symmetry the torque of interest is τ_y . This can be found as

$$\underline{\tau} = \int_V \underline{r} \times (\underline{J} \times \underline{B}) dV$$

or

$$\begin{aligned} \tau_y &= \int_S [x \underline{e}_x \times (\underline{K} \times \underline{B})] \cdot \underline{e}_y dx dy \\ &= \int_S x [(\underline{e}_x \cdot \underline{B}) \underline{K} - (\underline{e}_x \cdot \underline{K}) \underline{B}] \cdot \underline{e}_y dx dy \\ &= \int_S x [(\underline{e}_x \cdot \underline{B}) (\underline{K} \cdot \underline{e}_y) - (\underline{e}_x \cdot \underline{K}) (\underline{B} \cdot \underline{e}_y)] dx dy \\ &= \int_S x (B_x K_y - K_x B_y) dx dy \end{aligned}$$

or

$$\begin{aligned} \tau_y &= \int_{-\pi}^{\pi} \int_0^a \rho \cos \varphi [(B_\rho \cos \varphi - B_\varphi \sin \varphi) (K_\rho \sin \varphi + K_\varphi \cos \varphi) \\ &\quad - (K_\rho \cos \varphi - K_\varphi \sin \varphi) (B_\rho \sin \varphi + B_\varphi \cos \varphi)] \rho d\rho d\varphi \\ &= \int_{-\pi}^{\pi} \int_0^a \rho \cos \varphi (B_\rho K_\varphi - B_\varphi K_\rho) \rho d\rho d\varphi \\ &= 2 \int_0^{\pi} \int_0^a \rho \cos \varphi (B_\rho K_\varphi - B_\varphi K_\rho) \rho d\rho d\varphi \end{aligned}$$

where we have used the fact that B_ρ and K_φ are even in φ and the fact that B_φ and K_ρ are odd in φ . Using the symmetry from top to bottom of the disc we can write (where the integration is now only on the top of the disc)

$$\tau_y = 4\mu_0 \int_0^{\pi} \int_0^a (H_\rho^i H_\rho + H_\varphi^i H_\varphi) \rho^2 d\rho \cos \varphi d\varphi$$

Now transforming to spheroidal coordinates gives

$$\tau_y = 4\mu_0 a^2 \int_0^{\pi} \int_0^1 (H_\xi^i H_\xi + H_\varphi^i H_\varphi) \sqrt{1 - \xi^2} \xi d\xi \cos \varphi d\varphi$$

5.4 Expansion of Incident Field

The case where d is small but nonzero is now discussed. First the exciting or incident field must be expanded for small d . We write the incident field as

$$H_z^i(x, y, z) = H_z^i(\hat{\rho}, \hat{z})$$

$$H_z^i(\hat{\rho}, \hat{z}) = \frac{-I}{8\pi\sqrt{b\hat{\rho}}} k \left[-2K(k) + \left\{ (1 + b/\hat{\rho}) + \frac{1}{k'^2} (1 - b/\hat{\rho}) \right\} E(k) \right]$$

$$\hat{\rho} = \sqrt{(x+d)^2 + y^2} = \sqrt{\rho^2 + d^2 + 2d\rho \cos \varphi}$$

$$\hat{z} = z + h$$

$$k = \frac{2\sqrt{\hat{\rho}b}}{\sqrt{(b+\hat{\rho})^2 + \hat{z}^2}}, \quad k' = \sqrt{1 - k^2}$$

Now we write

$$\begin{aligned} H_z^i(x, y, z) &\approx H_z^i(\rho, \hat{z}) + \frac{\partial H_z^i}{\partial \hat{\rho}}(\rho, \hat{z}) \frac{\partial \hat{\rho}}{\partial x} d \approx H_z^i(\rho, \hat{z}) + \frac{\partial H_z^i}{\partial \hat{\rho}}(\rho, \hat{z}) \frac{x+d}{\hat{\rho}} d \\ &\approx H_z^i(\rho, \hat{z}) + \frac{\partial H_z^i}{\partial \hat{\rho}}(\rho, \hat{z}) d \cos \varphi \end{aligned}$$

Thus to evaluate the derivative we write

$$\frac{\partial k}{\partial \hat{\rho}} = \frac{k}{2\hat{\rho}} \left[1 - \left(\frac{b+\hat{\rho}}{2b} \right) k^2 \right] = \frac{k}{2\hat{\rho}} \left[\frac{(b^2 - \hat{\rho}^2) + \hat{z}^2}{(b+\hat{\rho})^2 + \hat{z}^2} \right]$$

$$K'(k) = \frac{1}{kk'^2} (E - k'^2 K)$$

$$E'(k) = \frac{1}{k} (E - K)$$

$$\begin{aligned} \frac{\partial H_z^i}{\partial \hat{\rho}} &= \frac{-I}{8\pi\sqrt{b\hat{\rho}}} k \left[-b/\hat{\rho}^2 + \frac{1}{k'^2} b/\hat{\rho}^2 + \frac{2k}{k'^4} \frac{\partial k}{\partial \hat{\rho}} (1 - b/\hat{\rho}) \right] E(k) \\ &+ \frac{-I}{8\pi\sqrt{b\hat{\rho}}} \left[-2K(k) + \left\{ (1 + b/\hat{\rho}) + \frac{1}{k'^2} (1 - b/\hat{\rho}) \right\} E(k) \right] \left(-\frac{1}{2} k/\hat{\rho} + \frac{\partial k}{\partial \hat{\rho}} \right) \\ &+ \frac{-I}{8\pi\sqrt{b\hat{\rho}}} k \left[-2K'(k) + \left\{ (1 + b/\hat{\rho}) + \frac{1}{k'^2} (1 - b/\hat{\rho}) \right\} E'(k) \right] \frac{\partial k}{\partial \hat{\rho}} \\ &= \frac{-I}{8\pi\sqrt{b\hat{\rho}}} k \left[-b/\hat{\rho}^2 + \frac{1}{k'^2} b/\hat{\rho}^2 + \frac{k^2}{\hat{\rho}k'^4} \left\{ 1 - \left(\frac{b+\hat{\rho}}{2b} \right) k^2 \right\} (1 - b/\hat{\rho}) \right] E \end{aligned}$$

$$\begin{aligned}
& + \frac{I}{8\pi\sqrt{b\hat{\rho}}} \left[-2K + \left\{ (1 + b/\hat{\rho}) + \frac{1}{k'^2} (1 - b/\hat{\rho}) \right\} E \right] \frac{k^3}{4b\hat{\rho}} (b + \hat{\rho}) \\
& + \frac{-I}{8\pi\sqrt{b\hat{\rho}}} k \left[-2 \frac{1}{kk'^2} (E - k'^2 K) + \left\{ (1 + b/\hat{\rho}) + \frac{1}{k'^2} (1 - b/\hat{\rho}) \right\} \frac{1}{k} (E - K) \right] \frac{k}{2\hat{\rho}} \left\{ 1 - \left(\frac{b + \hat{\rho}}{2b} \right) k^2 \right\}
\end{aligned}$$

5.5 Lateral Force for Small Displacement Approximation

The lateral force in the case where d is small is now treated. Taking the limit of the previous expression

$$\begin{aligned}
F_z &= 4\mu_0 \int_0^a \rho d\rho \int_0^\pi d\varphi (H_z^i H_\rho \cos \varphi - H_z^i H_\varphi \sin \varphi) \\
&= -4\mu_0 a^2 \int_0^1 \xi d\xi \int_0^\pi d\varphi (H_z^i H_\xi \cos \varphi + H_z^i H_\varphi \sin \varphi) \\
&\sim -4\mu_0 a^2 d \int_0^1 \xi d\xi \int_0^\pi d\varphi [(H_{z0}^i H_{\xi 1} + H_{z1}^i H_{\xi 0}) \cos^2 \varphi + H_{z0}^i H_{\varphi 1} \sin^2 \varphi] \\
&\sim -2\pi\mu_0 a^2 d \int_0^1 \xi d\xi [H_{z0}^i (H_{\xi 1} + H_{\varphi 1}) + H_{z1}^i H_{\xi 0}]
\end{aligned}$$

where

$$H_z^i(\hat{\rho}, h) \sim H_z^i(\rho, h) + \frac{\partial H_z^i}{\partial \rho}(\rho, h) d \cos \varphi$$

or

$$\begin{aligned}
H_z^i(\xi, \varphi, z=0) &\sim H_{z0}^i(\xi) + H_{z1}^i(\xi) d \cos \varphi \\
\phi_m &\sim \sum_{n, \text{odd}}^\infty A_n P_n(\xi) Q_n(j\zeta) + \cos \varphi \sum_{n, \text{even}}^\infty A_{1n} P_n^1(\xi) Q_n^1(j\zeta) \\
H_\xi &\sim - \sum_{n, \text{odd}}^\infty A_n \frac{1}{a\xi} \sqrt{1 - \xi^2} P_n'(\xi) Q_n(j0) - \cos \varphi \sum_{n, \text{even}}^\infty A_{1n} \frac{1}{a\xi} \sqrt{1 - \xi^2} P_n^{1'}(\xi) Q_n^1(j0) \\
&\sim \sum_{n, \text{odd}}^\infty A_n \frac{1}{a\xi} P_n^1(\xi) Q_n(j0) - \cos \varphi \sum_{n, \text{even}}^\infty A_{1n} \frac{1}{a\xi} \left[n(n+1) P_n(\xi) + \frac{\xi}{\sqrt{1 - \xi^2}} P_n^1(\xi) \right] Q_n^1(j0) \\
&\sim H_{\xi 0}(\xi) + H_{\xi 1}(\xi) d \cos \varphi \\
H_\varphi &\sim \sin \varphi \sum_{n, \text{even}}^\infty A_{1n} \frac{1}{a\sqrt{1 - \xi^2}} P_n^1(\xi) Q_n^1(j0) \\
&\sim H_{\varphi 1}(\xi) d \sin \varphi
\end{aligned}$$

$$\begin{aligned}
A_n &= \frac{3a/\pi}{jQ'_n(j0)} \int_0^1 \int_0^\pi H_z^i(\xi, \varphi, z=0) P_n(\xi) \xi d\xi d\varphi \\
&\sim \frac{3a}{jQ'_n(j0)} \int_0^1 H_{z0}^i(\xi) P_n(\xi) \xi d\xi \\
A_{1n} &= \frac{2a}{\pi(n+1)n} \frac{(2n+1)}{jQ_n^{1'}(j0)} \int_0^1 \int_0^\pi H_z^i(\xi, \varphi, z=0) P_n^1(\xi) \xi d\xi \cos \varphi d\varphi \\
&\sim \frac{ad}{(n+1)n} \frac{(2n+1)}{jQ_n^{1'}(j0)} \int_0^1 H_{z1}^i(\xi) P_n^1(\xi) \xi d\xi
\end{aligned}$$

Thus we find

$$\begin{aligned}
F_x &\sim 2\pi\mu_0 a \sum_{n, \text{even}}^\infty n(n+1) A_{1n} Q_n^1(j0) \int_0^1 H_z^i(\rho, h) P_n(\xi) d\xi \\
&\quad - 2\pi\mu_0 ad \sum_{n, \text{odd}}^\infty A_n Q_n(j0) \int_0^1 \frac{\partial H_z^i}{\partial \rho}(\rho, h) P_n^1(\xi) d\xi \\
&\sim 2\pi\mu_0 ad \sum_{n, \text{even}}^\infty n(n+1) \hat{A}_{1n} \frac{Q_n^1(j0)}{jQ_n^{1'}(j0)} \int_0^1 H_z^i(\rho, h) P_n(\xi) d\xi \\
&\quad - 2\pi\mu_0 ad \sum_{n, \text{odd}}^\infty \hat{A}_n \frac{Q_n(j0)}{jQ_n'(j0)} \int_0^1 \frac{\partial H_z^i}{\partial \rho}(\rho, h) P_n^1(\xi) d\xi
\end{aligned}$$

where the “hat” coefficients are the values given by the code (normalized values). The ratio of Legendre functions can be found from

$$\frac{jQ_n^{m'}(j0)}{Q_n^m(j0)} = (m+n)(n-m+1) \frac{Q_n^{m-1}(j0)}{Q_n^m(j0)} = -(m+n)(n-m+1) \frac{\Gamma(\frac{n+m}{2}) \Gamma(1+\frac{n-m}{2})}{2\Gamma(1+\frac{n-m+1}{2}) \Gamma(\frac{n+m+1}{2})}$$

5.6 Vertical Force for Small Displacement Approximation

Now consider the vertical force. The result is

$$\begin{aligned}
F_z &= -4\mu_0 \int_0^a \rho d\rho \int_0^\pi d\varphi (H_\rho^i H_\rho + H_\varphi^i H_\varphi) \\
&= -4\mu_0 a^2 \int_0^1 \xi d\xi \int_0^\pi d\varphi (H_\xi^i H_\xi + H_\varphi^i H_\varphi) \\
&\sim -4\mu_0 a^2 \pi \int_0^1 \xi d\xi H_{\xi 0}^i H_{\xi 0}
\end{aligned}$$

where

$$H_{\xi 0}^i = -H_\rho^i(\rho, \hat{z}) = -H_\rho^i(a\sqrt{1-\xi^2}, h)$$

$$H_{\xi 0} = \sum_{n, \text{odd}}^{\infty} A_n \frac{1}{a\xi} P_n^1(\xi) Q_n(j0)$$

Thus

$$\begin{aligned} F_z &\sim 4\mu_0 a \pi \sum_{n, \text{odd}}^{\infty} A_n Q_n(j0) \int_0^1 H_\rho^i(\rho, h) P_n^1(\xi) d\xi \\ &\sim 4\mu_0 a \pi \sum_{n, \text{odd}}^{\infty} \hat{A}_n \frac{Q_n(j0)}{jQ_n'(j0)} \int_0^1 H_\rho^i(\rho, h) P_n^1(\xi) d\xi \end{aligned}$$

where again the “hat” coefficients are normalized.

5.7 Torque for Small Displacement Approximation

Taking the limit of small d in the previous expression gives

$$\begin{aligned} \tau_y &= 4\mu_0 a^2 \int_0^\pi \int_0^1 (H_\xi^i H_\xi + H_\varphi^i H_\varphi) \sqrt{1 - \xi^2} \xi d\xi \cos \varphi d\varphi \\ &\sim 4\mu_0 a^2 \int_0^\pi \int_0^1 \{ (H_{\xi 0}^i + H_{\xi 1}^i d \cos \varphi) (H_{\xi 0} + H_{\xi 1} d \cos \varphi) + H_{\varphi 1}^i d \sin \varphi H_{\varphi 1} d \sin \varphi \} \sqrt{1 - \xi^2} \xi d\xi \cos \varphi d\varphi \\ &\sim 4\mu_0 a^2 d \int_0^\pi \int_0^1 (H_{\xi 0}^i H_{\xi 1} + H_{\xi 0} H_{\xi 1}^i) \sqrt{1 - \xi^2} \xi d\xi \cos^2 \varphi d\varphi \\ &\sim 2\pi \mu_0 a^2 d \int_0^1 (H_{\xi 0}^i H_{\xi 1} + H_{\xi 0} H_{\xi 1}^i) \sqrt{1 - \xi^2} \xi d\xi \end{aligned}$$

where

$$\begin{aligned} H_{\xi 1}^i &= \frac{\partial H_\rho}{\partial \rho}(\rho, \hat{z}) = \frac{\partial H_\rho}{\partial \rho}(\rho, h) \\ H_{\xi 1} &= - \sum_{n, \text{even}}^{\infty} A_{1n} \frac{1}{a d \xi} \left[n(n+1) P_n(\xi) + \frac{\xi}{\sqrt{1 - \xi^2}} P_n^1(\xi) \right] Q_n^1(j0) \end{aligned}$$

5.8 Strip Coil Excitation and Results

The above equations for small displacement d have been implemented in computer program. The exciting fields (and their derivatives with respect to d) have been integrated with respect to the loop diameter b to generate uniform current density circular strips. The levitation strip extends from a radius $b_{\ell \min}$ to a radius $b_{\ell \max}$ and has azimuthal current density $K_\ell = I_\ell n_\ell / (b_{\ell \max} - b_{\ell \min})$, where I_ℓ is the levitation current per turn and this coil is considered to consist of n_ℓ turns. The stability strip extends from a radius $b_{s \min}$ to a radius $b_{s \max}$ and has azimuthal current density $K_s = I_s / (b_{s \max} - b_{s \min})$, where I_s is the stability coil current.

The disc of radius a is a distance h above the coils and is displaced a small distance d from the coil center along the x axis. The parameters taken in this example are $a \approx 250 \mu\text{m}$, $b_{\ell \min} \approx 100 \mu\text{m}$, $b_{\ell \max} \approx 250 \mu\text{m}$,

$n_\ell = 3$, $b_{s\min} \approx 250 \mu\text{m}$, $b_{s\max} \approx 300 \mu\text{m}$, $h \approx 20 \mu\text{m}$. These choices correspond to a set of experimental apparatus that was constructed several years ago. Figure 3b shows a micrograph of the stator coils in this device. The outer coil was the stability coil. The next three coils inward were driven in series as the levitation coil (the inner circular strip was not used). The disc radius was the same as the small gap between the levitation and stability coils. A stable selection of currents used in the experiment were $I_s \approx -1.2 \text{ A}$ rms and $I_\ell \approx 0.9 \text{ A}$ rms at $f = 10 \text{ MHz}$.

The lateral force results from the disc can be written in terms of the two currents as (here we have arbitrarily set $d = 1 \mu\text{m}$)

$$F_x = AI_s^2 + BI_sI_\ell + CI_\ell^2$$

Three calculations thus determine the coefficients. If $I_s = 0$, $I_\ell = 0.9 \text{ A}$ we find

$$F_x \approx 1.476806 \times 10^{-8} \text{ N}$$

$$C = 1.823216 \times 10^{-8} \text{ N/A}^2$$

If $I_s = -1.2 \text{ A}$, $I_\ell = 0$ we find that

$$F_x \approx -3.9276033 \times 10^{-9} \text{ N}$$

$$A = -2.72750 \times 10^{-9} \text{ N/A}^2$$

If $I_s = -1.2 \text{ A}$, $I_\ell = 0.9 \text{ A}$ we find

$$F_x \approx -7.0259085 \times 10^{-8} \text{ N}$$

$$B = 7.509217 \times 10^{-8} \text{ N/A}^2$$

We then have the quadratic equation for zero force with $x = I_s/I_\ell$

$$0 = Ax^2 + Bx + C$$

The solutions are

$$x = I_s/I_\ell = \frac{-B \pm \sqrt{B^2 - 4AC}}{2A} \approx 27.77216, -0.240693$$

The fact that there is both a positive and negative solution is similar to the half plane model above (although the values are a little different). Figure 3c shows a plot of the disc lateral force (dotted curve). The half plane result that was illustrated in Figure 2d is also shown (solid curve). The simplified half plane result (small d and large b_ℓ) is also shown (dash-dot curve). Restoring force is indicated by negative values. Notice that the half plane analysis is fairly accurate in the region of reasonably sized currents.

Figure 3d shows the vertical disc force as a function of stability current for this example. Figure 3e shows the total azimuthal current density on the disc as a function of radius for various stability current levels. Notice that for $I_s < -0.2$ the current density at the edge $\rho = a$ is positive (the same sign as the levitation current below the disc). The change in sign of the edge current occurs at $I_s \approx -0.19 \text{ A}$. The change in sign of lateral force on the disc occurs in Figure 3c at $I_s \approx -0.21 \text{ A}$. These values are very nearly the same as in the half plane analysis.

5.9 Forces for Simplified Loop Geometries

This section simplifies the oblate spheroidal solution further by considering the case where a single loop stator coil and the disc are far apart in z . This gives a dipole field excitation of the disc that is unstable. Finally the case where the single loop stator is much larger in diameter than the disc is considered that is stable. Both treatments assume that d is small.

5.9.1 small displacement large distance apart

To simplify the problem further and develop some insight with regard to the stability issue, we will take the coil and disc to be far apart, such that the modal series in n can be approximated as well as approximating the incident field. It is convenient to start from the spherical loop expansion in this limit to approximate the incident field for $b \ll h$.

$$\begin{aligned} A_{\varphi}^i(r, \theta) &= \mu_0 I \sum_{n=0}^{\infty} \frac{(-1)^{n+1} (2n-1)!!}{2^{n+2} (n+1)!} \frac{br_{<}^{2n+1}}{r_{>}^{2n+2}} P_{2n+1}^1(\cos \theta) \\ &\sim -\frac{\mu_0 I b^2}{2^2 r^2} P_1^1(\cos \theta) + \frac{\mu_0 I b^4}{2^4 r^4} P_3^1(\cos \theta) \\ &\sim \frac{\mu_0 I b^2}{4 r^2} \sin \theta \left[1 + \frac{3 b^2}{8 r^2} (5 \sin^2 \theta - 4) \right] \end{aligned}$$

where

$$\begin{aligned} P_1^1(\xi) &= -\sqrt{1-\xi^2} \\ P_3^1(\xi) &= -\frac{3}{2} \sqrt{1-\xi^2} (5\xi^2 - 1) = -6\sqrt{1-\xi^2} + \frac{15}{2} (1-\xi^2)^{3/2} \end{aligned}$$

The first term is the dipole term

$$A_{\varphi}^i(r, \theta) \sim \frac{\mu_0 I \pi b^2}{4\pi r^2} \sin \theta$$

or

$$\underline{A} = \mu_0 \frac{\underline{m} \times \underline{r}}{4\pi r^3} = -\frac{\mu_0}{4\pi} \underline{m} \times \nabla \left(\frac{1}{r} \right)$$

where the dipole moment is

$$\underline{m} = I \pi b^2 \underline{e}_z$$

We can also find the field of the dipole via the scalar potential

$$\phi_m = \frac{\underline{m} \cdot \underline{r}}{4\pi r^3}$$

or

$$\phi_m^{id} = \frac{mz}{4\pi (x^2 + y^2 + z^2)^{3/2}}$$

$$H_z^{id} = -\frac{\partial \phi_m^{id}}{\partial z} = \frac{m(2z^2 - x^2 - y^2)}{4\pi(x^2 + y^2 + z^2)^{5/2}}$$

If $x^2 + y^2 = \rho^2 = 0$ then $H_z^{id} = m/(2\pi z^3)$. The exact field on the axis of a loop is $H_z^i = (Ib^2/2)/(b^2 + z^2)^{3/2}$. Let us take $z = h$ and $x \rightarrow x + d$

$$H_z^{id} = \frac{m[2h^2 - (x+d)^2 - y^2]}{4\pi[(x+d)^2 + y^2 + h^2]^{5/2}}$$

Now let us take d small, $x = \rho \cos \varphi$, and $y = \rho \sin \varphi$

$$H_z^{id} = \frac{m[2h^2 - 2\rho d \cos \varphi - \rho^2]}{4\pi[2\rho d \cos \varphi + \rho^2 + h^2]^{5/2}} \sim \frac{m(2h^2 - \rho^2)}{4\pi(\rho^2 + h^2)^{5/2}} - \frac{m\rho}{4\pi(\rho^2 + h^2)^{5/2}} \left(2 + 5\frac{2h^2 - \rho^2}{\rho^2 + h^2}\right) d \cos \varphi$$

Thus setting $\rho = a\sqrt{1 - \xi^2}$ gives

$$H_z^{id} \sim H_{z0}^{id}(\xi) + H_{z1}^{id}(\xi) d \cos \varphi$$

$$H_{z0}^{id}(\xi) = \frac{m\{2h^2 - a^2(1 - \xi^2)\}}{4\pi\{h^2 + a^2(1 - \xi^2)\}^{5/2}}$$

$$H_{z1}^{id}(\xi) = -\frac{ma\sqrt{1 - \xi^2}}{4\pi\{h^2 + a^2(1 - \xi^2)\}^{5/2}} \left\{2 + 5\frac{2h^2 - a^2(1 - \xi^2)}{h^2 + a^2(1 - \xi^2)}\right\}$$

The approximation of the series in n also requires $h \gg a$ so that the dipole incident field remains smooth over the disc radius. Thus we might further simplify to

$$H_{z0}^{id} \sim \frac{m}{2\pi h^3}$$

$$H_{z1}^{id}(\xi) \sim -\frac{3ma}{\pi h^5} \sqrt{1 - \xi^2}$$

The dipole field force is

$$F_x^d \sim -2\pi\mu_0 a^2 d \int_0^1 \xi d\xi [H_{z0}^{id}(H_{\xi1} + H_{\varphi1}) + H_{z1}^{id}H_{\xi0}]$$

where now we can take only the first two terms of the modal expansion

$$\begin{aligned} H_\xi &\sim -A_1 \frac{1}{a\xi} \sqrt{1 - \xi^2} P_1'(\xi) Q_1(j0) - \cos \varphi A_{12} \frac{1}{a\xi} \sqrt{1 - \xi^2} P_2^{1'}(\xi) Q_2^1(j0) \\ &\sim A_1 \frac{1}{a\xi} P_1^1(\xi) Q_1(j0) - \cos \varphi A_{12} \frac{1}{a\xi} \left[6P_2(\xi) + \frac{\xi}{\sqrt{1 - \xi^2}} P_2^1(\xi) \right] Q_2^1(j0) \\ &\sim H_{\xi0}(\xi) + H_{\xi1}(\xi) d \cos \varphi \end{aligned}$$

$$H_\varphi \sim \sin \varphi A_{12} \frac{1}{a\sqrt{1-\xi^2}} P_2^1(\xi) Q_2^1(j0) \\ \sim H_{\varphi 1}(\xi) d \sin \varphi$$

$$A_1 \sim \frac{3a}{jQ_1'(j0)} \int_0^1 H_{z0}^i(\xi) P_1(\xi) \xi d\xi$$

$$A_{12} \sim ad \frac{5/6}{jQ_2^{1'}(j0)} \int_0^1 H_{z1}^i(\xi) P_2^1(\xi) \xi d\xi$$

The Legendre functions are

$$P_1(\xi) = \xi$$

$$P_2(\xi) = \frac{1}{2} (3\xi^2 - 1)$$

$$P_1^1(\xi) = -\sqrt{1-\xi^2}$$

$$P_2^1(\xi) = -3\xi\sqrt{1-\xi^2}$$

$$\frac{jQ_n^{m'}(j0)}{Q_n^m(j0)} = (m+n)(n-m+1) \frac{Q_n^{m-1}(j0)}{Q_n^m(j0)} = -(m+n)(n-m+1) \frac{\Gamma(\frac{n+m}{2}) \Gamma(1+\frac{n-m}{2})}{2\Gamma(1+\frac{n-m+1}{2}) \Gamma(\frac{n+m+1}{2})}$$

$$\frac{jQ_1'(j0)}{Q_1(j0)} = -\frac{\pi}{2}$$

$$\frac{jQ_2^{1'}(j0)}{Q_2^1(j0)} = -\frac{3\pi}{4}$$

Using these we find

$$A_1 \sim \frac{3a}{jQ_1'(j0)} \int_0^1 H_{z0}^{id}(\xi) \xi^2 d\xi$$

$$A_{12} \sim -ad \frac{5/2}{jQ_2^{1'}(j0)} \int_0^1 H_{z1}^{id}(\xi) \sqrt{1-\xi^2} \xi^2 d\xi$$

$$H_{\xi 0}(\xi) = -A_1 \frac{1}{a\xi} \sqrt{1-\xi^2} Q_1(j0)$$

$$H_{\xi 1}(\xi) d = -A_{12} \frac{3}{a\xi} (2\xi^2 - 1) Q_2^1(j0)$$

$$H_{\varphi 1}(\xi) d = -A_{12} \frac{3\xi}{a} Q_2^1(j0)$$

or upon inserting the coefficients

$$\begin{aligned}
H_{\xi 0}(\xi) &\sim \frac{6}{\pi \xi} \sqrt{1 - \xi^2} \int_0^1 H_{z0}^{id}(\xi) \xi^2 d\xi \\
H_{\xi 1}(\xi) &\sim -\frac{10}{\pi \xi} (2\xi^2 - 1) \int_0^1 H_{z1}^{id}(\xi) \sqrt{1 - \xi^2} \xi^2 d\xi \\
H_{\varphi 1}(\xi) &\sim -\frac{10\xi}{\pi} \int_0^1 H_{z1}^{id}(\xi) \sqrt{1 - \xi^2} \xi^2 d\xi
\end{aligned}$$

Now inserting the approximated dipole fields gives

$$\begin{aligned}
H_{\xi 0}(\xi) &\sim \frac{m}{\pi^2 h^3} \frac{1}{\xi} \sqrt{1 - \xi^2} \\
H_{\xi 1}(\xi) &\sim \frac{4ma}{\pi^2 h^5} \frac{1}{\xi} (2\xi^2 - 1) \\
H_{\varphi 1}(\xi) &\sim \frac{4ma}{\pi^2 h^5} \xi
\end{aligned}$$

Inserting these and the approximated dipole fields into the force gives

$$\begin{aligned}
H_{z0}^{id} &\sim \frac{m}{2\pi h^3} \\
H_{z1}^{id}(\xi) &\sim -\frac{3ma}{\pi h^5} \sqrt{1 - \xi^2}
\end{aligned}$$

The dipole field force is

$$\begin{aligned}
F_x^d &\sim -2\pi\mu_0 a^2 d \int_0^1 \xi d\xi [H_{z0}^{id} \{H_{\xi 1} + H_{\varphi 1}\} + H_{z1}^{id} H_{\xi 0}] \\
&\sim -\mu_0 d \frac{2m^2 a^3}{\pi^2 h^8} \int_0^1 d\xi [2\{(2\xi^2 - 1) + \xi^2\} - 3(1 - \xi^2)] \\
&\sim -\mu_0 d \frac{2m^2 a^3}{\pi^2 h^8} \int_0^1 d\xi [(9\xi^2 - 5)] \\
&\sim -\mu_0 d \frac{2m^2 a^3}{\pi^2 h^8} (3 - 5) \\
&\sim \mu_0 d \frac{4m^2 a^3}{\pi^2 h^8}
\end{aligned}$$

This case appears to be unstable since the coil is centered at $x = -d$ and the force is in the positive x direction. We really need to also look at the torque τ_y to see if the movement is accompanied by any tilt that might in turn change the force. But first we calculate the vertical force.

$$F_z^d \sim -4\mu_0 a^2 \pi \int_0^1 \xi d\xi H_{\xi 0}^{id} H_{\xi 0}$$

$$\phi_m^{id} = \frac{mz}{4\pi(\rho^2 + z^2)^{3/2}}$$

$$H_\rho^{id} = -\frac{\partial \phi_m^{id}}{\partial \rho} = \frac{3m\rho z}{4\pi(\rho^2 + z^2)^{5/2}}$$

Setting $z = h$ and $\rho = a\sqrt{1 - \xi^2}$ gives

$$H_\xi^{id} = -\frac{3mha\sqrt{1 - \xi^2}}{4\pi\{a^2(1 - \xi^2) + h^2\}^{5/2}}$$

Expanding for large h

$$H_\xi^{id} \sim -\frac{3ma}{4\pi h^4} \sqrt{1 - \xi^2}$$

Inserting into the force formula gives

$$F_z^d \sim \mu_0 \frac{3m^2 a^3}{\pi^2 h^7} \int_0^1 d\xi (1 - \xi^2)$$

$$\sim \mu_0 \frac{2m^2 a^3}{\pi^2 h^7}$$

5.9.2 small displacement large exciting loop

Next we take the limit that $b \gg h$. The magnetic field from the loop in this limit is

$$A_\varphi^i(r, \theta) = \mu_0 I \sum_{n=0}^{\infty} \frac{(-1)^{n+1} (2n-1)!!}{2^{n+2} (n+1)!} \frac{br_{<}^{2n+1}}{r_{>}^{2n+2}} P_{2n+1}^1(\cos \theta)$$

$$= \mu_0 I \sum_{n=0}^{\infty} \frac{(-1)^{n+1} (2n-1)!!}{2^{n+2} (n+1)!} \frac{r^{2n+1}}{b^{2n+1}} P_{2n+1}^1(\cos \theta)$$

$$\sim \mu_0 I \frac{r}{4b} \sin \theta - \mu_0 I \frac{3r^3}{32b^3} \sin \theta (5 \cos^2 \theta - 1)$$

or

$$A_\varphi^{ib} = \mu_0 I \frac{\rho}{4b} - \mu_0 I \frac{3\rho}{32b^3} (4z^2 - \rho^2)$$

The field for large b is

$$\mu_0 H_z^{ib} = \frac{\partial A_\varphi^{ib}}{\partial \rho} + \frac{1}{\rho} A_\varphi^{ib} = \mu_0 I \frac{1}{2b} \left[1 - \frac{3}{4b^2} (2z^2 - \rho^2) \right]$$

$$\mu_0 H_\rho^{ib} = -\frac{\partial A_\varphi^{ib}}{\partial z} = \mu_0 I \frac{3\rho}{4b^3} z$$

Now we displace ρ to $\hat{\rho}$ (in the unit vector as well).

$$\underline{e}_\rho = \underline{e}_x \cos \varphi + \underline{e}_y \sin \varphi$$

The final term resulting from $H_{z1}^{ib}H_{\xi0}$ is larger in magnitude than the first terms resulting from $H_{z0}^{ib}(H_{\xi1} + H_{\varphi1})$. Thus the final term is the term responsible for flipping the sign of the force to a negative quantity. The total result is

$$F_x^b \sim -\mu_0 I^2 \frac{a^3}{b^4} d \left[1 + \frac{2a^2}{5b^2} - \frac{3h^2}{2b^2} \right]$$

If the first term is dominant, then the force is negative and stability is indicated. Perhaps it is $\partial H_z^i / \partial \rho > 0$ that is required as in the case of the loop.

Now the axial force is

$$\begin{aligned} F_z^b &\sim -4\mu_0 a^2 \pi \int_0^1 \xi d\xi H_{\xi0}^{ib} H_{\xi0} \\ &\sim 2\mu_0 I^2 \frac{a^3}{b^4} h \left[1 - \frac{3}{2b^2} (h^2 - a^2/5) \right] \end{aligned}$$

If the first term is dominant, then the force is positive and levitation is possible.

5.10 Torques for Simplified Loop Geometries

This section looks at the corresponding torque for the two simplified geometries of large z spacing and large loop diameter. Again both treatments assume that d is small.

5.10.1 small displacement large distance apart

Now we take in addition that h is large

$$\tau_y^d \sim 2\pi\mu_0 a^2 d \int_0^1 (H_{\xi0}^{id} H_{\xi1} + H_{\xi0} H_{\xi1}^{id}) \sqrt{1 - \xi^2} \xi d\xi$$

where

$$\begin{aligned} H_{\xi0}(\xi) &\sim \frac{m}{\pi^2 h^3} \frac{1}{\xi} \sqrt{1 - \xi^2} \\ H_{\xi1}(\xi) &\sim \frac{4ma}{\pi^2 h^5} \frac{1}{\xi} (2\xi^2 - 1) \end{aligned}$$

The dipole potential is

$$\phi_m^{id} = \frac{mz}{4\pi (x^2 + y^2 + z^2)^{3/2}}$$

Taking $x \rightarrow x + d$

$$\begin{aligned} \phi_m^{id} &= \frac{mz}{4\pi \left\{ (x+d)^2 + y^2 + z^2 \right\}^{3/2}} \sim \frac{mz}{4\pi \left\{ \rho^2 + 2\rho d \cos \varphi + z^2 \right\}^{3/2}} \\ H_\rho^{id} &= -\frac{\partial \phi_m^{id}}{\partial \rho} \sim \frac{3mz(\rho + d \cos \varphi)}{4\pi \left\{ \rho^2 + 2\rho d \cos \varphi + z^2 \right\}^{5/2}} \sim \frac{3mz\rho}{4\pi (\rho^2 + z^2)^{5/2}} \left\{ 1 + \left(\frac{1}{\rho} - \frac{5\rho}{\rho^2 + z^2} \right) d \cos \varphi \right\} \end{aligned}$$

$$\phi_m^{id} = \frac{mz}{4\pi(\rho^2 + z^2)^{3/2}}$$

$$H_\rho^{id} = -\frac{\partial \phi_m^{id}}{\partial \rho} = \frac{3m\rho z}{4\pi(\rho^2 + z^2)^{5/2}}$$

Setting $z = h$ and $\rho = a\sqrt{1 - \xi^2}$ gives

$$H_\xi^{id} = -\frac{3mha\sqrt{1 - \xi^2}}{4\pi\{a^2(1 - \xi^2) + h^2\}^{5/2}}$$

Expanding for large h

$$H_\xi^{id} \sim -\frac{3ma}{4\pi h^4} \sqrt{1 - \xi^2}$$

Inserting into the force formula gives

$$F_z^d \sim \mu_0 \frac{3m^2 a^3}{\pi^2 h^7} \int_0^1 d\xi (1 - \xi^2)$$

$$\sim \mu_0 \frac{2m^2 a^3}{\pi^2 h^7}$$

5.9.2 small displacement large exciting loop

Next we take the limit that $b \gg h$. The magnetic field from the loop in this limit is

$$A_\varphi^i(r, \theta) = \mu_0 I \sum_{n=0}^{\infty} \frac{(-1)^{n+1} (2n-1)!!}{2^{n+2} (n+1)!} \frac{br_{<}^{2n+1}}{r_{>}^{2n+2}} P_{2n+1}^1(\cos \theta)$$

$$= \mu_0 I \sum_{n=0}^{\infty} \frac{(-1)^{n+1} (2n-1)!!}{2^{n+2} (n+1)!} \frac{r^{2n+1}}{b^{2n+1}} P_{2n+1}^1(\cos \theta)$$

$$\sim \mu_0 I \frac{r}{4b} \sin \theta - \mu_0 I \frac{3r^3}{32b^3} \sin \theta (5 \cos^2 \theta - 1)$$

or

$$A_\varphi^{ib} = \mu_0 I \frac{\rho}{4b} - \mu_0 I \frac{3\rho}{32b^3} (4z^2 - \rho^2)$$

The field for large b is

$$\mu_0 H_z^{ib} = \frac{\partial A_\varphi^{ib}}{\partial \rho} + \frac{1}{\rho} A_\varphi^{ib} = \mu_0 I \frac{1}{2b} \left[1 - \frac{3}{4b^2} (2z^2 - \rho^2) \right]$$

$$\mu_0 H_\rho^{ib} = -\frac{\partial A_\varphi^{ib}}{\partial z} = \mu_0 I \frac{3\rho}{4b^3} z$$

Now we displace ρ to $\hat{\rho}$ (in the unit vector as well).

$$\underline{e}_\rho = \underline{e}_x \cos \varphi + \underline{e}_y \sin \varphi$$

$$\begin{aligned}
\mathbf{e}_{\hat{\rho}} &= \mathbf{e}_x \cos \hat{\varphi} + \mathbf{e}_y \sin \hat{\varphi} \\
&= \mathbf{e}_x \frac{x+d}{\hat{\rho}} + \mathbf{e}_y \frac{y}{\hat{\rho}} = \mathbf{e}_x \frac{x+d}{\sqrt{(x+d)^2 + y^2}} + \mathbf{e}_y \frac{y}{\sqrt{(x+d)^2 + y^2}} \\
&\sim \mathbf{e}_x \frac{(x+d)}{\rho} \left(1 - \frac{d}{\rho^2} x\right) + \mathbf{e}_y \frac{y}{\rho} \left(1 - \frac{d}{\rho^2} x\right)
\end{aligned}$$

or

$$\begin{aligned}
\mathbf{e}_{\hat{\rho}} &\sim \mathbf{e}_x \cos \varphi \left(1 - \frac{d}{\rho^2} x\right) + \mathbf{e}_y \sin \varphi \left(1 - \frac{d}{\rho^2} x\right) + \mathbf{e}_x \frac{d}{\rho} \\
&\sim \mathbf{e}_x \frac{d}{\rho} + \mathbf{e}_{\rho} \left(1 - \frac{d}{\rho} \cos \varphi\right) \sim \mathbf{e}_{\rho} - \mathbf{e}_{\varphi} \frac{d}{\rho} \sin \varphi \\
\mathbf{e}_x &= \mathbf{e}_{\rho} \cos \varphi - \mathbf{e}_{\varphi} \sin \varphi \\
\hat{\rho} &= \sqrt{(x+d)^2 + y^2} = \rho \left(1 + \frac{d}{\rho} \cos \varphi\right)
\end{aligned}$$

Thus setting $z = h$ gives

$$\begin{aligned}
H_z^{ib} &\sim I \frac{1}{2b} \left[1 - \frac{3}{4b^2} (2h^2 - \hat{\rho}^2)\right] \sim I \frac{1}{2b} \left[1 - \frac{3}{4b^2} (2h^2 - \rho^2 - 2d\rho \cos \varphi)\right] \\
&\sim H_{z0}^{ib} + H_{z1}^{ib} d \cos \varphi
\end{aligned}$$

or

$$\begin{aligned}
H_{z0}^{ib} &\sim \frac{I}{2b} \left[1 - \frac{3}{4b^2} (2h^2 - \rho^2)\right] = \frac{I}{2b} \left[1 - \frac{3}{4b^2} \{2h^2 - a^2 (1 - \xi^2)\}\right] \\
H_{z1}^{ib} &\sim I \frac{3\rho}{4b^3} = I \frac{3}{4b^3} a \sqrt{1 - \xi^2} \\
H_{\rho}^{ib} &\sim I \frac{3h\hat{\rho}}{4b^3} \sim I \frac{3h}{4b^3} (\rho + d \cos \varphi) \sim H_{\rho 0}^{ib} + H_{\rho 1}^{ib} d \cos \varphi \\
H_{\rho 0}^{ib} &\sim I \frac{3h}{4b^3} a \sqrt{1 - \xi^2} \sim -H_{\xi 0}^{ib} \\
H_{\rho 1}^{ib} &\sim I \frac{3h}{4b^3} \sim -H_{\xi 1}^{ib} \\
H_{\varphi}^{ib} &\sim -I \frac{3\hat{\rho}}{4b^3} \frac{d}{\rho} h \sin \varphi \sim -I \frac{3d}{4b^3} h \sin \varphi \sim H_{\varphi 1}^{ib} d \sin \varphi \\
H_{\varphi 1}^{ib} &\sim -I \frac{3h}{4b^3}
\end{aligned}$$

Because of the smoothness of the exciting field at the disc we can approximate the field with only a few terms. The force is again

$$F_x^b \sim -2\pi\mu_0 a^2 d \int_0^1 \xi d\xi [H_{z0}^{ib} (H_{\xi 1} + H_{\varphi 1}) + H_{z1}^{ib} H_{\xi 0}]$$

where

$$\begin{aligned} H_{\xi 0}(\xi) &\sim \frac{6}{\pi\xi} \sqrt{1-\xi^2} \int_0^1 H_{z0}^{ib}(\xi) \xi^2 d\xi \\ &\sim \frac{3I}{\pi b} \frac{1}{\xi} \sqrt{1-\xi^2} \int_0^1 \left[1 - \frac{3}{4b^2} \{2h^2 - a^2(1-\xi^2)\} \right] \xi^2 d\xi \\ &\sim \frac{I}{\pi b} \left[1 - \frac{3}{2b^2} (h^2 - a^2/5) \right] \frac{1}{\xi} \sqrt{1-\xi^2} \\ H_{\xi 1}(\xi) &\sim -\frac{10}{\pi\xi} (2\xi^2 - 1) \int_0^1 H_{z1}^{ib}(\xi) \sqrt{1-\xi^2} \xi^2 d\xi \\ &\sim -I \frac{15a}{2\pi b^3} \frac{1}{\xi} (2\xi^2 - 1) \int_0^1 (1-\xi^2) \xi^2 d\xi \\ &\sim -I \frac{a}{\pi b^3} \frac{1}{\xi} (2\xi^2 - 1) \\ H_{\varphi 1}(\xi) &\sim -\frac{10\xi}{\pi} \int_0^1 H_{z1}^{ib}(\xi) \sqrt{1-\xi^2} \xi^2 d\xi \\ &\sim -I \frac{15a}{2\pi b^3} \xi \int_0^1 (1-\xi^2) \xi^2 d\xi \\ &\sim -I \frac{a}{\pi b^3} \xi \end{aligned}$$

Inserting into the force formula gives

$$\begin{aligned} F_x^b &\sim -2\pi\mu_0 a^2 d \int_0^1 \xi d\xi [H_{z0}^{ib} (H_{\xi 1} + H_{\varphi 1}) + H_{z1}^{ib} H_{\xi 0}] \\ &\sim \mu_0 I^2 \frac{a^3}{b^4} d \int_0^1 d\xi \left[\left(1 - \frac{3}{4b^2} \{2h^2 - a^2(1-\xi^2)\} \right) \{-(1-2\xi^2) + (\xi^2)\} - \frac{3}{2} \left\{ 1 - \frac{3}{2b^2} (h^2 - a^2/5) \right\} (1-\xi^2) \right] \\ &\sim \mu_0 I^2 \frac{a^3}{b^4} d \int_0^1 d\xi \left[- \left(1 - \frac{3}{4b^2} \{2h^2 - a^2(1-\xi^2)\} \right) (1-3\xi^2) - \frac{3}{2} \left\{ 1 - \frac{3}{2b^2} (h^2 - a^2/5) \right\} (1-\xi^2) \right] \\ &\sim \mu_0 I^2 \frac{a^3}{b^4} d \left[-\frac{2a^2}{5b^2} - 1 + \frac{3h^2}{2b^2} \right] \end{aligned}$$

The final term resulting from $H_{z1}^{ib}H_{\xi0}$ is larger in magnitude than the first terms resulting from $H_{z0}^{ib}(H_{\xi1} + H_{\varphi1})$. Thus the final term is the term responsible for flipping the sign of the force to a negative quantity. The total result is

$$F_x^b \sim -\mu_0 I^2 \frac{a^3}{b^4} d \left[1 + \frac{2a^2}{5b^2} - \frac{3h^2}{2b^2} \right]$$

If the first term is dominant, then the force is negative and stability is indicated. Perhaps it is $\partial H_z^i / \partial \rho > 0$ that is required as in the case of the loop.

Now the axial force is

$$\begin{aligned} F_z^b &\sim -4\mu_0 a^2 \pi \int_0^1 \xi d\xi H_{\xi0}^{ib} H_{\xi0} \\ &\sim 2\mu_0 I^2 \frac{a^3}{b^4} h \left[1 - \frac{3}{2b^2} (h^2 - a^2/5) \right] \end{aligned}$$

If the first term is dominant, then the force is positive and levitation is possible.

5.10 Torques for Simplified Loop Geometries

This section looks at the corresponding torque for the two simplified geometries of large z spacing and large loop diameter. Again both treatments assume that d is small.

5.10.1 small displacement large distance apart

Now we take in addition that h is large

$$\tau_y^d \sim 2\pi\mu_0 a^2 d \int_0^1 (H_{\xi0}^{id} H_{\xi1} + H_{\xi0} H_{\xi1}^{id}) \sqrt{1 - \xi^2} \xi d\xi$$

where

$$H_{\xi0}(\xi) \sim \frac{m}{\pi^2 h^3} \frac{1}{\xi} \sqrt{1 - \xi^2}$$

$$H_{\xi1}(\xi) \sim \frac{4ma}{\pi^2 h^5} \frac{1}{\xi} (2\xi^2 - 1)$$

The dipole potential is

$$\phi_m^{id} = \frac{mz}{4\pi (x^2 + y^2 + z^2)^{3/2}}$$

Taking $x \rightarrow x + d$

$$\phi_m^{id} = \frac{mz}{4\pi \left\{ (x+d)^2 + y^2 + z^2 \right\}^{3/2}} \sim \frac{mz}{4\pi \left\{ \rho^2 + 2\rho d \cos \varphi + z^2 \right\}^{3/2}}$$

$$H_\rho^{id} = -\frac{\partial \phi_m^{id}}{\partial \rho} \sim \frac{3mz(\rho + d \cos \varphi)}{4\pi \left\{ \rho^2 + 2\rho d \cos \varphi + z^2 \right\}^{5/2}} \sim \frac{3mz\rho}{4\pi (\rho^2 + z^2)^{5/2}} \left\{ 1 + \left(\frac{1}{\rho} - \frac{5\rho}{\rho^2 + z^2} \right) d \cos \varphi \right\}$$

Now setting $z = h$

$$H_\rho^{id} \sim \frac{3mh\rho}{4\pi(\rho^2 + h^2)^{5/2}} \left\{ 1 + \left(\frac{1}{\rho} - \frac{5\rho}{\rho^2 + h^2} \right) d \cos \varphi \right\}$$

Transforming to spheroidal coordinates

$$H_\xi^{id} \sim -\frac{3mha\sqrt{1-\xi^2}}{4\pi\{h^2 + a^2(1-\xi^2)\}^{5/2}} \left[1 + \left\{ \frac{1}{a\sqrt{1-\xi^2}} - \frac{5a\sqrt{1-\xi^2}}{a^2(1-\xi^2) + h^2} \right\} d \cos \varphi \right]$$

Thus for large h

$$H_{\xi 0}^{id} = -\frac{3mha\sqrt{1-\xi^2}}{4\pi\{h^2 + a^2(1-\xi^2)\}^{5/2}} \sim -\frac{3ma}{4\pi h^4} \sqrt{1-\xi^2}$$

$$H_{\xi 1}^{id} = -\frac{3mha\sqrt{1-\xi^2}}{4\pi\{h^2 + a^2(1-\xi^2)\}^{5/2}} \left\{ \frac{1}{a\sqrt{1-\xi^2}} - \frac{5a\sqrt{1-\xi^2}}{a^2(1-\xi^2) + h^2} \right\} \sim -\frac{3m}{4\pi h^4}$$

Inserting into the torque formula yields

$$\tau_y^d \sim -2\mu_0 \frac{3m^2 a^2}{\pi^2 h^7} d \int_0^1 \left[-\frac{a^2}{h^2} (1-2\xi^2) + \frac{1}{4} \right] (1-\xi^2) d\xi$$

$$\sim -2\mu_0 \frac{2m^2 a^2}{\pi^2 h^7} d \left(-\frac{3}{5} \frac{a^2}{h^2} + \frac{1}{4} \right) \sim -\mu_0 \frac{m^2 a^2}{\pi^2 h^7} d$$

Thus the contribution from $H_{\xi 0}^i H_{\xi 1}^i$ is dominant for large h .

5.10.2 small displacement large exciting loop

Now we take in addition that b is large

$$\tau_y^b \sim 2\pi\mu_0 a^2 d \int_0^1 (H_{\xi 0}^{ib} H_{\xi 1}^i + H_{\xi 0}^i H_{\xi 1}^{ib}) \sqrt{1-\xi^2} \xi d\xi$$

The field coefficients are

$$H_{\xi 0}^{ib} \sim -I \frac{3h}{4b^3} a \sqrt{1-\xi^2}$$

$$H_{\xi 1}^{ib} \sim -I \frac{3h}{4b^3}$$

$$H_{\xi 0}^i(\xi) \sim \frac{I}{\pi b} \left[1 - \frac{3}{2b^2} (h^2 - a^2/5) \right] \frac{1}{\xi} \sqrt{1-\xi^2}$$

$$H_{\xi 1}^i(\xi) \sim -I \frac{a}{\pi b^3} \frac{1}{\xi} (2\xi^2 - 1)$$

Thus

$$\tau_y^b \sim \mu_0 I^2 \frac{3ha^2}{2b^4} d \int_0^1 \left[-\frac{a^2}{b^2} (1-2\xi^2) - \left\{ 1 - \frac{3}{2b^2} (h^2 - a^2/5) \right\} \right] (1-\xi^2) d\xi$$

$$\sim \mu_0 I^2 \frac{ha^2}{b^4} d \left[-\frac{3}{5} \frac{a^2}{b^2} - \left\{ 1 - \frac{3}{2b^2} (h^2 - a^2/5) \right\} \right] = \mu_0 I^2 \frac{ha^2}{b^4} d \left(-\frac{3}{10} \frac{a^2}{b^2} - 1 + \frac{3}{2} \frac{h^2}{b^2} \right)$$

$$\sim -\mu_0 I^2 \frac{ha^2}{b^4} d$$

Now for large b the $H_{\xi 0} H_{\xi 1}^{ib}$ contribution is dominant and the torque is negative.

6 CONCLUSIONS

This report discusses the levitation forces and lateral restoring forces for a perfectly conducting disc above stator electrodes. Oblate spheroidal coordinates are used to solve for the disc currents excited by uniformly distributed stator strip electrodes. Results are simplified by considering small lateral displacements of the disc about the electrodes. This allows only the symmetric and first asymmetric modes to be included in the series. Note in this limit that the contributions from both sets of cross terms (one set is the symmetric excitation field interacting with the asymmetric current and the other set is the asymmetric source field interacting with the symmetric current) in the quadratic force expression are of the same order and must be included. The forces are determined by the Coulomb force method. Calculations based on the formulas clearly demonstrate stability characteristics observed in previous experiments. For example, levitation forces overcome the disc weight. In addition, reversal of stability coil currents relative to the levitation coil currents results in lateral restoring forces and stable levitation at low currents (this non-intuitive approach was eventually used in the prior experiments). The calculation also shows that with extremely large stability currents (much larger than could be achieved in the experiments) of the same sign as the levitation coil currents, lateral restoring forces can also be attained (this was intuitively thought to be the simplest approach to stable levitation at the outset of the experiments). Calculations also show that by increasing the size of the stability coil (leaving a dead space between the disc and stability coil) stability coil currents, with the same sign as the levitation coil currents, can be reduced in magnitude but are still required to be larger than the reversed sign case. Thus the disc model reproduces the experimental results as well as indicates improvements that can be attempted.

To understand the results, in particular the lateral restoring forces, simplified models were introduced. The edge of the disc was modeled as a half plane conductor above electrodes. The first model took the half plane above a ground plane stator, in which the stator magnetic field was excited by magnetic line charges. This model furnished simple results for both lateral and vertical forces. In particular, it led to an understanding that when the stability current is reversed from the levitation current, the induced current on the half plane near the edge reverses sign (becomes the same sign as the levitation current beneath the half plane) and thus is repelled by the stability coil. This appears to be the source of stability observed in these cases. This sign reversal near the edge of the disc is also observed in the oblate spheroidal solution as the stability point is approached. The two dimensional model also showed that stability can be achieved with the same current direction on the stability coil (as the levitation coil) but with larger current magnitudes.

Finally, the half plane conductor (representing the disc edge) was placed above uniform current density strips for both the levitation and stability electrodes. This led to similar results as the previous simplified model except that the predicted forces are directly tied to the strip or coil current densities. Comparisons between the predicted lateral forces in this model and in the disc model are relatively good if the stability coil current is not too large.

7 APPENDIX - UNIT VECTORS IN SPHEROIDAL SYSTEM

This short appendix derives some relations between the unit vectors in the oblate spheroidal system and the Cartesian and cylindrical systems. The position vector is

$$\underline{r} = x\underline{e}_x + y\underline{e}_y + z\underline{e}_z$$

The relation between Cartesian and cylindrical coordinates and oblate spheroidal coordinates is

$$x = a\sqrt{1+\zeta^2}\sqrt{1-\xi^2}\cos\varphi$$

$$y = a\sqrt{1+\zeta^2}\sqrt{1-\xi^2}\sin\varphi$$

$$\rho = a\sqrt{1+\zeta^2}\sqrt{1-\xi^2}$$

$$z = a\zeta\xi$$

The metric coefficients are

$$h_\xi = a\sqrt{\frac{\xi^2 + \zeta^2}{1 - \xi^2}} = \sqrt{\left(\frac{\partial x}{\partial \xi}\right)^2 + \left(\frac{\partial y}{\partial \xi}\right)^2 + \left(\frac{\partial z}{\partial \xi}\right)^2}$$

$$h_\zeta = a\sqrt{\frac{\xi^2 + \zeta^2}{1 + \zeta^2}} = \sqrt{\left(\frac{\partial x}{\partial \zeta}\right)^2 + \left(\frac{\partial y}{\partial \zeta}\right)^2 + \left(\frac{\partial z}{\partial \zeta}\right)^2}$$

$$h_\varphi = a\sqrt{(1 + \zeta^2)(1 - \xi^2)} = \sqrt{\left(\frac{\partial x}{\partial \varphi}\right)^2 + \left(\frac{\partial y}{\partial \varphi}\right)^2 + \left(\frac{\partial z}{\partial \varphi}\right)^2}$$

Thus the unit vectors are

$$\begin{aligned} \underline{e}_\xi &= \frac{\partial \underline{r} / \partial \xi}{|\partial \underline{r} / \partial \xi|} = \frac{\underline{e}_x \partial x / \partial \xi + \underline{e}_y \partial y / \partial \xi + \underline{e}_z \partial z / \partial \xi}{h_\xi} \\ &= \frac{(\underline{e}_x \cos \varphi + \underline{e}_y \sin \varphi) \partial \rho / \partial \xi + \underline{e}_z \partial z / \partial \xi}{h_\xi} = \frac{\underline{e}_\rho \partial \rho / \partial \xi + \underline{e}_z \partial z / \partial \xi}{h_\xi} \end{aligned}$$

or

$$\begin{aligned} \underline{e}_\xi &= \frac{-\underline{e}_\rho \xi \sqrt{1 + \zeta^2} + \underline{e}_z \zeta \sqrt{1 - \xi^2}}{\sqrt{\xi^2 + \zeta^2}} \\ \underline{e}_\zeta &= \frac{\partial \underline{r} / \partial \zeta}{|\partial \underline{r} / \partial \zeta|} = \frac{\underline{e}_x \partial x / \partial \zeta + \underline{e}_y \partial y / \partial \zeta + \underline{e}_z \partial z / \partial \zeta}{h_\zeta} \\ &= \frac{(\underline{e}_x \cos \varphi + \underline{e}_y \sin \varphi) \partial \rho / \partial \zeta + \underline{e}_z \partial z / \partial \zeta}{h_\zeta} = \frac{\underline{e}_\rho \partial \rho / \partial \zeta + \underline{e}_z \partial z / \partial \zeta}{h_\zeta} \end{aligned}$$

or

$$\begin{aligned}\underline{e}_\zeta &= \frac{\underline{e}_\rho \zeta \sqrt{1-\xi^2} + \underline{e}_z \xi \sqrt{1+\zeta^2}}{\sqrt{\xi^2 + \zeta^2}} \\ \underline{e}_\varphi &= \frac{\partial \underline{r} / \partial \varphi}{|\partial \underline{r} / \partial \varphi|} = \frac{\underline{e}_x \partial x / \partial \varphi + \underline{e}_y \partial y / \partial \varphi + \underline{e}_z \partial z / \partial \varphi}{h_\varphi} \\ &= \frac{(-\underline{e}_x \sin \varphi + \underline{e}_y \cos \varphi) \rho}{h_\varphi} = \frac{\underline{e}_\varphi \rho}{h_\varphi} = \underline{e}_\varphi\end{aligned}$$

The limit $\zeta = 0$ gives

$$\underline{e}_\zeta = -\underline{e}_\rho \operatorname{sgn}(\xi) = -(\underline{e}_x \cos \varphi + \underline{e}_y \sin \varphi) \operatorname{sgn}(\xi)$$

$$\underline{e}_\zeta = \underline{e}_z \operatorname{sgn}(\xi)$$

$$\underline{e}_\varphi = -\underline{e}_x \sin \varphi + \underline{e}_y \cos \varphi$$

References

- [1] C. Shearwood, C. B. Williams, P. H. Mellor, R. B. Yates, M. R. J. Gibbs, and A. D. Mattingley, "Levitation of a micromachined rotor for application in a rotating gyroscope," *Electronics Letters*, 12 October 1995, Vol. 31, No. 21, pp. 1845-1846.
- [2] R. Yates, C. Williams, C. Shearwood, P. Mellor, "A micromachined rotating yaw rate sensor," October 1996, SPIE Vol. 2882, pp. 161-168.
- [3] J. A. Stratton, *Electromagnetic Theory*, McGraw-Hill Book Co., New York, 1941.
- [4] W. R. Smythe, *Static and Dynamic Electricity*, McGraw-Hill Book Co., New York, 1968.
- [5] M. Abramowitz and I. A. Stegun (editors), *Handbook of Mathematical Functions*, National Bureau of Standards, Dec. 1972.
- [6] I. S. Gradshteyn and I. M. Ryzhik, *Table of Integrals, Series, and Products*, Academic Press, New York, 1980.
- [7] M. R. Spiegel, *Vector Analysis*, Schaum's Outline Series, McGraw-Hill Book Co., New York, 1959.

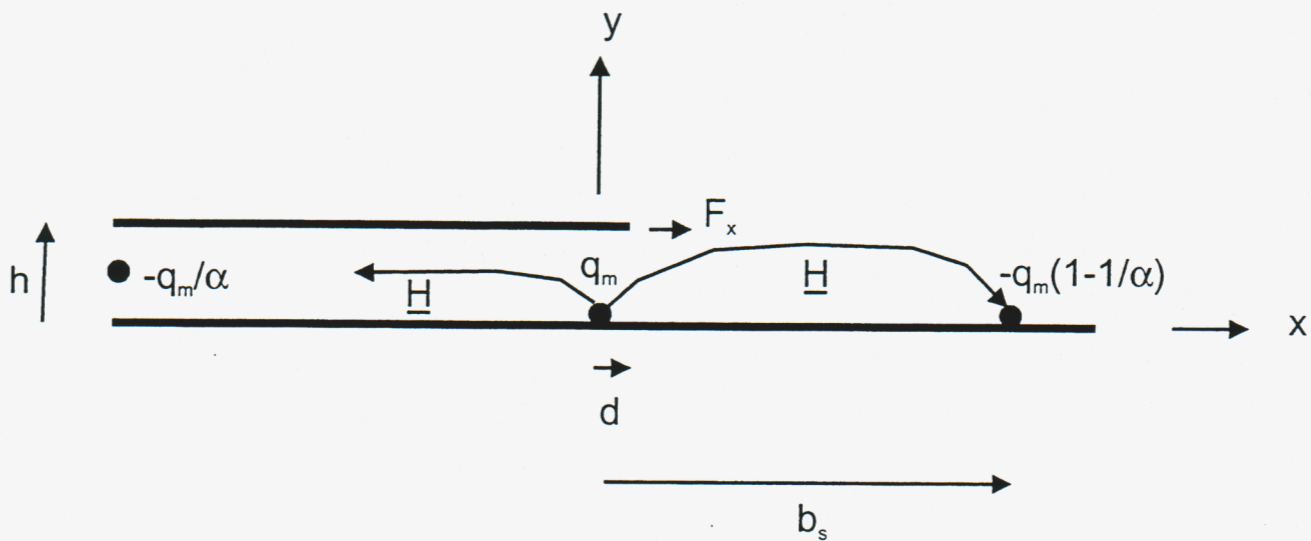


Figure 1a. Half plane edge model for disc. Stator field excitation provided by magnetic line charges.

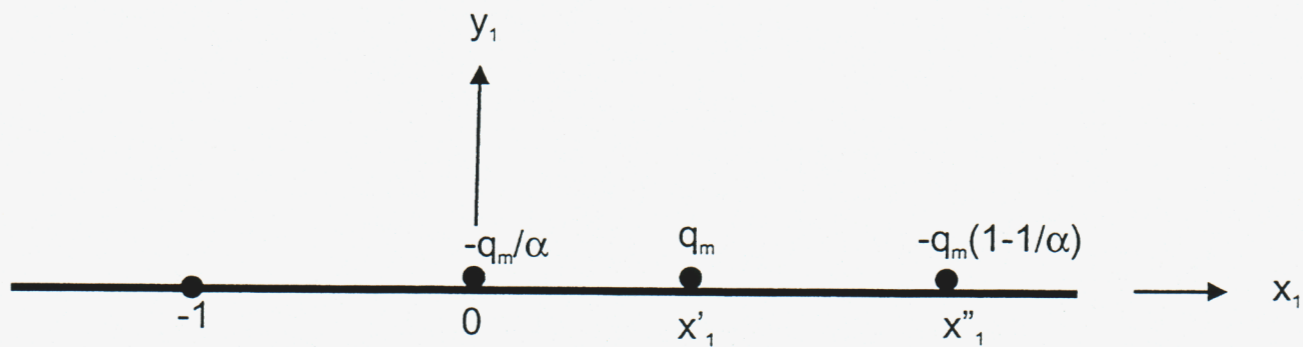


Figure 1b. Conformal mapping for solution of problem in 1a.

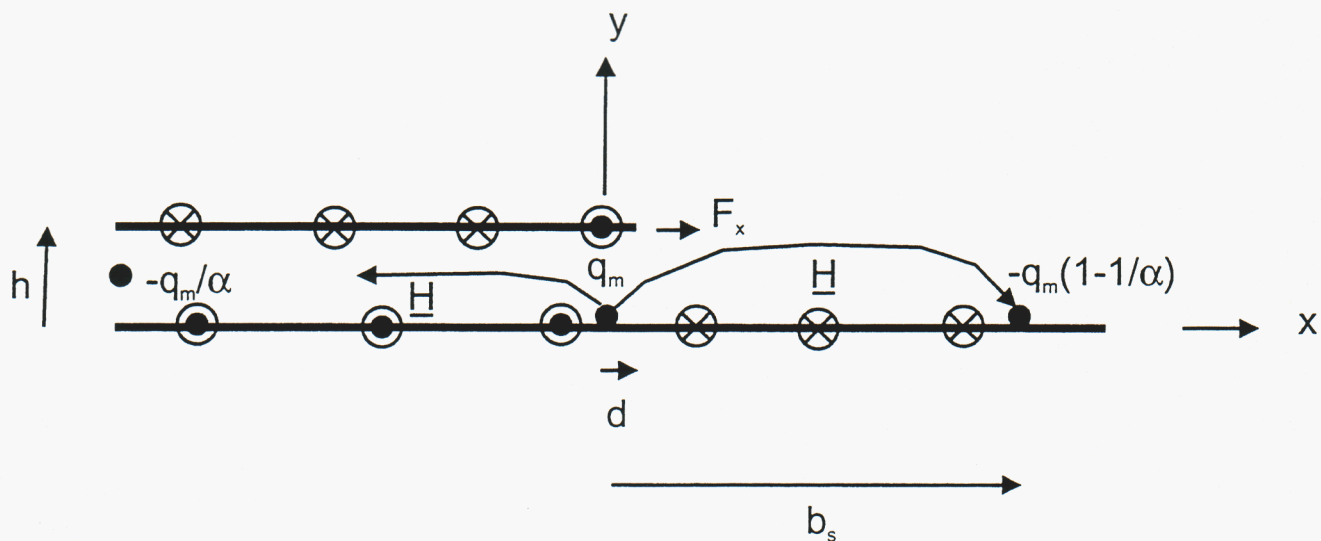


Figure 1c. Illustration of current density reversal at edge of half plane. This provides repulsive restoring force with respect to stability electrode current.

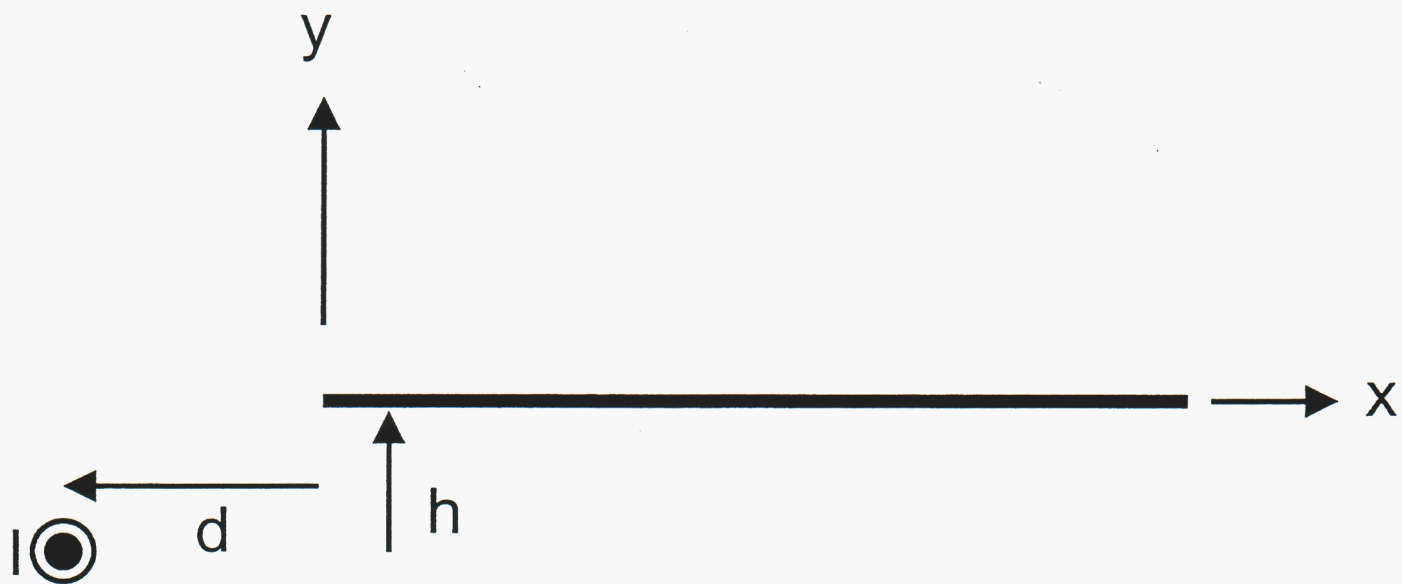


Figure 2a. Half plane excited by electric line current.

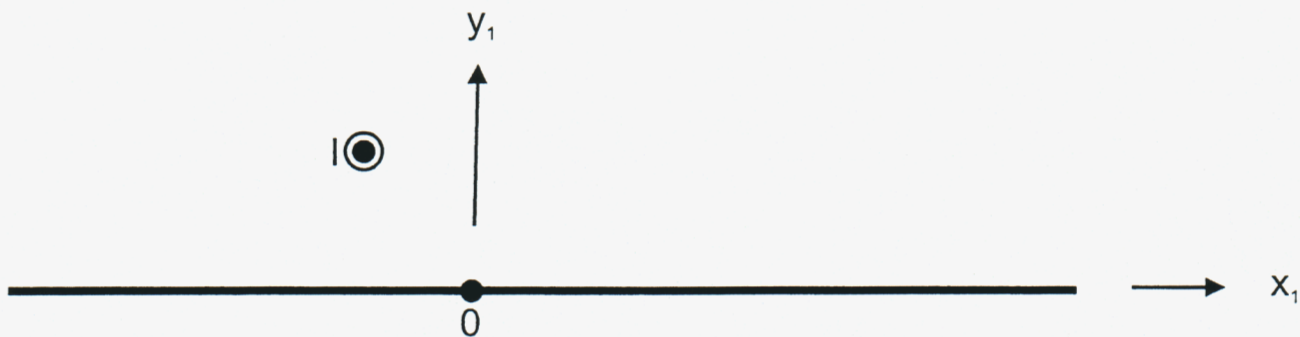


Figure 2b. Conformal mapping for solution of problem in 2a.

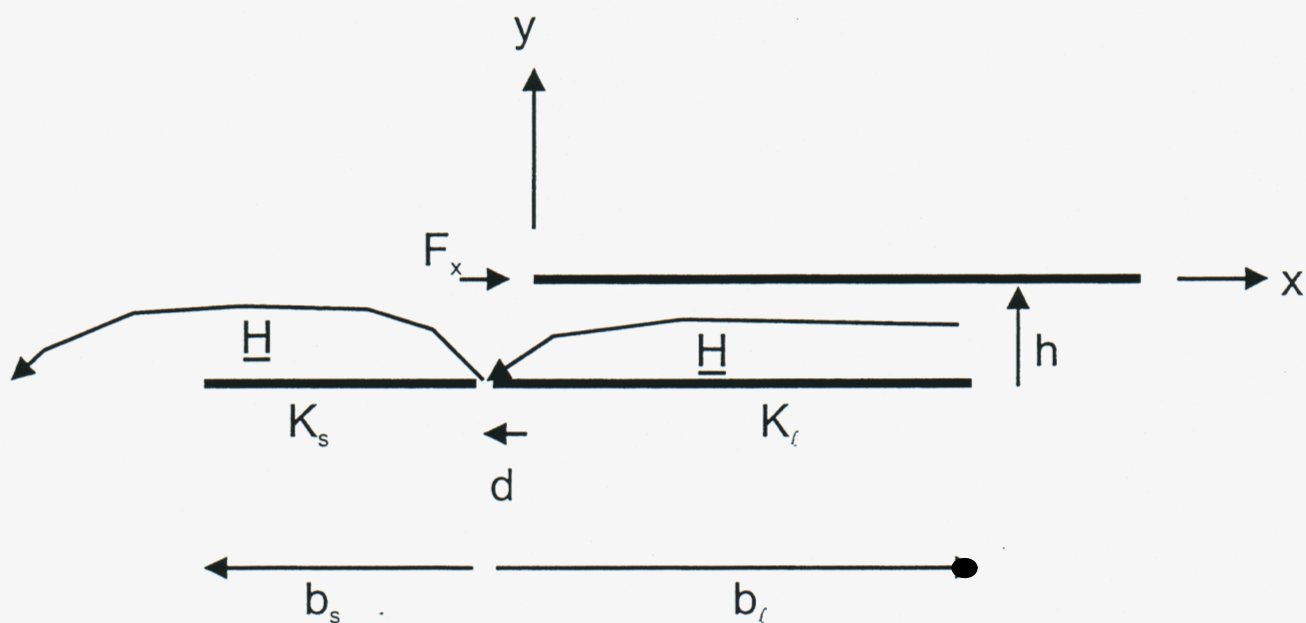


Figure 2c. Half plane edge model for disc. Stator field excitation provided by uniform current density electric current strip electrodes.

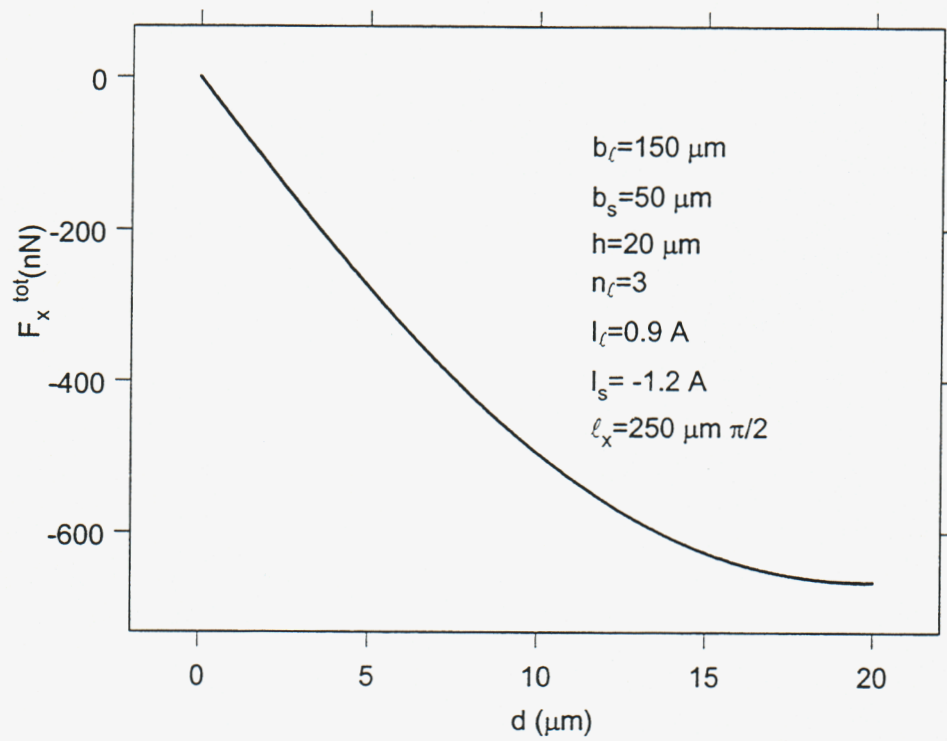


Figure 2d. Total lateral force from half plane edge model with current strip excitation.

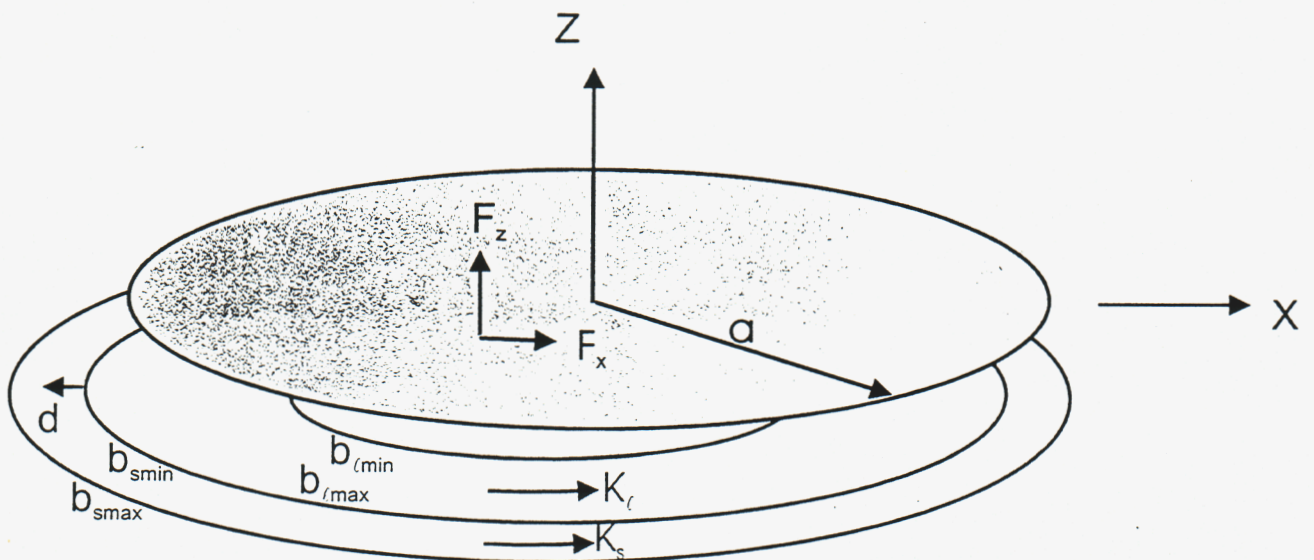
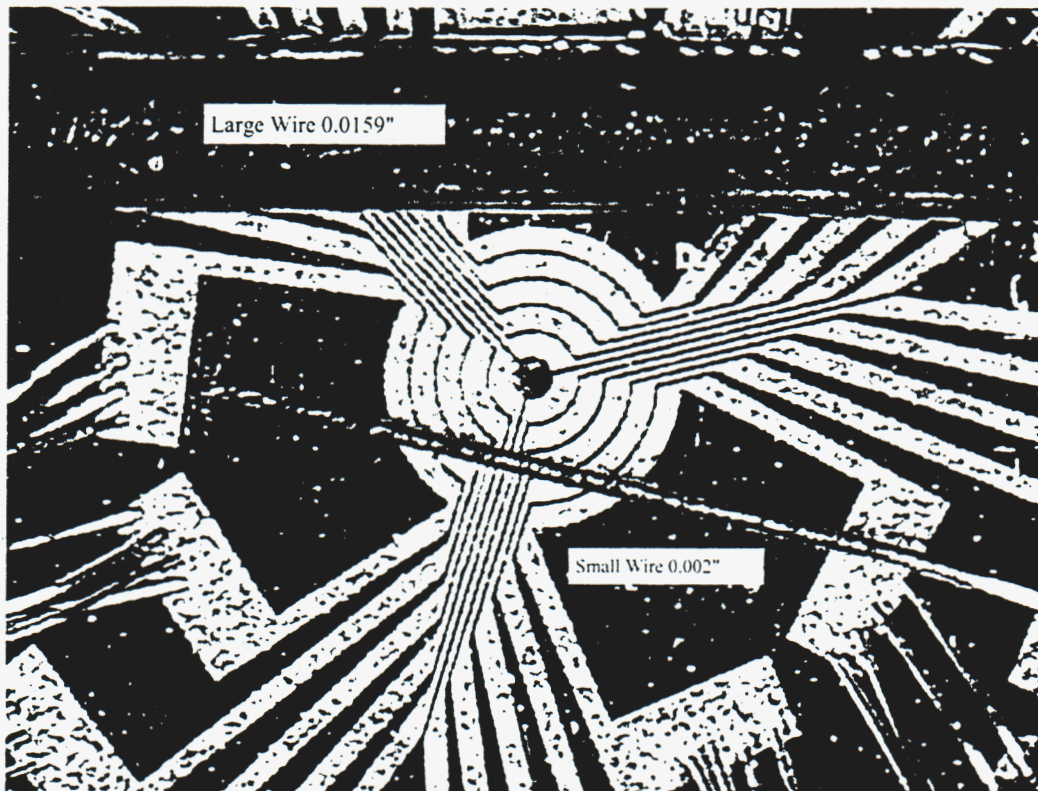


Figure 3a. Disc geometry above circular strip electrodes for stator coils.



Coil 2 - Concentric Coils

Figure 3b. Stator coils used in previous experiments.

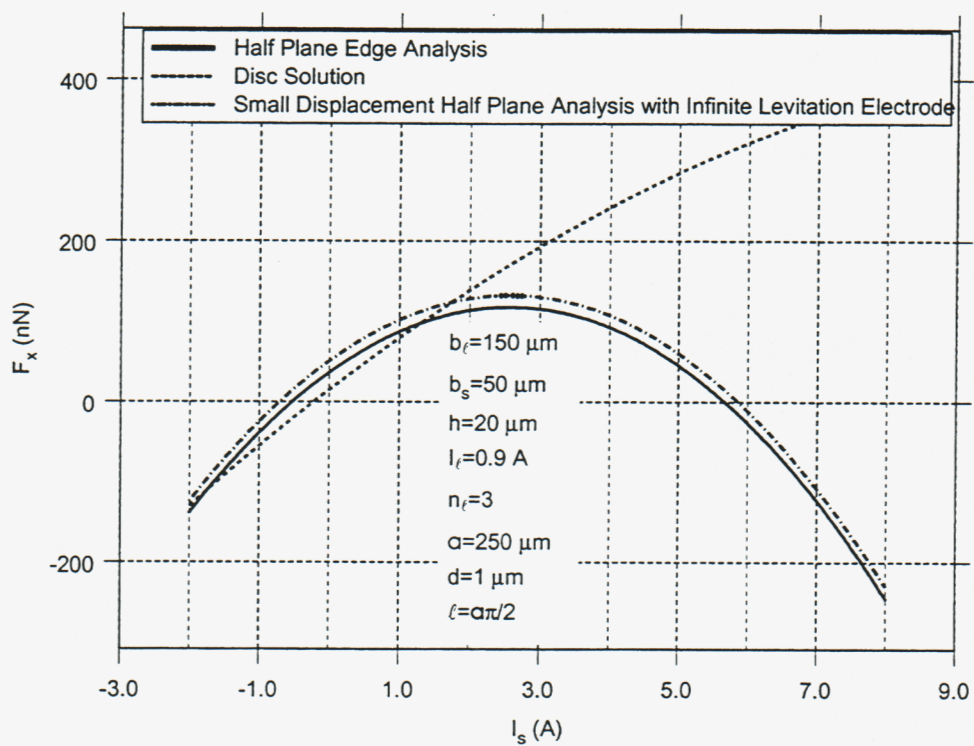


Figure 3c. Lateral force on disc and from half plane edge model (with current strip excitation) as a function of stability coil current.

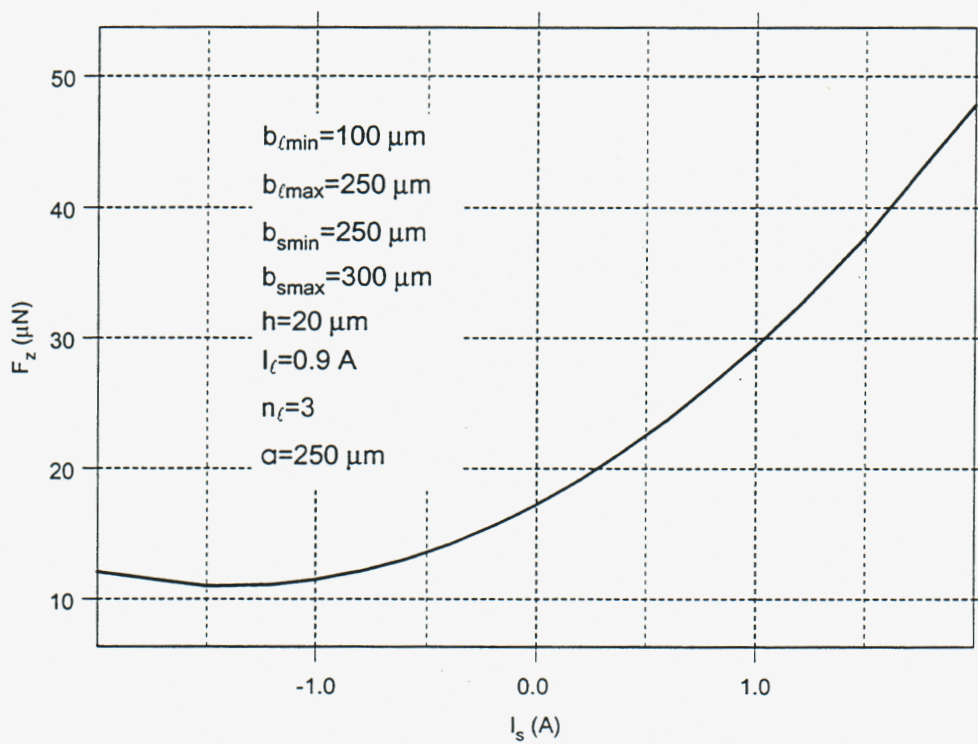


Figure 3d. Vertical force on disc as a function of stability coil current.

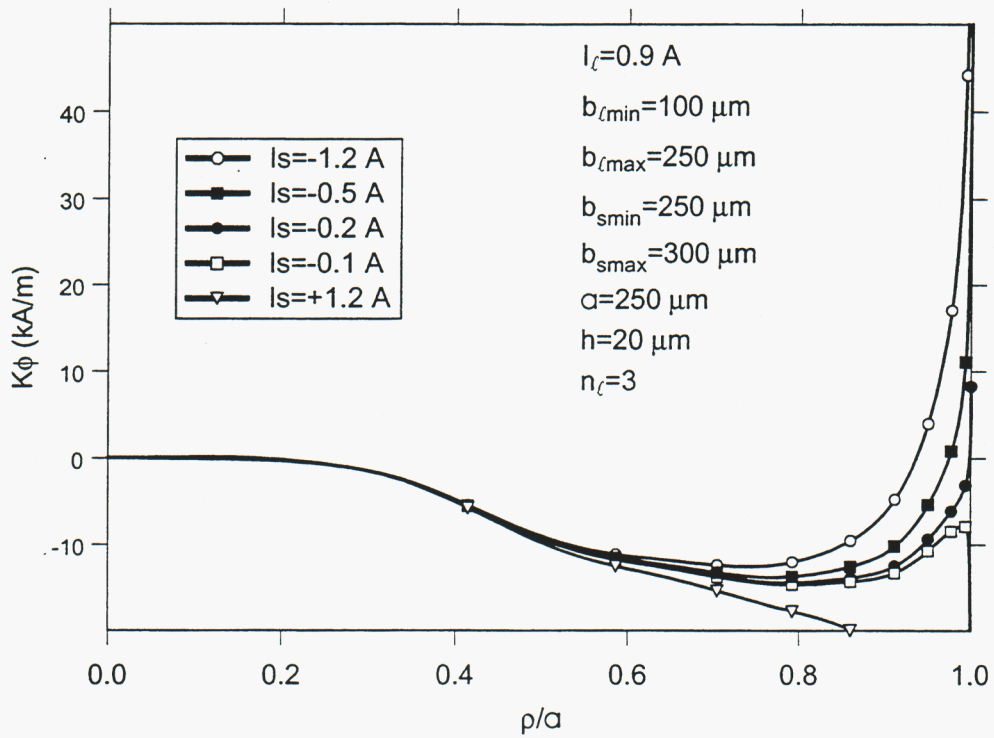


Figure 3e. Total azimuthal current density on disc as a function of radius when disc is centered above stator electrodes.

DISTRIBUTION LIST

1	MS	1221	J.A. Tegneila, 15000
1		1002	G.R. Langheim, 15200
1		1003	R.D. Robinett, 15211
1		1004	R.W. Harrigan, 15221
1		1125	A.K. Miller, 15252
1		1006	L. Shippers, 15272
1		1152	M.L. Keifer, 1642
1		0980	R. Mata Jr., 5714
1		0329	G.E. Sleeffe, 2614
1		0329	F.J. Peter, 2614
10		1003	J.T. Feddema, 15211
5		1152	L.K. Warne, 1642
5		1152	W.A. Johnson, 1642
5		0980	A.J. Ogden, 5714
5		0329	D.L. Armour, 2614
1		1088	LDRD Office
1		9018	Central Technical Files, 8945-1
2		0899	Technical Library, 9616
1		0612	Review & Approval Desk, 9612

for DOE/OSTI